Investigation of Energy Absorption in a Multi-Body System Under Impact

A THESIS
SUBMITTED TO THE FACULTY OF THE GRADUATE SCHOOL
OF THE UNIVERSITY OF MINNESOTA
BY

Jonathan Paul Robelia

IN PARTIAL FULFILLMENT OF THE REQUIREMENTS
FOR THE DEGREE OF
MASTER OF SCIENCE

Thomas R. Chase, Adviser
Arthur G. Erdman, Adviser

December 2009

Acknowledgments

I would like to thank Professor Thomas R. Chase, my advisor, for his patience and the tremendous support throughout this process. I would also like to express my gratitude to my co-advisor, Professor Arthur G. Erdman, for the allowing me this research opportunity and the support he has provided. I would like to thank Michael Meyer and Nathanial Pearson for their help with the experiments. Finally, I would like thank Beth Robelia and ReAnn Dargus Robelia for their editorial and motivational support.

Dedication

This thesis is dedicated to my family, whose support continues to guide me through life's adventures.

Abstract

This thesis investigates the energy absorption of a multi-body system impacted by a suddenly contracting pretensioned helical extension spring. The system consists of a helical extension spring and other common components used in a consumer application.

Impact tests were performed on the system with varying input energies; resulting damage included plastic and brittle failure. Impact tests were also performed on individual components from the system to characterize the amount of energy each component absorbed given a specific energy input.

Component models were created by carrying out regression analysis on the results from each of the components, including the helical extension spring. Through inverse prediction, component models were used to determine the amount of energy each component absorbed during system tests. System models were created, estimating the amount of energy transfered from the helical extension spring to each of the components in the system. Further analysis of the data from a prior study on the energy absorption of helical extension springs was also conducted.

The energy absorption models developed in this thesis provide an understanding of the energy being absorbed in the system due to an impact event. The system models predicted energy absorption between 88 and 120 percent of the initial potential energy stored in the helical extension spring. Energy absorptions of over 100 percent indicate that the component models have over-predicted the amount of energy actually absorbed. The helical extension spring was found to absorb between 37 and 68 percent of its own potential energy during coil impact.

Contents

List of Tables

List of Figures

Nomenclature

F	Spring Force $[N]$ or $[lb_f]$
k	Spring Constant $[N/m]$ or $[lb_f/in]$
x	Spring Extension $[m]$ or $[in]$
F_0	Spring Preload $[N]$ or $[lb_f]$
E_0	Potential Energy Stored in the Spring $[J]$ or $[ft - lb_f]$
E_{avail}	Potential Energy Available After Spring Coil Impact $[J]$ or $[ft - lb_f]$
y_i	Observed Values/Dependent Variables of a Data Set
β_0	Intercept Parameter of a Simple Linear Regression Model
β_1	Slope Parameter of a Simple Linear Regression Model
x_i	Explanatory/Independent Variables of a Data Set
ϵ_i	Error Terms of a Data Set
y	Dependent Variable
x	Independent Variable
E_{abs}	Energy Absorbed by Spring Coil Impact $[J]$ or $[ft - lb_f]$
m	Mass of Spring $[Kg]$ or $[lb_m]$
g	Gravitational Constant, 9.81 m/sec^2 or 32.2 ft/sec^2
h	Height of Spring Travel $[m]$ or $[in]$

Chapter 1

Introduction

1.1 Background

This research originated as the result of a need to investigate how a helical extension spring performed in a multi-body internal impact test. The system is proprietary so all references to it will be generic. There was little prior research done on the system in question so literature reviewed is related to other impact test methods. The spring involved stores a considerable amount of potential energy. The author performed tests on the system in question to determine how energy was absorbed in the event that the spring's stored energy was suddenly released and impacted other components. The main focus of this research was how energy flowed through the system including its many components.

1.2 Literature Review

Literature directly relating to the research described in thesis was limited. However, secondary literature describing other methods of multi-body impact testing and analysis was found and is described below.

Impact is defined as the collision of two or more objects. The forces created during the collision are exerted and removed over a very brief period of time. During this brief period of time the forces involved do not have time to propagate throughout the objects undergoing impact. Loading during impact is different than static loading where a state of equilibrium is reached. Both objects involved in an impact can be subjected to elastic and/or plastic deformations (Goldsmith [1]), elastic deformation

being temporary and plastic being permanent.

There are a number of ways kinetic energy can be removed from an object due to an impact event. The energy flow in the direction of an impact begins at an initial kinetic energy of an object and ends with a final kinetic energy. During the impact some energy is stored as elastic strain and some energy can be absorbed through stress wave propagation, plastic deformation, material dampening, or other phenomenon such as sound or heat(Gilardi [2]).

Systems undergoing permanent deformation, such as the one studied here, require complex analytical descriptions using time-dependent analyses (Stronge [3]). A static analysis cannot be used for this type of impact scenario due to the large plastic deformations the system experiences during impact. During impact, as local deformations progress, the forces involved in the impact continue to change. These changing forces require a dynamic model to be used to describe such an event.

Typically, these dynamic impact events are simulated using time-based Finite Element Analysis. A full finite element analysis of the multi-body system investigated here was not practical. But, insight can be gained from the methods used to verify these models. Gobbi et al. [4] seeks to accurately model, using finite element analysis, the plastic deformations in steel bars undergoing impacts with medium velocities (approx. 6 m/s). Using numerical dynamic analyses, models are created for a simply supported steel bar being impacted by a bar shaped sledge. Models were verified using test rigs consisting of rigidly placed pins holding the steel bar to be impacted. Sledges were accelerated in a track to ensure proper orientation during impact. Findings indicate that the friction during impact between bars and pins used in the test setup was not negligible.

In his simulation of a motor-scooter drop test, Frendo [5] seeks to describe a low-velocity (approx. 3 m/s) multi-body impact with permanent deformation. He does this by first creating a system model to determine forces the motor-scooter experiences over a given period of time. These forces are incorporated into a time-based static Finite Element Analysis to determine the permanent deformations of the frame during the impact event. A drop test is performed using gravity to accelerate the scooter, the complete system, to the appropriate impact velocity. This allows all components in the system to be experimentally tested at one time. Data collected during this test was shown to agree with the predicted performance from his model.

When testing multi-body systems the complexities involved with multiple component interactions can be removed by testing individual components. Chou et al. [6] describes the use of component level testing relating to side impact testing in the automotive industry. Here, component level tests are used to expedite the development of subsystems or components for better performance when integrated and tested at the system level. For example, impact tests can be performed on car doors by themselves and give some insight into how the door will perform when installed in a complete car during an impact test. In the research presented in this paper component level tests were also performed. Components were removed from the system and tested to better understand their role in the energy absorption of the system as a whole. The methods presented by Chou et al. [6] make the assumption that components tested under impact at a subsystem level behave similarly to components tested under impact when part of the larger system.

A review of the dynamics of helical springs was published by Pearson [7]. Forced and transient vibration, wave propagation and damping are discussed. No literature concerning the energy absorption of collapsing helical extension spring coils was found.

1.3 Overview

Chapter 2 describes the multi-body system under investigation, including the subsystems and components that make up the system. Chapter 3 discusses the motivation, methods and results of testing conducted on components from the system. Chapter 4 discusses the models created for each of the components and for the system, with special attention paid to the helical extension spring. Chapter 5 summarizes the conclusions made in this thesis and recommends future work.

Chapter 2

System Description

The system under investigation is a multi-body system that experiences an internal impact event. This means the system is made up of many components that physically interact with one another. This investigation concerns the analysis of the energy flow through the system due to an energy input from one of the system's components, a helical extension spring. The spring collides with one or more components inside the system, discharging a large amount of energy in the form of an impact event. This chapter will present a description of the system, its subsystems and components, and the nature of system/subsystem/component relationships.

2.1 System

The system under investigation is used in a consumer application and operated by a human. It fills an envelope with approximate dimensions of 1.8 m (6 ft) by 0.9 m (3 ft) by 0.9 m (3 ft). It is semi-rigid and is constructed of wood, steel, and polymer composites. The system mass is approximately 36 kg (80 lb). The system is attached to ground around its perimeter by means of a flexible coupling held in place by approximately 20 wood screws. This creates a firm but slightly flexible union.

The system consists of 3 major subsystems each made up of a number of components. The system is of proprietary nature and therefore will be described using generic terms, i.e. component I , subsystem A, etc. The 3 subsystems will be referred to as subsystem A, subsystem B, and subsystem C. Please refer to Fig. 2.1.

The system is comprised of a single occurrence of subsystem C, four occurrences of

subsystem A and two occurrences of subsystem B. One occurrence of subsystem B and two occurrences of subsystem A form one of two identical assemblies. For simplicity we will call each of these identical assemblies Assembly AAB. For the purposes of this research only one of the two instances of Assembly AAB will be discussed, as they operate similarly and independently of each other. A representation of the relative size of each subsystem and the location they take in the system can be seen in Fig. 2.1.

The impact event is located in one of Subsystem A's two identical occurrences within Assembly AAB. Energy for the impact is supplied by a helical extension spring, which is a component in Subsystem A. Under normal operating conditions the energy stored in the spring is released slowly and in a controlled manner. Under these conditions an impact event does not occur. Only when the spring is suddenly released due to a component failure does the system experience an impact event.

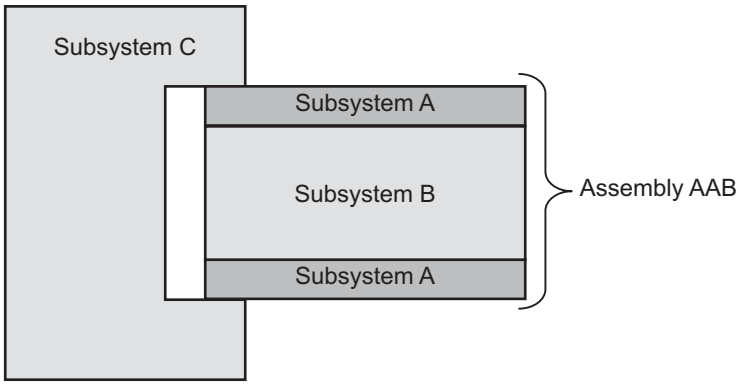

Figure 2.1: Representation of Nesting Subsystem Assembly

2.2 Subsystems

As mentioned above the system is composed of three main subsystems: A, B, and C. For the purposes of this report the system contains a single occurrence of Subsystem B and C and two occurrences of Subsystem A. From this point on when the System is mentioned it will refer to this combination of subsystems. As seen in Fig. 2.1, both occurrences of Subsystem A are attached to Subsystem B and the resulting Assembly AAB attaches to Subsystem C.

2.2.1 Subsystem C

Subsystem C is the largest of the three subsystems and through it the system is attached to ground. It fills an envelope of 1.8 m (6 ft) by 0.9 m (3 ft) by 0.25 m (1 ft). Subsystem C accounts for approximately 33% of the system's mass. Each occurrence of Subsystem A connects to Subsystem C through one pin joint. This leaves a small contact area for energy to be transfered between Subsystems A and B into Subsystem C. See Fig. 2.2 for a diagram of the pin placement.

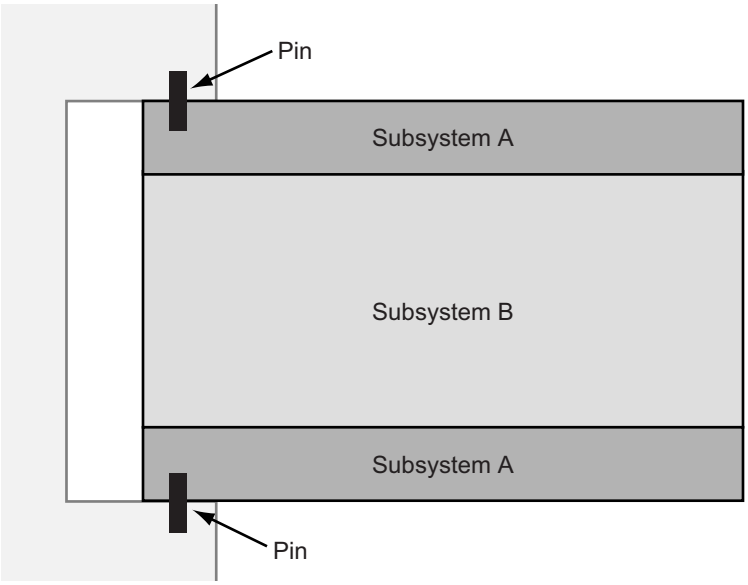

Figure 2.2: Pin Placement Connecting Subsystem A to Subsystem C

2.2.2 Subsystem B

Subsystem B fills a rectangular envelope approximately 0.9 m (3 ft) by 0.9 m (3 ft) by 0.15 m (0.5 ft). It makes up approximately 58% of the system's mass. It houses both occurrences of Subsystem A and does not come into contact with Subsystem C.

Subsystem B and A are in intimate contact with each other along the three sides of a channel in Subsystem B. This channel, along with two mounting blocks integrated into Subsystem B, hold both instances of Subsystem A to Subsystem B. The mounting blocks, Components 11 and 12, are made of polyvinyl chloride (PVC). See Fig. 2.3 for a diagram of the contact between Subsystem B and Subsystem A.

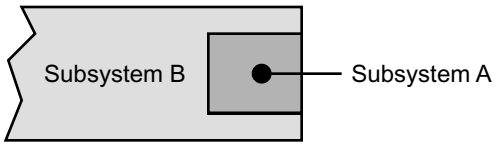

Figure 2.3: Right Side: 3-Sided Contact of Subsystem A and B

2.2.3 Subsystem A

Subsystem A, the location of the impact event, is of the most interest due to the localized damage created by the impact event. This damage absorbs the energy that was stored in the helical extension spring. This relates to the main purpose of this research: determine where in the system energy is being absorbed and how much of it is being absorbed.

Subsystem A is a mechanism that fills a rectangular envelope approximately 0.6 m (2 ft) by 2 cm (0.8 in) by 2 cm (0.8 in). Both instances make up approximately 9% of the system's mass. As mentioned in the previous section, three sides of Subsystem A are in contact with Subsystem B, as shown in Fig. 2.3.

Ten components make up Subsystem A, three of which are movable. The three movable components are Components 8 and 9 and the helical extension spring. The movable components allow potential energy to be stored in the spring and transfered to the remaining seven stationary components. The stationary components are used to attach Subsystem A to Subsystem B and transfer the energy of the helical extension spring to Subsystems B and C. The seven stationary components are Components 1-5, 7 and 10.

Each instance of Subsystem A is connected to Subsystem B by two screws: a short screw, Component 4, and a long screw, Component 7. The screws are fastened to the mounting blocks in Subsystem B. See Fig. 2.4 for a diagram of the screw placement.

The short screw mounting block, Component 11, has a 3 mm (0.1 in) thick section where the short screw is fastened. This leaves only a small section of the short screw in contact with the mounting block. The long screw mounting block, Component 12, is thicker, allowing the entire length of the long screw to be supported. The different mounting block geometries play an interesting role in the energy absorption and transmission properties of the system, and will be discussed in Chapter 3.

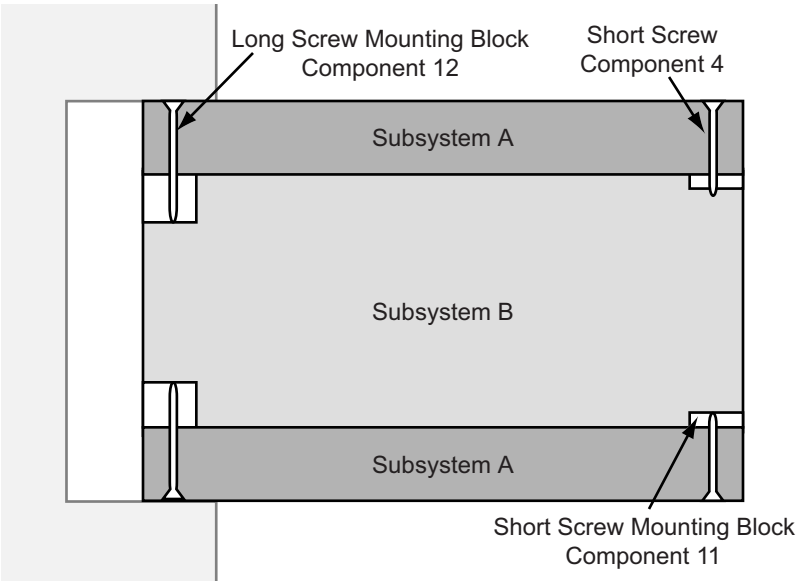

Figure 2.4: Cross Section - Screw Placement and Material Geometry

2.2.4 Assembly AAB

Four different types of AAB assemblies were tested, AAB1, AAB2, AAB3, and AAB4. All of these assemblies were the same size, the only differences being the presence or lack of components 5 and 12. Table 2.1 lists which assembly contains which components.

Subsystem	Component Number	Assembly			
		AAB1	AAB2	AAB3	AAB4
A	1	x	x	x	x
	2	x	x	x	x
	3	x	x	x	x
	4	x	x	x	x
	5			x	x
	6	x	x	x	x
B	11	x	x	x	x
	12		x		x

Table 2.1: Component Presence in Subsystems and Assemblies

2.3 Helical Extension Spring

As previously described, the helical extension spring is one of the three movable components in Subsystem A. It is an energy storage device whose sudden release

is the cause of the impact event within the system. Its properties and use will be discussed in this section.

The helical extension spring found in Subsystem A has a preload of 209 N (47 lb). During manufacture residual stresses were created inside the spring. This creates a initial force (or preload) that must be applied to the spring before its coils can be stretched apart. The spring's force versus deflection curve can be seen in Figure 2.5.

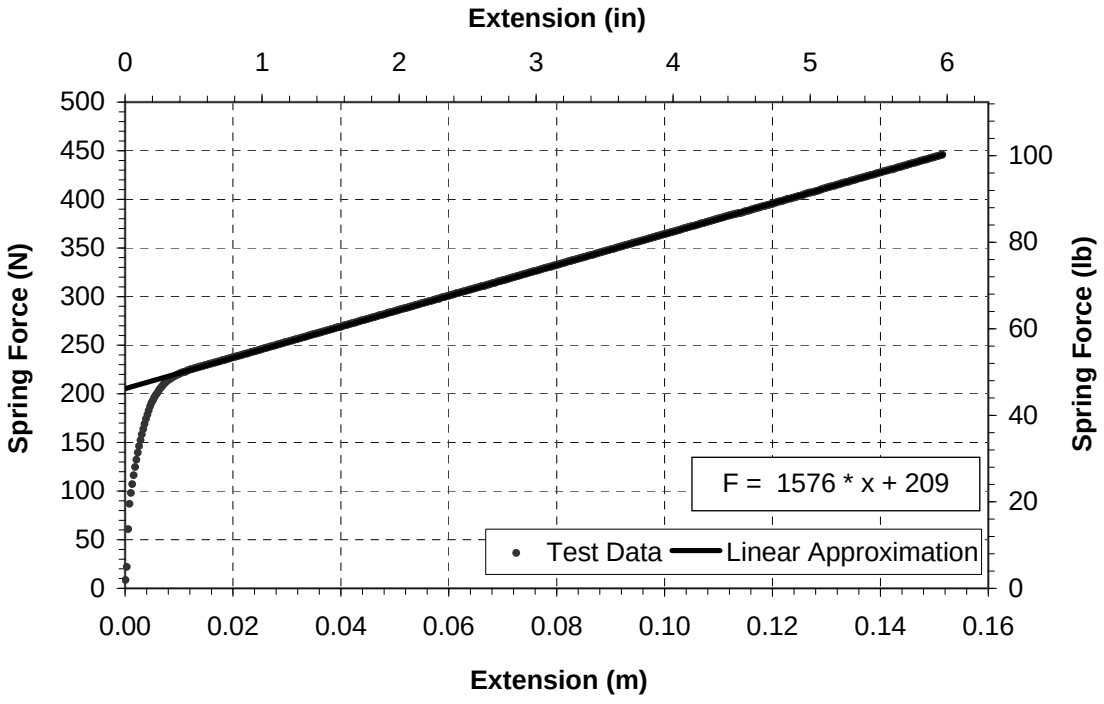

Figure 2.5: Measured Force Deflection Curve of Helical Extension Spring from Subsystem A

A spring's force versus deflection curve can be approximated by Eq. (2.1).

$$F = k \cdot x + F_0 \tag{2.1}$$

Eq. (2.1) is a linear approximation and disregards the non-linearity present at small extensions. The force deflection curve of the helical extension spring found in Subsystem A is approximated by Eq. (2.2), where $k = 1576\ N/m$ $(9\ lb/in)$ and $F_0 = 209\ N$ $(47\ lb)$.

$$F = 1576 \cdot x + 209 \tag{2.2}$$

The spring stores a considerable amount of energy, up to 102 J (75 ft-lb). The amount of potential energy stored in a spring is given by Eq. (2.3).

$$E_0 = \frac{1}{2} \cdot k \cdot x^2 + F_0 \cdot x \tag{2.3}$$

Therefore, for the helical extension spring found in Subsystem A:

$$E_0 = 788 \cdot x^2 + 209 \cdot x \tag{2.4}$$

where x is measured in meters and the units of E_0 are Joules. An energy versus deflection curve of the spring is illustrated in Fig. 2.6.

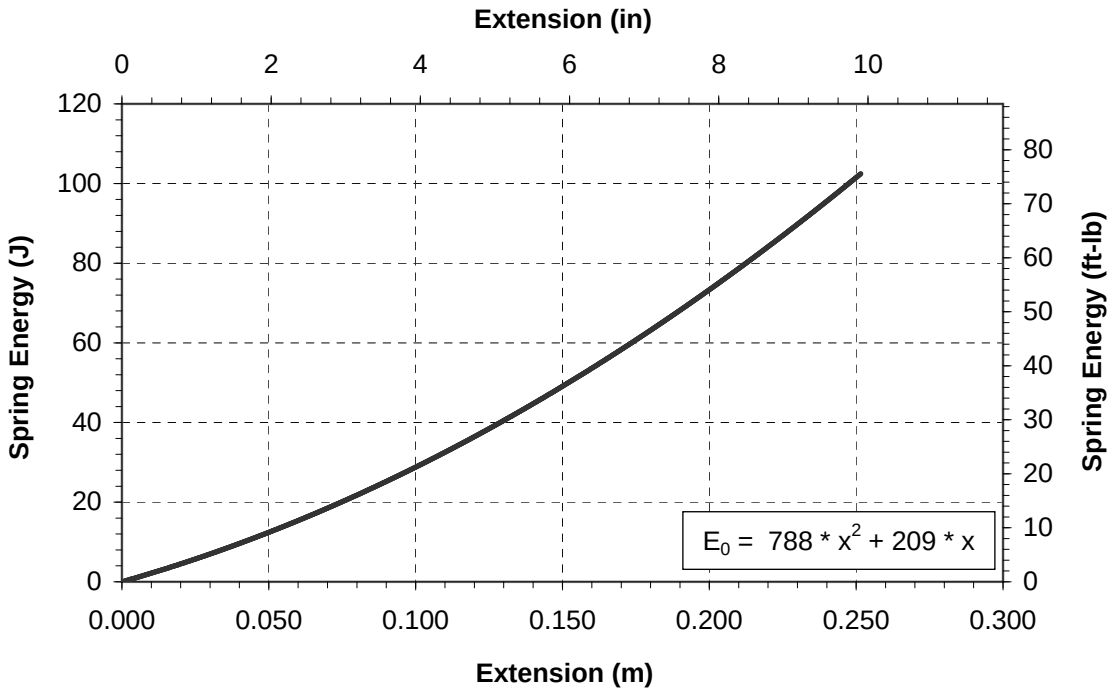

Figure 2.6: Potential Energy vs. Deflection of Helical Extension Spring from Subsystem A

When the spring is in an extended position and then suddenly released it impacts other components within the assembly. This impact event transfers the energy from the spring to the rest of the assembly and in turn the rest of the system. This was investigated through a series of tests. These tests and others are described in the following chapter.

Chapter 3

Testing

Discussed in this chapter are the testing methods used to quantify the the energy absorption characteristics for the system undergoing an impact event. In order to gain a better understanding of the system behavior during and after the sudden release of spring energy, two series of tests were performed. The first series of tests involved the system as a whole. These tests mimic the response of the system as it would occur in its intended installation location.

The second series of tests were conducted to better understand the behavior of the components in the system tests. The component tests involved select components from Subsystems A and B. The component tests mimic the response of individual components to impact as it would occur in the components' intended location within the system.

3.1 System Tests

The system tests involved Subsystems A, B and C. They were conducted for three reasons: one, to understand what was physically happening to the system during and after the impact event; two, to determine which components were being damaged and how much damage was occurring; three, to determine if the amount of energy input to the system during the impact event would cause the complete separation of Subsystem A from Subsystem B.

The system tests will be discussed in three parts: the test setup, the test procedure and the test results. The test setup subsection will discuss the items used to conduct

the tests, the test procedure subsection will discuss the methods used to conduct the tests and the test results section will discuss the data obtained from the tests.

3.1.1 System Tests Setup

A fixture was built to emulate the size, shape and material of a typical installation of the system. The system was installed in the fixture per the manufacturer's instructions. As mentioned in Section 2.1, the system was attached to the grounding fixture using 20 screws around its perimeter, forming a firm, yet semi-flexible, union.

The extension of the spring in Subsystem A depends on the position of Assembly AAB relative to Subsystem C. The rotation of Assembly AAB relative to Subsystem C about the pins shown in Fig. 2.2 does not cause spring extension. Spring extension is caused by the vertical movement of Assembly AAB relative to Subsystem C. The extension of the spring varies from between 0 and 178 mm (0 and 7 in). These extensions can be converted to energies using Fig. 2.6.

Figure 3.1 represents the setup for the system test. An additional support fixture was created to hold Assembly AAB in place relative to Subsystem C. The fixture keeps Assembly AAB from rotating about the pin joints seen in Fig. 2.2 and moving vertically relative to Subsystem C. The assembly rested on the support fixture but the fixture did not hold the assembly rigidly. This allowed the assembly to move freely when an impact event occurred.

A standard commercial digital video camera was used to record each system test. The camera recorded video at 30 frames per second. The camera was aimed at the interface between Subsystem B and Subsystem A when a spring was released. The rate of 30 frames per second was not fast enough to capture all of the details that occurred during an impact event. A high speed camera would have been needed in order to capture all of these details. However, the lower frame rate camera did enable review of the general damage incurred during each test and allowed a record to be kept of the final state of the system.

3.1.2 System Test Procedure

The procedure used for the system tests consists of three steps. First, Assembly AAB is placed in the desired position within Subsystem C. The position of the spring in Subsystem A is recorded to determine its extension and the corresponding energy

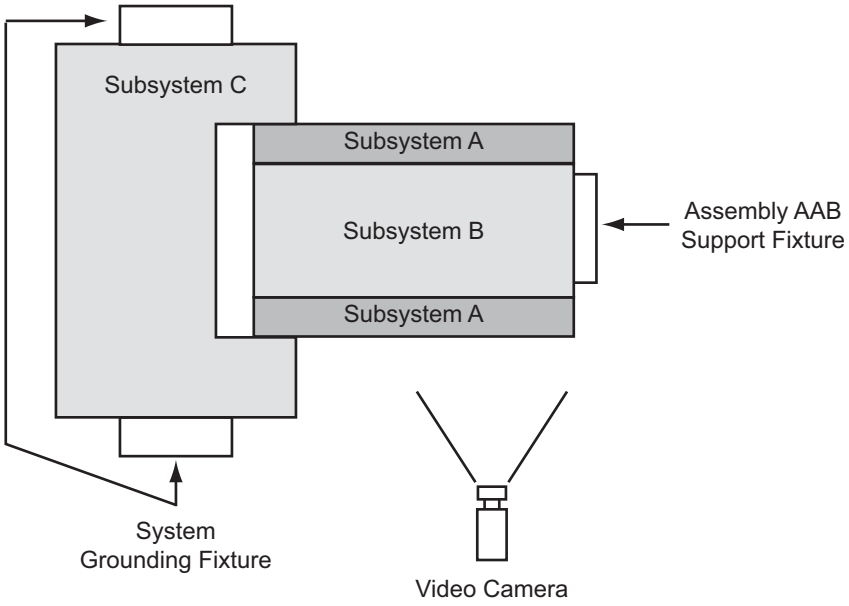

Figure 3.1: Setup for System Tests

stored.

Second, a nylon cord, Component 8, holding the spring in place is cut using a hand held propane torch. A torch is used to sever the cord because it acts quickly and does not exert an external force on the system. Alternatively, using a mechanical means to cut the cord, such as a knife or scissors, introduces an external force to the system which may influence its behavior. Also, using mechanical means to sever the cord may cause the cord to fray and shorten the extension of the spring prior to its complete release. This causes the initial energy stored in the spring to decrease before release.

Third, observe the behavior of the system after the impact event and measure significant damage done to any of the components from each of the subsystems. The final state of the subsystems is recorded. Assembly AAB is removed from Subsystem C and Subsystem A is removed from Subsystem B. Components that are damaged are recorded and the amount of damage incurred by each component is recorded.

This procedure was repeated at approximately thirty different initial spring potential energy levels between 20 J (15 ft-lb) and 112 J (83 ft-lb). A variety of results were produced at each energy level with more damage occurring at higher energy levels.

3.1.3 System Test Results

This subsection describes the results of the system tests. This includes the methods of energy absorption, the kinds of deformation the absorbed energy creates and some examples of this deformation. A list of deformed components is given and the method used to measure the amount of deformation is discussed.

Results from the system tests included measurements of damage sustained and a record of which components were damaged. The components that were damaged give an indication of where energy is being absorbed in the system. The amount of damage they sustain relates to the amount energy they absorb. The maximum energy input into the system during any one test was 112 Nm (83 ft-lb), resulting in a theoretical spring velocity after coil contraction of 22 m/s (49 miles/hr).

The components in the system generally absorbed energy in one or more of the following four ways: elastic deformation, plastic deformation, ductile fracture or brittle fracture. Energy is absorbed through elastic deformation when a component deforms during impact and then returns to its original state. When the component returns to its original state it releases almost all of the energy it stored temporarily. Measuring elastic deformation is not possible after impact has occurred. For this reason elastic deformation of components in the system test was not measured. We assume that the amount of elastic deformation energy is small compared to the amount of plastic deformation energy.

Plastic deformation or plastic flow occurs when a component permanently deforms during an impact event. Plastic deformation may take the form of elongation or bending of material. The energy used to deform components plastically removes it from the energy imparted by the impacting spring. Because plastic deformation is permanent it can be observed after a test has been run. This allows a measurement of the extent of damage following a test. An example of the large plastic deformation of Component 1, which is typical of the system tests, can be seen in Fig. 3.2. This type of large plastic deformation occurred as the result of pin-loading on a sheet metal hole in Component 1 during an impact event.

A possible explanation for the large plastic deformation seen in Fig. 3.2 is a decrease in the local flow stress, as described by Macaulay [8]. While the material is pin-loaded by the impact event, a high local strain rate occurs. This causes a build up of heat that does not have time to escape. The increase in temperature lowers the local flow

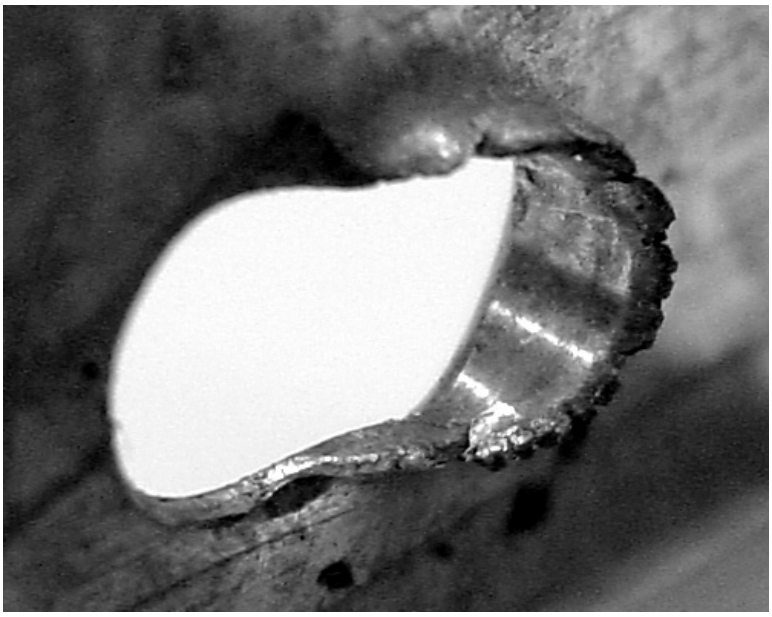

(a) Inside of Hole

(b) Outside of Hole

Figure 3.2: Typical Plastic Deformation of Component 1 - Material: Steel Sheet Metal

stress of the material and allows large strains to occur. These strains occur locally and the nearby material is left undeformed.

In some cases ductile fracture occurred along with plastic deformation. The fracture seen in Fig. 3.3 occurred along with large plastic deformation. In our analysis we did not differentiate between plastic deformation without ductile fracture and plastic deformation with ductile fracture.

Brittle fracture of material was also observed in the system tests. An example of a typical brittle fracture occurring in Component 2 can be seen in Fig. 3.4. This type of fracture occurs when a component breaks in two with no signs of plastic material flow. This may present itself as a component that, after fracturing, can be fit back together perfectly with no sign of failure except for a crack at the fracture point. The Brittle fracture observed during the system tests occurred in a fiberglass reinforced nylon component. This type of material failure is also permanent so it can be observed easily after a test and an amount of energy assigned to its presence.

The components from Subsystem A and B that were damaged during the system tests due to either plastic deformation or brittle failure were recorded. The component damage observed in the system tests included: bent steel screws (Components 4 and 7), pin-loaded deformation at hole locations of different materials (Components 1 and 11), brittle fractured polymer components (Components 2 and 12), buckling of sheet metal steel structures (Component 5) and shearing of circular cross sections (Component 3). As an exception, the helical extension spring does not exhibit either plastic deformation or brittle failure but absorbs energy elastically. The raw system test data can be found in Appendix B.

Component deformation was measured using a dial caliper for elongation or compression of material. A protractor was used to measure components that bent at an angle. This generated data that could be used to relate the damage done to each component to the energy that component absorbed. Component tests were conducted to obtain the relationship between component damage and energy absorption, as described in the next section.

3.2 Component Tests

Component tests were performed to determine the relationship between the energy absorption of certain components and the damage done to them by an impact event.

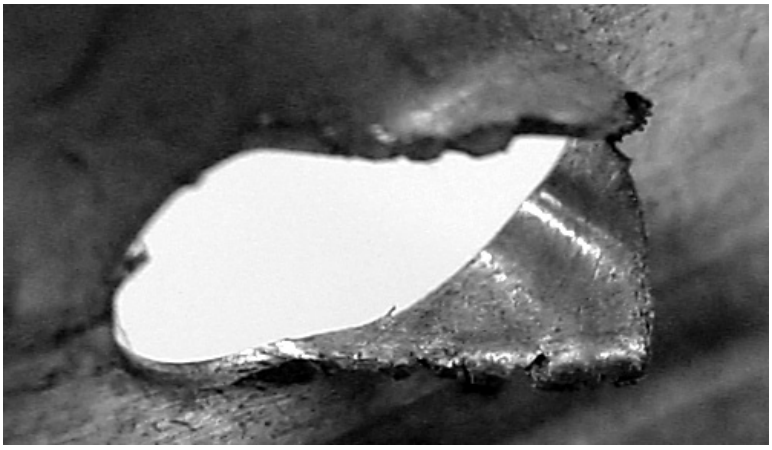

(a) Inside of Hole

(b) Closeup of Fracture

Figure 3.3: Typical Plastic Deformation with Ductile Fracture of Component 1 - Material: Steel Sheet Metal

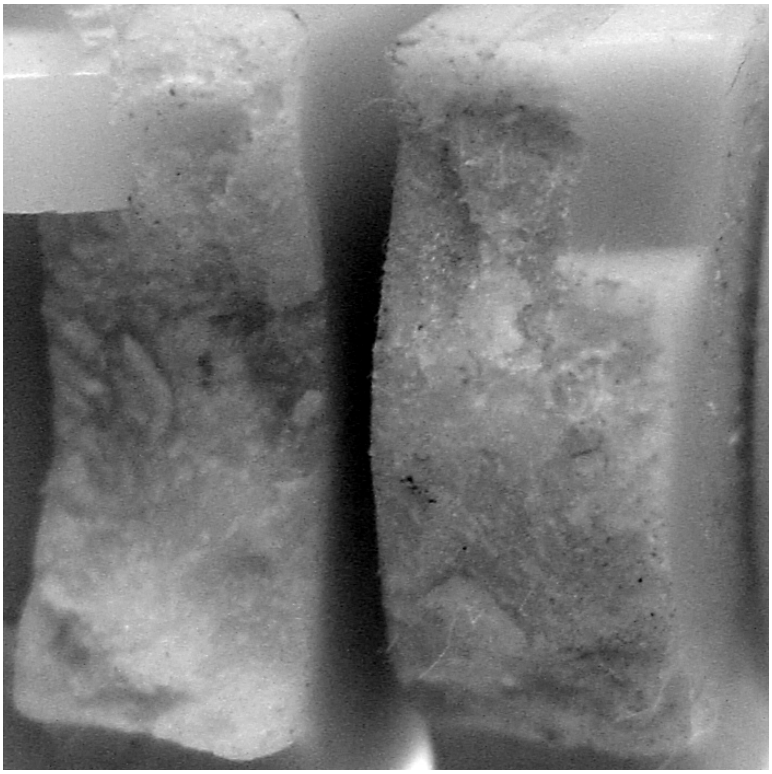

Figure 3.4: Two Halves of the Typical Brittle Fracture of Component 2 - Material: Fiberglass Reinforced Nylon

The component tests were conducted using components from Subsystem A and B. No components in Subsystem C were used for the component tests. Components from Subsystem C were far enough removed from the impact location that they did not sustain any permanent damage.

Eight component tests were performed: six components from Subsystem A and two components from Subsystem B. This section describes the general concept and procedure used to determine the energy absorption properties of a generic component similar to ones found in Subsystems A and B. The component tests will be described in three sections: setup, procedure and results. The setup section will describe the apparatus used to conduct a typical component test. The test procedure section will discuss the method used to carry out a typical component test. Each of the component tests were set up and conducted in a similar manner, making a single description of the setup and procedure of a component test sufficient to understand the process. The results section will briefly discuss the trends found in the test results and examples of typical results.

3.2.1 Component Test Setup

A test stand was created for each of the eight components tested. Seven of the eight test stands mimicked the geometric properties of the location in which the component was installed within the system. The materials used to mimic the system geometry were made of harder and more rigid materials than were found in the original system. These materials were replaced to ensure that the component being tested absorbed the majority of the energy being supplied.

The test stand created for each component included a helical extension spring, identical to the one found in Subsystem A, and a rigid base to fix the stand to ground. The spring was used to impact each component. The spring imparts similar loads at similar velocities to those found in the system under normal conditions. The rigid base was used to ensure that little or no energy was transfered into kinetic energy from the movement of the test stand. A generic component test stand is represented in Fig. 3.5. A slot located in the rigid base ensures the spring travels in the correct direction. Two smaller slots were also placed in the rigid base parallel to the direction of impact. The two slots guide the spring end adapter guide pin, ensuring proper placement of the spring end during impact.

The one component that needed a dissimilar test stand was the helical extension

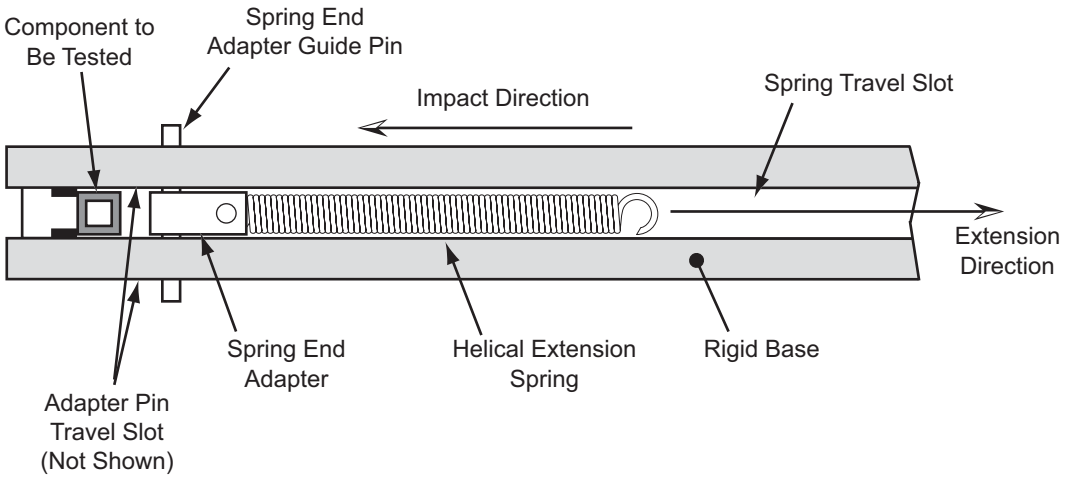

(a) Top View

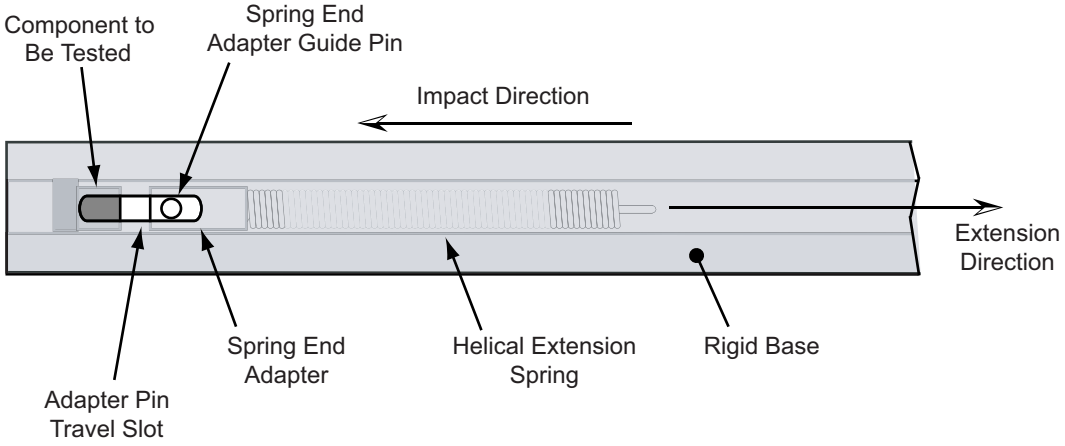

(b) Side View

Figure 3.5: Test Setup for Generic Component

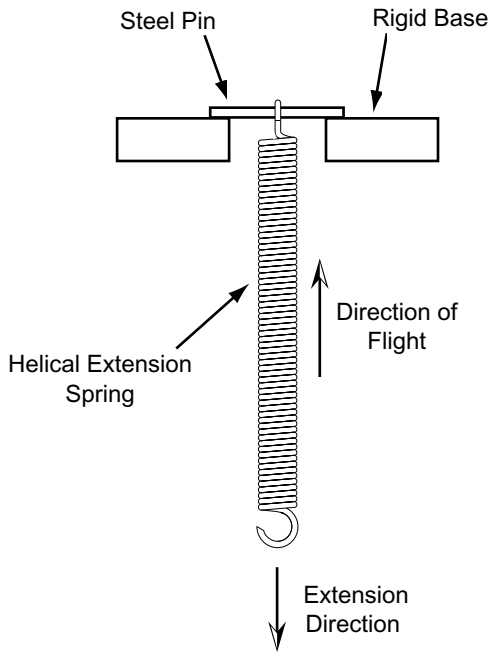

Figure 3.6: Test Setup for Helical Extension Spring

spring. The test setup for the spring can be seen in Fig. 3.6. The spring was found to absorb a portion of its own energy during contraction. The energy absorption is attributed to the impact between the adjacent spring coils. A test stand was created to measure the energy absorbed by the spring. The test stand enabled the spring to be launched vertically. The initial potential energy of the spring was compared to the potential energy associated with the maximum height reached by the spring. The loss of energy was determined by their difference.

3.2.2 Component Test Procedure

The procedure for the component tests involve five steps. First, the spring is extended to a desired energy level. This energy level, E_{avail}, is found from the available spring energy versus extension graph provided in Fig. 3.7. This graph is obtained from the helical extension spring component test which will be discussed later in this section. Second, the spring is held at the desired extension by tying the free end back with a section of nylon cord, Component 8. Third, the cord is cut using a handheld propane torch. A handheld propane torch was used for the same reasons give in Section 3.1.2.

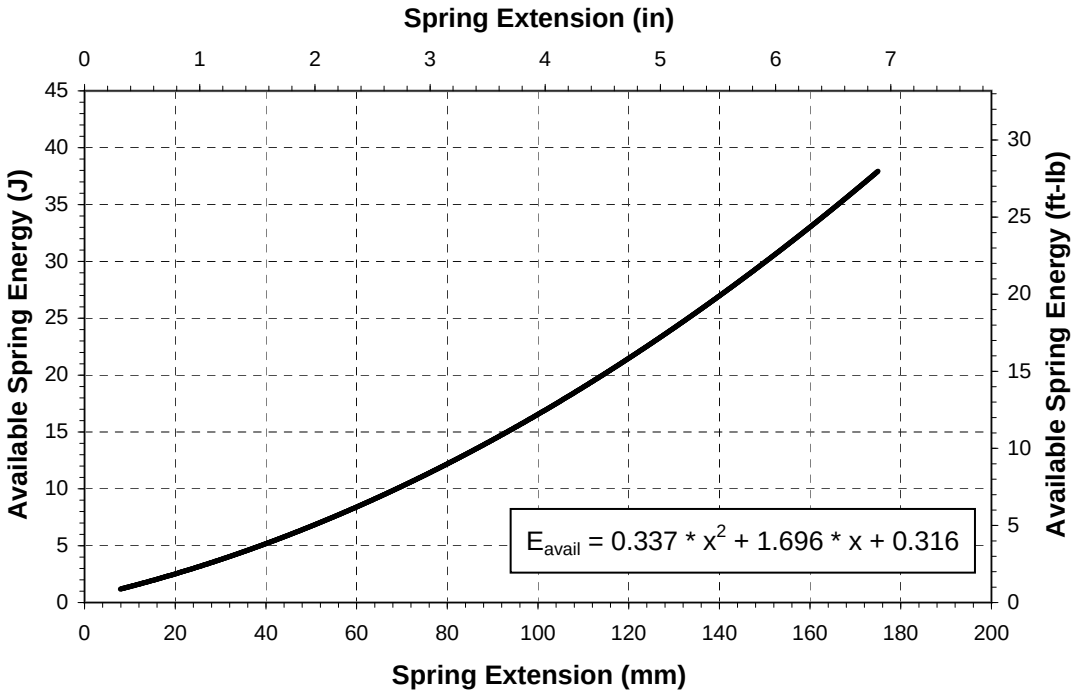

Figure 3.7: Available Spring Energy After Coil Impact vs. Deflection of Helical Extension Spring from Subsystem A

Step four varies according to the type of component damage incurred during the system tests. If the component sustains non-continuous damage, then the energy level for each test is steadily increased until the component fails. The test is repeated at the energy level where failure occurs to verify the result.

If the component damage occurs in a continuous manner, the input energy level is steadily increased from zero. The energy level is increased until the damage done to the component exceeds the damage that occurred in the system tests for that component. A new component is used for every test in both cases to avoid cumulative damage effects.

The procedure for the helical extension spring component test is similar to the component tests that exhibited plastic deformation. Instead of increasing the potential energy in the spring and measuring the deformation of the component, the maximum vertical rise of the spring is measured.

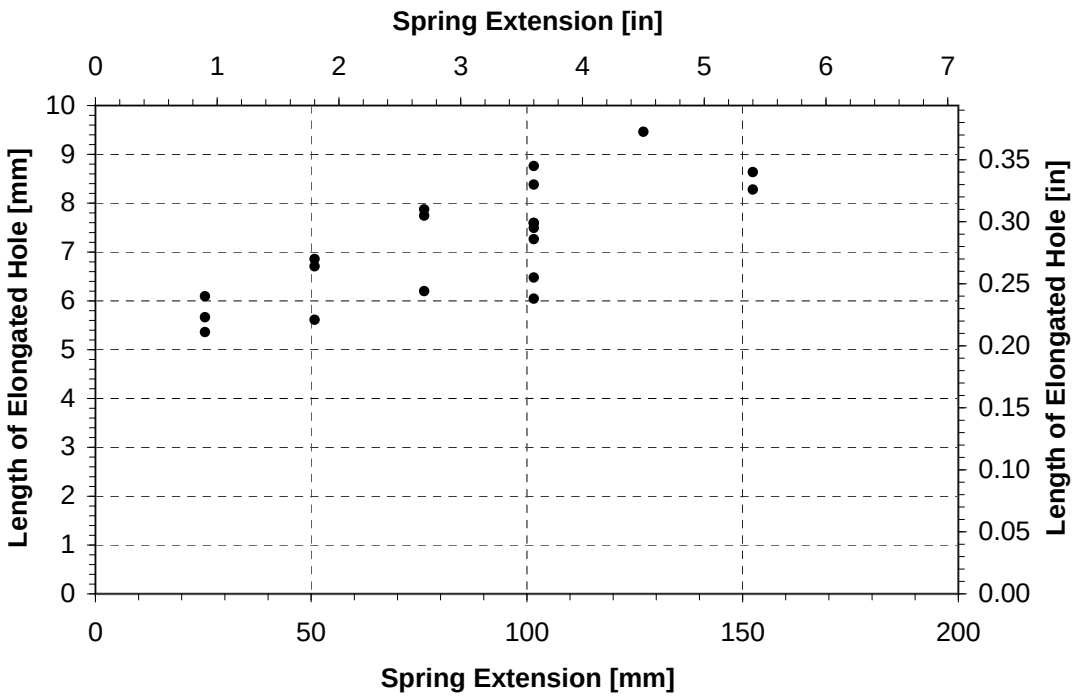

Figure 3.8: Continuous Trend Example from Component 1 - Pin-Loaded Hole Elongation vs. Spring Extension

3.2.3 Component Test Results

Results from the component tests included measurements of damage for each component and the corresponding amount of energy input. The amount of damage each component sustained relates to the amount of energy they absorbed. As an exception, one component did not incur damage but did absorb energy: the helical extension spring. The raw component test data can be found in Appendix A.1.

Two trends were noticed as a result of the component tests. One, the components that exhibit plastic deformation appear to deform continuously as energy input is increased, within the range of input energies used in the component tests. Two, the components that exhibit a non-continuous behavior do so at a given energy level and all energy levels above the given level. Below the energy level failure does not occur. This behavior leads to a non-continuous trend when the data is plotted. Examples of these trends can be seen in Fig. 3.8 and Fig. 3.9.

The spring is an exception to these trends. The spring does not exhibit either brittle failure or plastic deformation. However, the spring does absorb energy elastically.

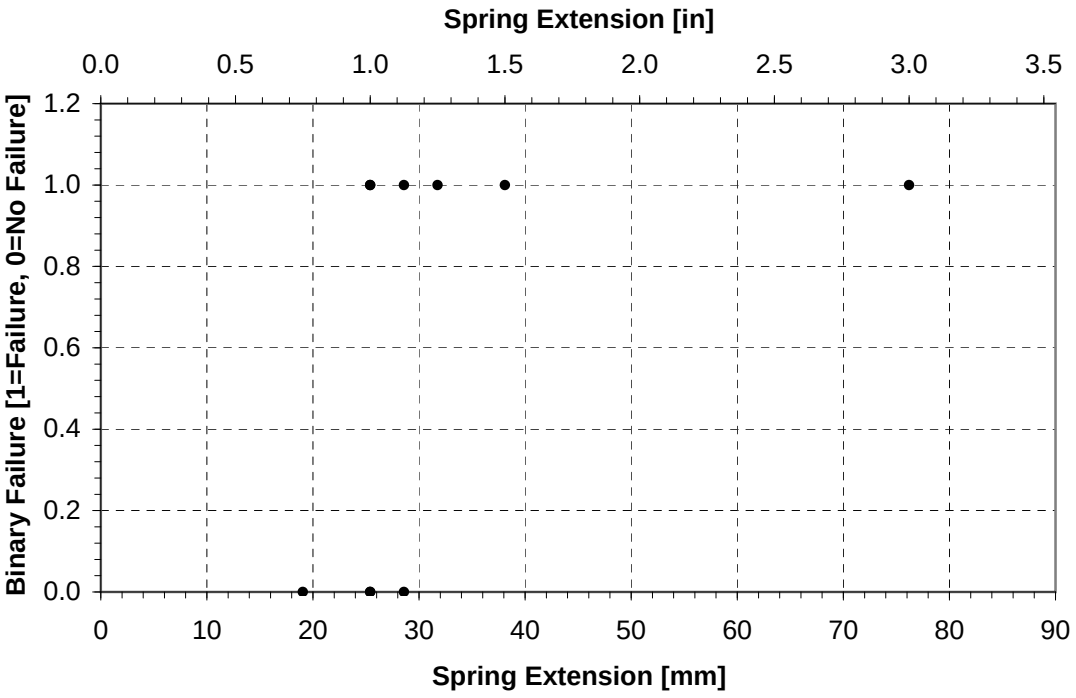

Figure 3.9: Non-Continuous Trend Example from Component 2 - Fracture State vs. Spring Extension

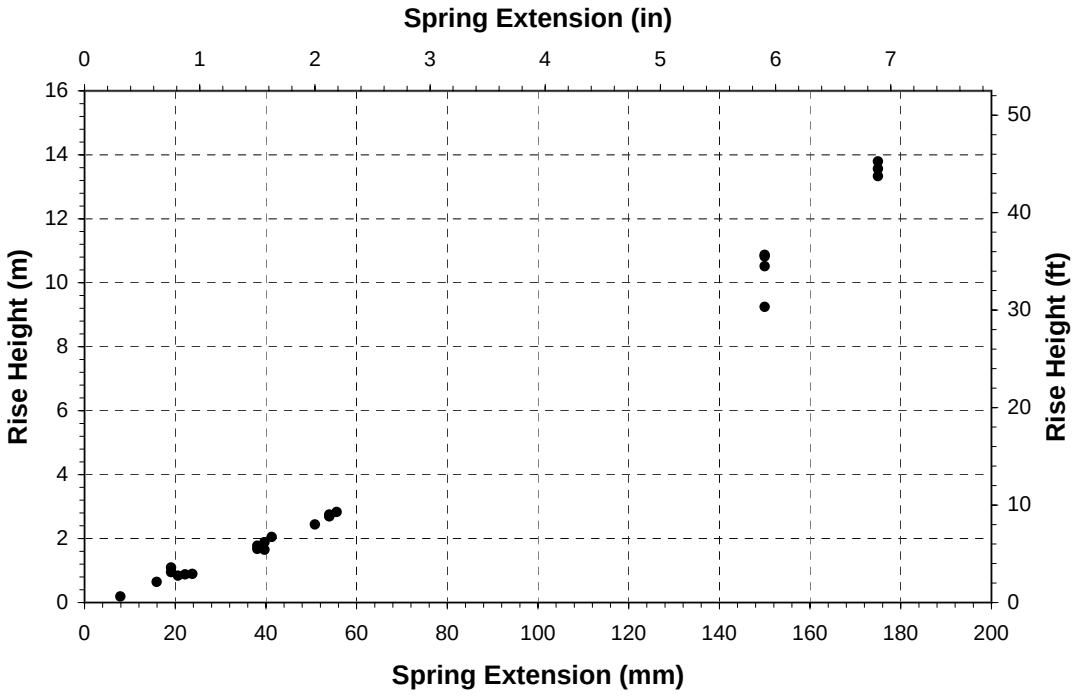

Figure 3.10: Results of Helical Extension Spring Component Test - Spring Travel Height vs. Spring Extension

This is of importance not only because the spring is a part of the system but because the spring was used to impart energy to the components in each of the component tests. For this reason Fig. 3.7 was used to determine the energy input to each component in the component tests. The results of the helical spring component test can be seen in Fig. 3.10.

The data obtained from both the system and component tests can now be used to create a model of the system and determine the energy absorption trends in the system.

Chapter 4

Modeling

As described in the previous section, component tests were conducted to help quantify the behavior of the components and subsystems observed in the system tests. The results of the component tests must be analyzed and models generated before they can be used in the system tests. These models are used to assign an energy absorption value to the component damage that was present in the system tests.

The quantification of the damage occurring in the system tests allows trends to be observed in the system tests. These trends can be displayed visually and conclusions about critical energy levels can be made. This chapter describes the models of the components and system, the process used to create them and the way in which the information was presented visually.

4.1 Component Modeling

Component models were created for each of the components tested. The models were created by analyzing the data obtained from the component tests. An equation relating the amount of energy absorbed to the amount of component damage is obtained. This results in models representing the energy absorption characteristics of the components under component test conditions.

The models discussed here are the simplified representations of the complex behavior of a system or component undergoing impact. They do not describe the variability of local material properties associated with high strain rates and they do not describe the complex material deformations seen in these tests. The models provide a sim-

plified manner in which to better understand the general trends of the components undergoing high strain rates and are based on exclusively on experiments.

4.1.1 Energy Absorption Assumptions for Modeling

The components tested absorbed energy through a number of different mechanisms, as discussed in Section 3.2.3. For the purposes of modeling the energy absorption of components, we group components into two different model types based on the state of the component after an impact event, with the exception of the Helical Extension Spring.

The first model type we call Continuous Models. As the name implies, the models result in continuous equations describing the behavior of the components. Components with this type of model generally absorb the majority of the energy transmitted to them through plastic deformation. We assume that the more energy absorbed by a component with a Continuous Model the more plastic deformation occurs to that component.

The second model type we call Non-Continuous Models. These models result in non-continuous equations. Components with this type of model generally absorb the majority of the energy transmitted to them as stress before failing catastrophically. We assume that a component with a Non-Continuous Model absorbs a certain amount of energy then fractures, stopping the absorption of energy.

These assumptions are used to describe the behavior of components as they plastically deform or experience a fracture that compromises the structure of the component. The helical extension spring is an exception to these assumptions and will be discussed in Section 4.1.4.1.

4.1.2 Continuous Models

The Continuous Models were created by relating the amount of damage done to each component and the amount of energy absorbed by that component. This relationship was found by performing a regression analysis on the data set from each component test in which the majority of energy was absorbed through plastic deformation.

The regression analysis consisted of a simple linear regression, which is commonly know as fitting a straight line to a data set. The simple linear regression model is

represented by the following equation [9]:

$$y_i = \beta_0 + \beta_1 x_i + \epsilon_i \tag{4.1}$$

The ϵ of each point is taken to be an error term derived from an error variance for the data set, σ^2. Using the method of least squares a line is fit to the data of the form:

$$y = \beta_0 + \beta_1 x \tag{4.2}$$

The regression analyses were performed with the help of a computer with sample results given in Fig. 4.1(a) and Fig. 4.1(b). Component 1 is used as a representative component and discussed below.

Figure 4.1(a) describes the change in length of a hole in Component 1 versus the energy input into Component 1. The material around the hole in Component 1, a sheet metal part, deformed plastically due to side loading from a pin inserted into the hole, see Fig. 3.3. The resulting equation, Eq. 4.3,

$$y = 0.0057x + 0.0337 \tag{4.3}$$

agrees with the first assumption concerning continuous components mentioned above: the more energy absorbed by a component the more deformation occurs.

An upper and lower confidence interval about the regression line were plotted in Fig. 4.1(a). They are used to give an idea of how close the regression line is to the true regression line for the current data set 95% of the time [10]. This means they only refer to the location of the regression line for this data set and do not indicate the response of future observations. The true regression line represents the true relationship between the amount of hole elongation and the amount of energy absorbed by the hole elongation. The confidence intervals in Fig. 4.1(a) are wider than desirable but this kind of variability in the observations is expected from large plastic deformations generated by an impact event.

The standardized residuals of the regression were plotted to ensure the simple linear regression was an appropriate fit for the data (see Fig. 4.1(b)). Residuals are the difference, or error, between the observed values of the dependent variable and the corresponding fitted values [9]. Standardized residuals are the quotient of this error and the error's standard deviation. The residuals in Fig. 4.1(b) are evenly distributed

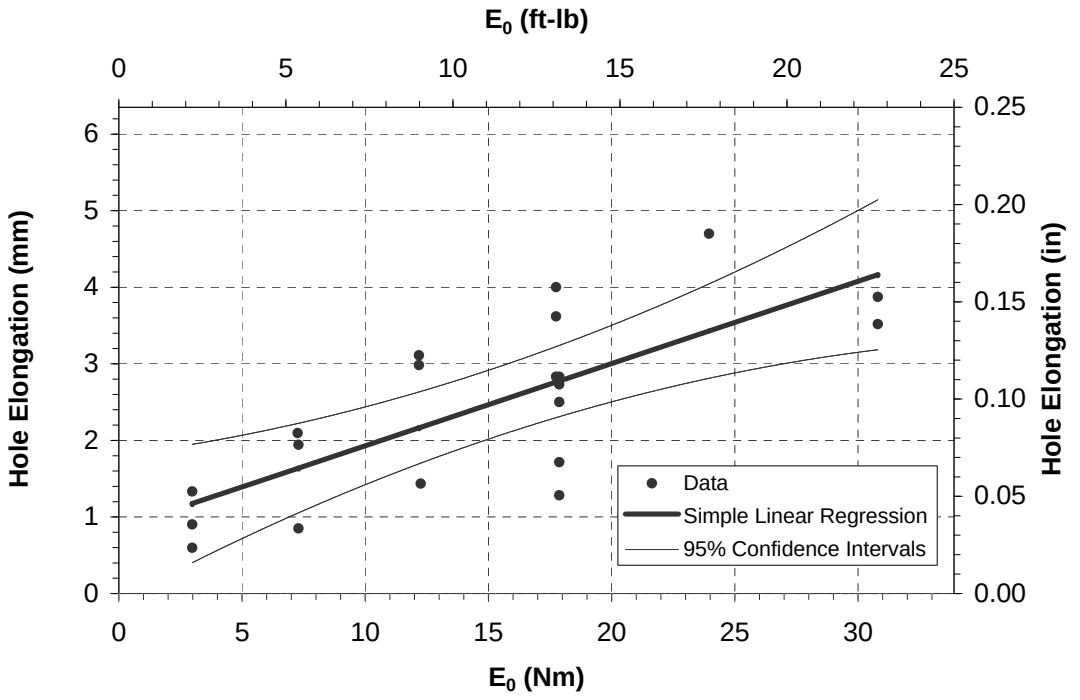

(a) Regression Analysis with Confidence Intervals

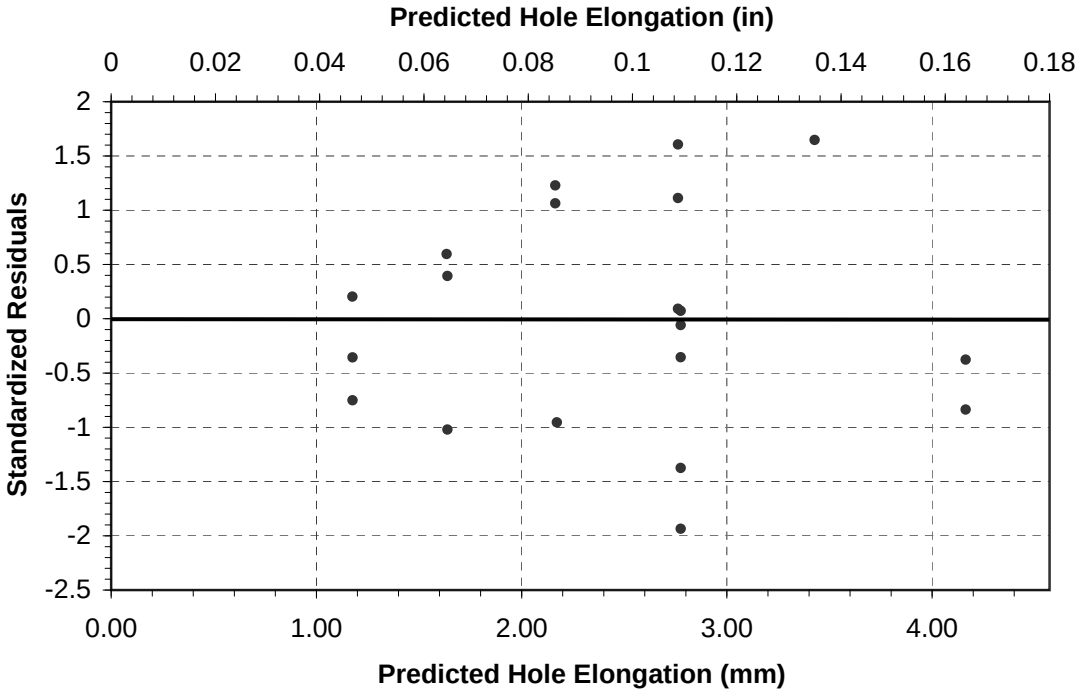

(b) Standardized Residuals from Regression Analysis

Figure 4.1: Model of Component 1

about 0, leading us to believe that the data is normally distributed about the regression line. This means that generally the simple linear regression is properly fit to the data.

From this analysis we now have a means to determine quantitatively how much energy was absorbed by Component 1 for a given deformation. This will be helpful later in analyzing the system tests. Similar analyses were conducted for Components 4, 5 and 7; the results can be found in Appendix A.2.

4.1.3 Non-Continuous Models

The Non-Continuous Models were created to mathematically describe the the non-continuous behavior of the test data taken for components 2, 3 and 6. The non-continuous behavior of these components was the result of different failure mechanisms. Component 2 and 6 failed due to brittle fracture while component 3 failed due to the total shearing of a tube. The tube shearing was believed to be caused by ductile fracture. The non-continuous model for Component 2 can be seen in Fig. 4.2.

The model seen in Fig. 4.2 describes the behavior of Component 2 during an impact event. Below 2.9 Nm (2.2 ft-lb) the energy absorbed by Component 2 is 0 Nm (0 ft-lbs). Above 2.9 Nm (2.2 ft-lb) the energy absorbed by Component 2 is 2.9 Nm (2.2 ft-lb).

From this model we now have a means to determine quantitatively how much energy was absorbed by Component 2 when it fractures during a system test. Similar analyses were conducted for Components 3 and 6; the results can be found in Appendix A.3.

4.1.4 Helical Extension Spring

As mentioned in previous sections, the helical extension spring stores a considerable amount of energy. When this energy is abruptly released, an impact event occurs in the system. The helical extension spring is unique among the system components because it absorbs energy but does not permanently deform. While other components in the system may have also absorbed small amounts of energy without deformation, the helical extension spring absorbs a large amount of energy. The model created to predict this energy absorption is discussed below.

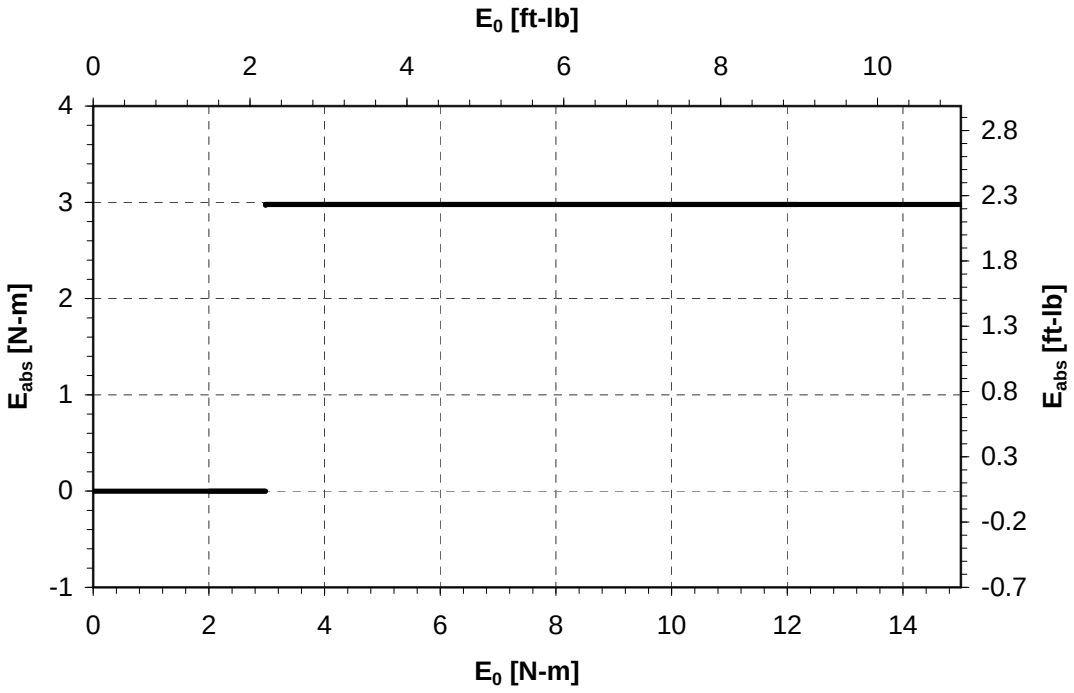

Figure 4.2: Graphical Representation of Component 2 Non-Continuous Model

4.1.4.1 Helical Extension Spring Model

The helical extension spring exhibited energy absorption behavior that was continuous and approximately linear. This can be seen in Fig. 4.3(a). The model shown in Fig. 4.3(a) was generated using the results of the Helical Extension Spring Component Test shown in Fig. 3.10.

Potential Energy In Spring, E_0, was calculated using Eq. 2.3 given in Section 2.3. The energy absorbed by spring coil impact, E_{abs}, was found using the maximum height of the spring and the initial potential energy corresponding to the maximum height, see Eq. 4.4.

$$E_{abs} = E_0 - E_{avail} \tag{4.4}$$

The Available Spring Energy, E_{avail}, was found using Eq. 4.5.

$$E_{avail} = m * g * h \tag{4.5}$$

The model shown in Fig. 4.3(a) was created using a linear regression, the same method utilized in Subsection 4.1.2. The lack of a random distribution of residuals suggests

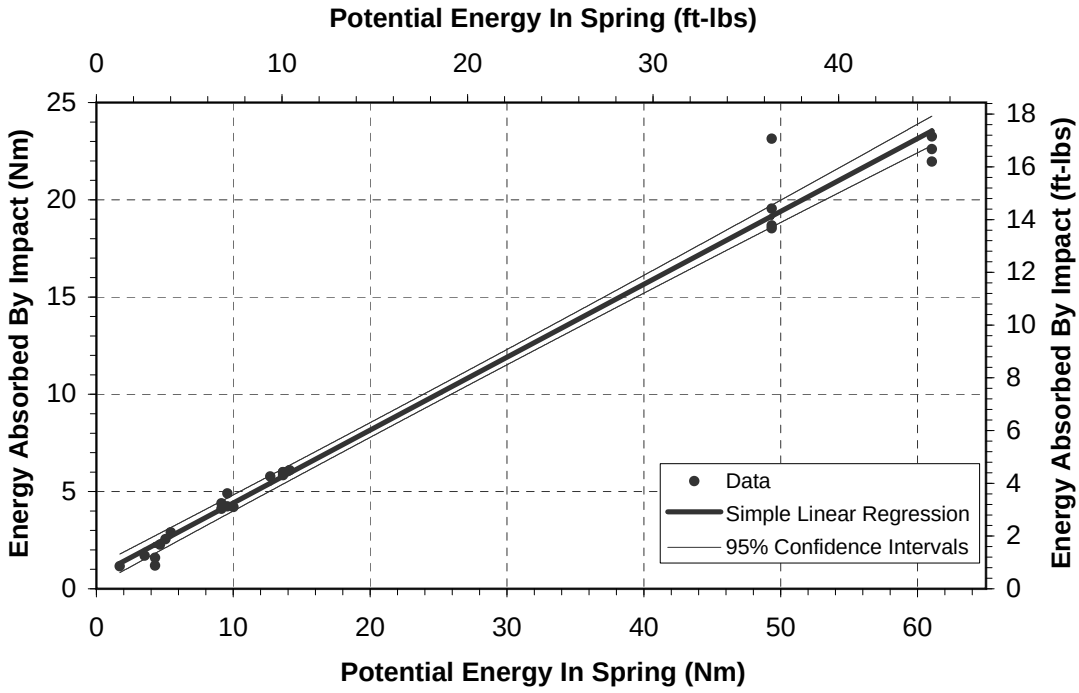

(a) Regression Analysis with Confidence Intervals

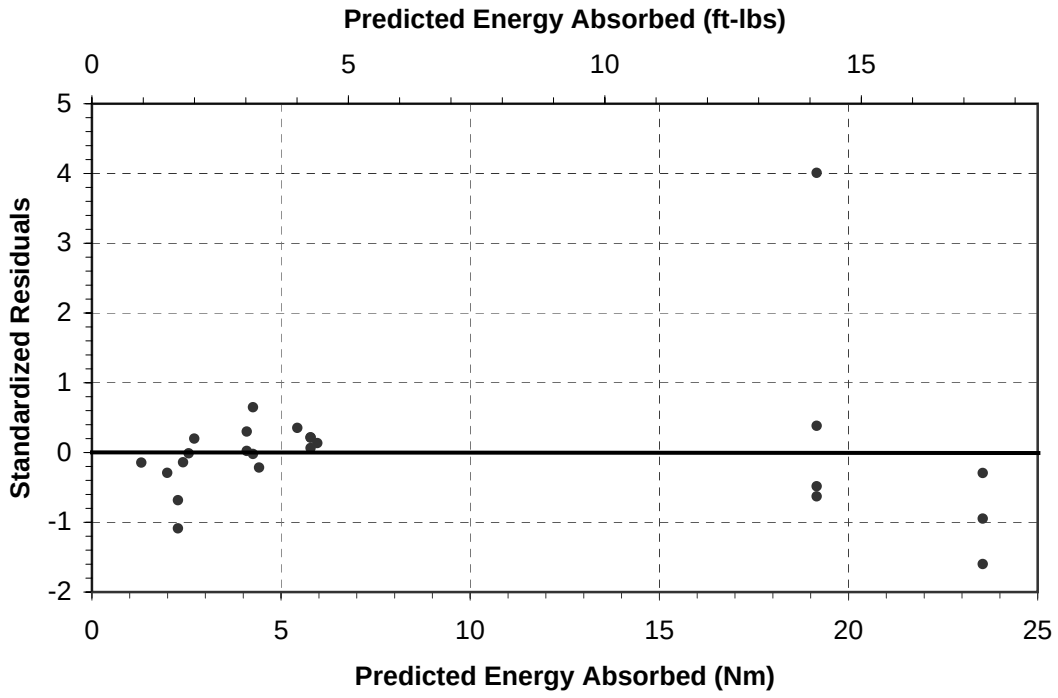

(b) Standardized Residuals from Regression Analysis

Figure 4.3: Model of Helical Extension Spring

that a linear approximation may not be the most ideal fit of this data. For the purposes of this research we will assume the linear approximation is sufficient.

This model shows that when the Helical Extension Spring is suddenly released in a system test, some of the energy stored in its coils is absorbed before the remainder is transfered to the rest of the system. Further investigation of this phenomenon was performed using a variety of different springs and detailed in Meyer [11]. A summary and further analysis of data from this investigation is given in the next section.

4.1.4.2 Energy Absorption in Helical Extension Springs

In Meyer [11] the energy absorption characteristics of three different helical extension springs (Springs S, M and H) was experimentally determined, a comparison of these characteristics was made and similarities discussed. A computer model of a generic spring was also created to predict the energy absorption of a spring with a given set of characteristics.

One of the springs discussed in Meyer, Spring H, was the helical extension spring found in the system described in Chapter 2. For this reason the data obtained in Meyer 2006 will be reexamined here to see if further interpretations of the data can be made.

The three springs selected for study in Meyer, Springs S, M and H, have three different Spring Constants, k [N/m (lb/in)]: 291.3(1.66), 1481.5(8.46) and 1587.3(9.06) respectively. The three different sizes of springs were used to represent a range of helical extension spring sizes. Each spring was found to absorb some percentage of the potential energy stored in its coils when released and allowed to contract freely. This energy absorption was displayed in a number of ways including as the percent of energy absorbed by spring coils during impact versus the amount of potential energy stored in the spring coils before release.

The energy absorption characteristics of the three springs in Meyer were obtained using two types of tests. The first method used was Free Flight experiments, which we described above in Section 3.2 and called the Helical Extension Spring Component Test. The second method used was Accelerometer Experiments, which involved instrumenting the springs with accelerometers and performing a test similar to the Free Flight Experiments but with lower initial potential energy levels.

4.1.4.2.1 Free Flight Experiments The data obtained by Meyer for Spring H, the Helical Extension Spring, using the free flight experiments is given in this section. Three models of each experiment and the corresponding residuals are given along with a brief description. Models for data obtained using spring S and M are given in the Appendix, Section A.4.1.

The three models used to evaluate the data obtained by Meyer are: Final Potential Energy vs. Initial Potential Energy, Percent Energy Absorbed vs. Initial Potential Energy and Energy Absorbed vs. Initial Potential Energy. The models were created to help understand how much of the springs' own energy is being absorbed and compare the energy absorption between spring sizes. The first two models were used by Meyer and are presented here with measurement errors and an evaluation of the regression fit, the plotting of residuals, for clarity. The third model is presented as a new way to look at the data: it compares the amount of energy absorbed to the amount of energy stored in the spring. Each model is discussed in order below.

The data and model given in Fig. 4.4 relates the kinetic energy remaining, after contraction, in Spring H to the initial potential energy stored in Spring H for a number of spring extensions. Error bars are included to provide an indication of the measurement error for both the independent and dependent variable.[1] A simple linear regression was used to model this relationship, Fig. 4.4(a). Based on the residuals given in Fig. 4.4(b) the linear model is not ideal, as the distribution is not entirely random, but will represent the relationship adequately. The model shows us that as initial potential energy increases the amount of kinetic energy remaining after contraction also increases.

The data and model given in Fig. 4.5 relates the percentage of energy absorbed by Spring H during contraction to the initial potential energy stored in Spring H for a number of spring extensions. Error bars are included to provide an indication of the measurement error for both the independent and dependent variable. A simple linear regression was used to model this relationship, Fig. 4.5(a). The residuals in Fig. 4.5(b) appear to be randomly distributed about zero given the data selection of initial potential energies. Based on this, the model seems adequate. The model shows us that as initial potential energy increases, the percent of energy absorbed

[1]Horizontal error bars are shown to clarify that measurement error occurred in the independent variable. The amount of initial potential energy stored in the springs before release was imparted by extending the springs a given amount. The amount of extension was variable for a given energy level because of error in the measurement device used to measure extension.

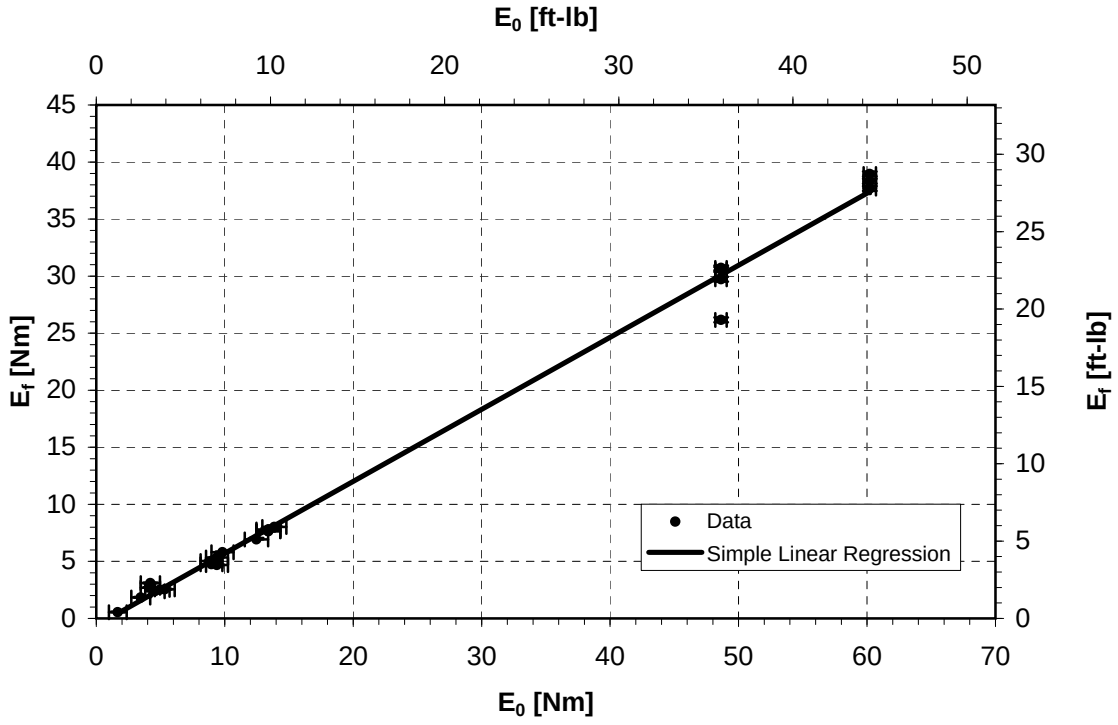

(a) Simple Linear Regression with Error Bars

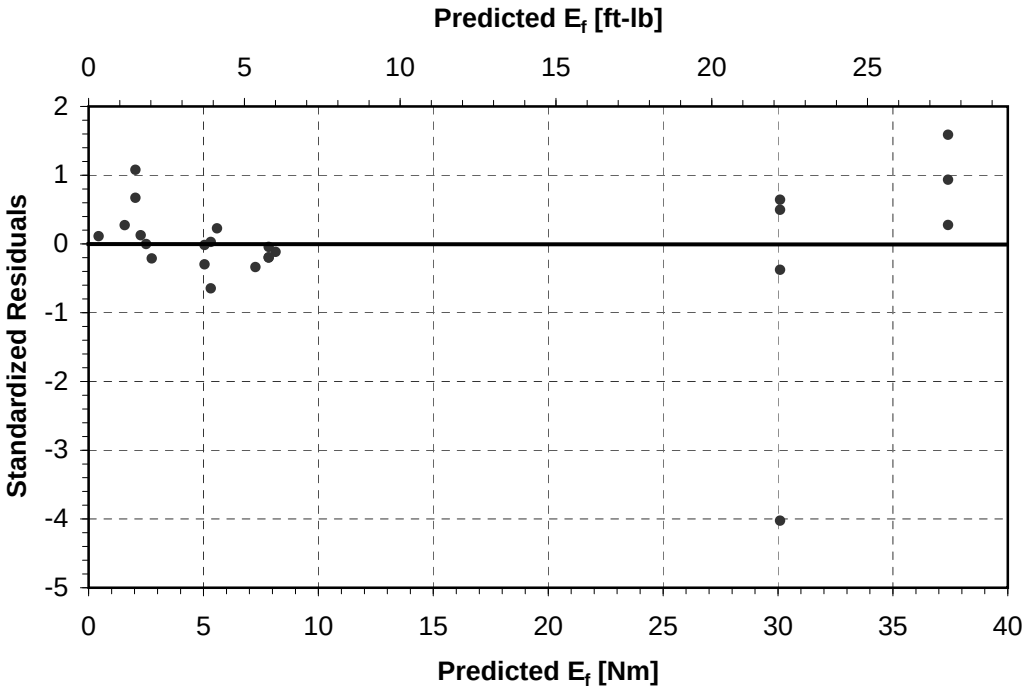

(b) Standardized Residuals from Regression Analysis

Figure 4.4: Final Kinetic Energy vs Initial Potential Energy, Spring H, Free Flight Experiments

during contraction decreases. It should be noted that the measurement error of the percent of energy absorbed increases at low initial potential energies. This makes us less certain of the inversely proportional relationship given in the above model.

If we plot the energy absorbed by contraction versus the initial potential energy of Spring H, we obtain a model in units that can be easily compared to Springs S and M. This relationship can be seen in Figure 4.6. Error bars are included to provide an indication of the measurement error for both the independent and dependent variable. A simple linear regression was used to model this relationship, Fig. 4.6(a). The residuals given in Fig. 4.6(b) appear similar to those found in Fig. 4.4, making the model adequate for our purposes. The small amount of measurement error also reaffirms that the model is adequate.

When energy absorbed vs. initial potential energy is compared for all three springs, similarities in energy absorption can be observed (see Fig. 4.7). Each of the three springs absorbs energy in a similar manner with models that have similar slopes. At the scale shown in Fig. 4.7(a), only Spring H and Spring M are visible. The relatively small energies stored by Spring S are too small to be seen in this figure. Figure 4.7(b) is plotted on a log-log scale; a log-log scale was used for its ability to compress points of lower values. This allows the small energies stored by Spring S to be compared to the much higher energies stored by Springs H and M. Since the y-intercept of these data sets is theoretically zero they continue to appear linear on the log-log plot and allow a qualitative comparison of all three springs.

Given three energy absorption relationships for three example springs, a theoretical relationship for all helical extension springs may be postulated. Assuming the data sets for all three springs are from the same population, combining them and performing a simple linear regression on the resulting combined data set yields Fig. 4.8. Looking closely at Fig. 4.8 we see that the linear regression is a good fit for both Spring M and Spring H, falling within the error bars for each of their respective data sets. However, the linear regression does not appear to be as good a fit for Spring S as it does not fall within the error bars of its data set. The linear regression does come within 0.1 Nm (14.2 in-lb) of the data set.

Prediction intervals for the data set are also plotted. This allows us to predict the response for future observations. Taking this into account we can say for a given helical extension spring with a given initial potential energy in *Joules* it is possible to

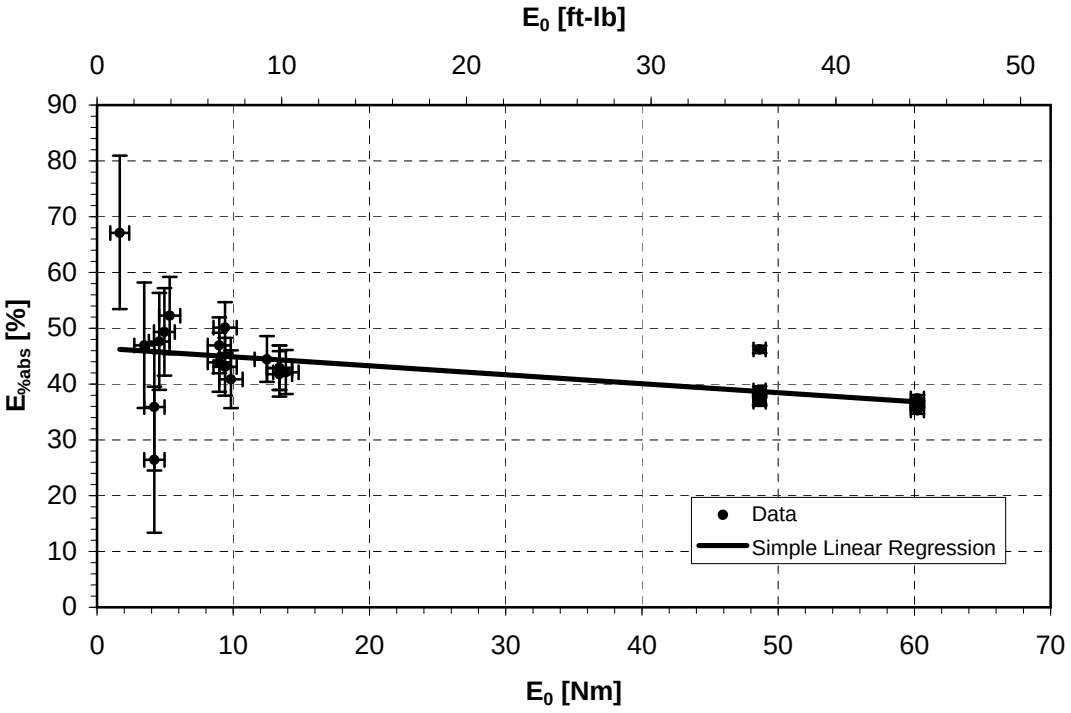

(a) Simple Linear Regression with Error Bars

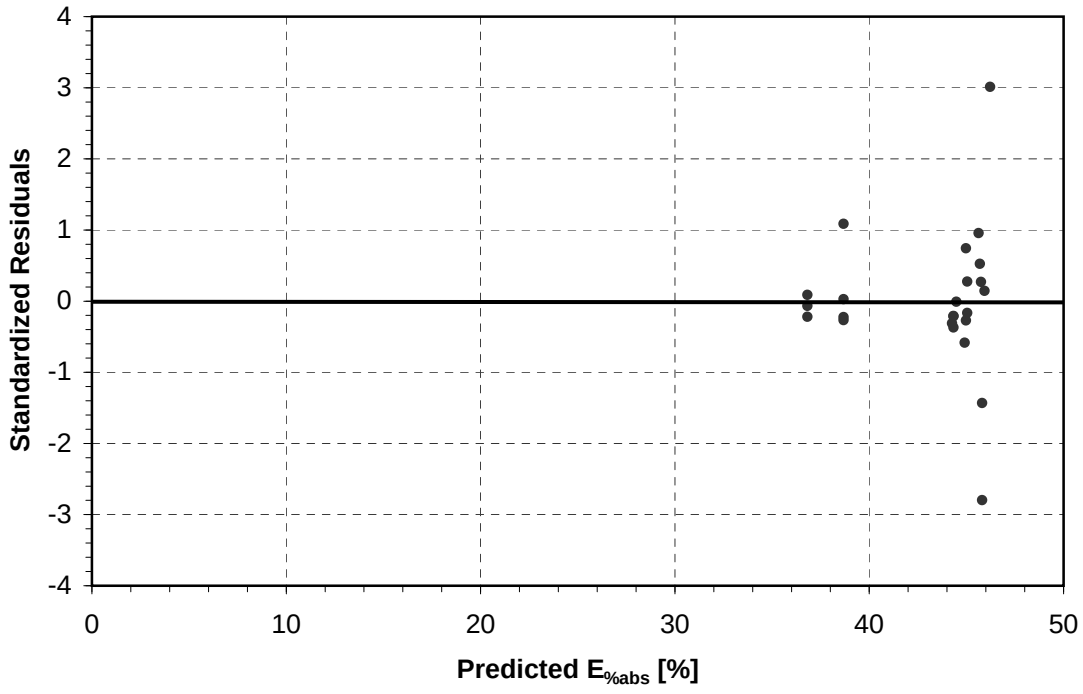

(b) Standardized Residuals from Regression Analysis

Figure 4.5: Percent Energy Absorbed vs Initial Potential Energy, Spring H, Free Flight Experiments

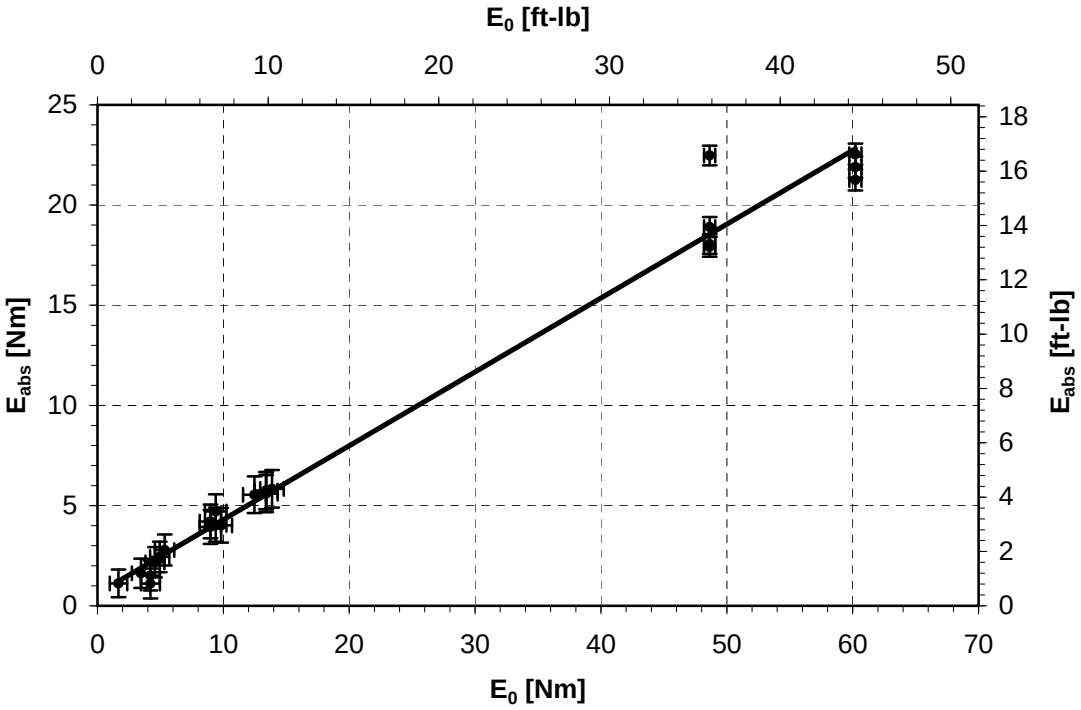

(a) Simple Linear Regression with Error Bars

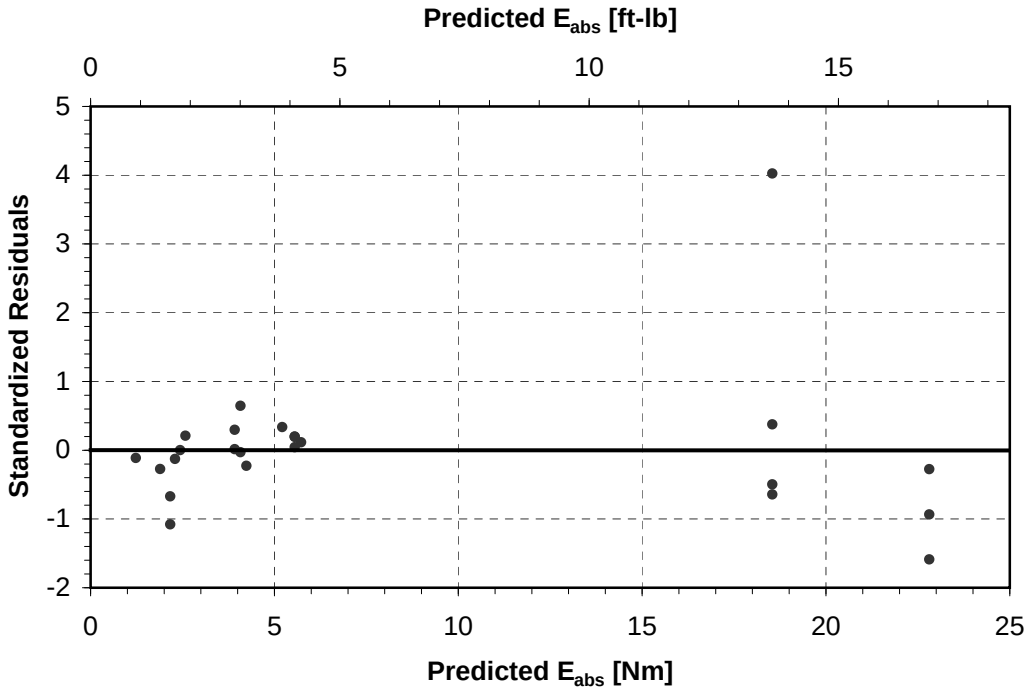

(b) Standardized Residuals from Regression Analysis

Figure 4.6: Energy Absorbed vs Initial Potential Energy, Spring H, Free Flight Experiments

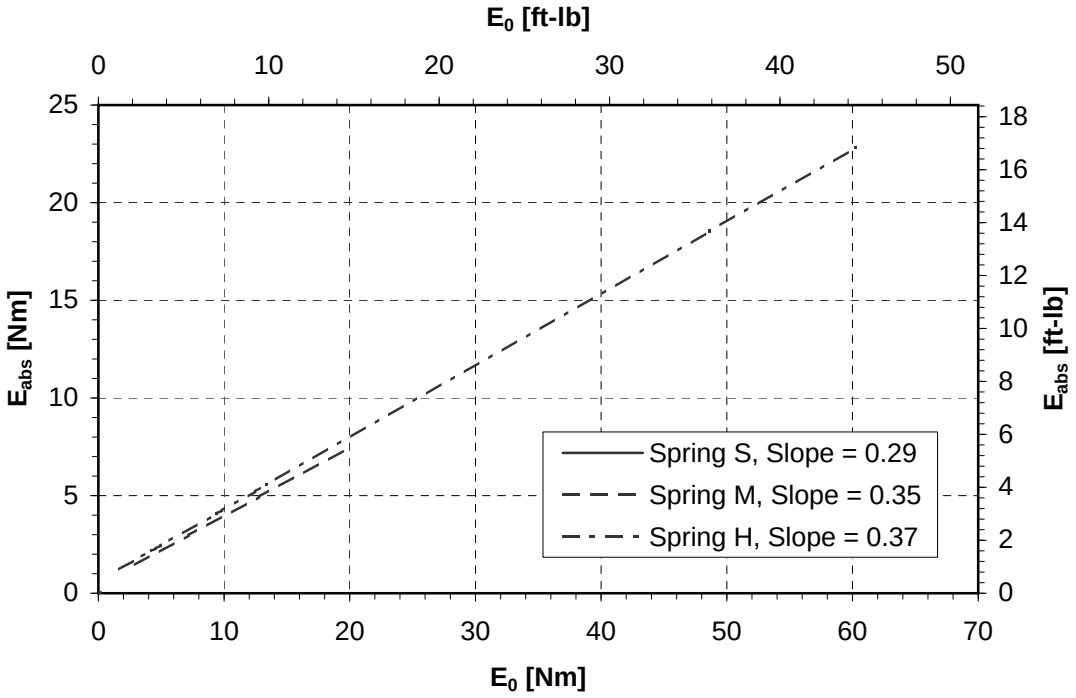

(a) Simple Linear Regressions of Spring S, M, and H

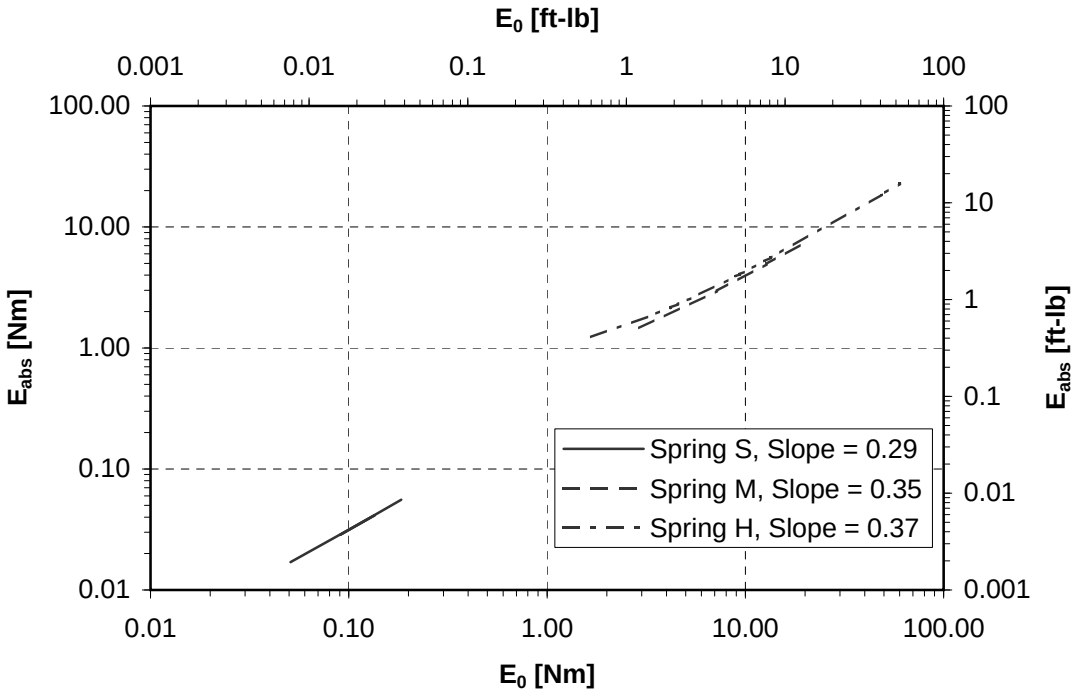

(b) Simple Linear Regressions of Spring S, M, and H plotted on Log-Log Axes

Figure 4.7: Energy Absorbed by Spring Coil Impact vs. Initial Potential Energy, Free Flight Experiments

estimate the mean energy it will absorb, within the prediction interval, using Eq. 4.6.

$$E_{abs} = 0.38E_0 + 0.22 \tag{4.6}$$

Four observations can be made about the data from the free flight experiments. First, using energy absorbed instead of percent energy absorbed to compare the energy absorption characteristics of different springs yields a more straight forward comparison, as seen in Fig. 4.7. Second, the slope of each linear model decreases as the spring constant of each spring decreases. Third, the slope of each linear model is less than one; therefore, the majority of energy stored in the helical extension springs tested was not absorbed when the spring was released. Fourth, a prediction of energy absorption can be made for helical extension springs with a certain initial potential energy given by Eq. 4.6.

4.1.4.2.2 Accelerometer Experiments The data obtained by Meyer for Spring H, the Helical Extension Spring, using the accelerometer experiments is given in this section. Three models of each experiment and the corresponding residuals is given along with a brief description. Models for data obtained using spring S and M are given in the Appendix, Section A.4.2.

Similar to the Free Flight Models, three models are used to evaluate the Accelerometer data obtained by Meyer: Final Potential Energy vs. Initial Potential Energy, Percent Energy Absorbed vs. Initial Potential Energy and Energy Absorbed vs. Initial Potential Energy. The models were created to help understand how much of the springs' own energy is being absorbed and compare the energy absorption between spring sizes. The first two models were used by Meyer and are presented here with measurement errors and an evaluation of the regression fit, the plotting of residuals, for clarity. The third model in presented as a new way look at the data: it compares the amount of energy absorbed to the amount of energy stored in the spring. Each model is discussed in order below.

The data and model given in Fig. 4.9 relates the kinetic energy remaining in Spring H after contraction to the initial potential energy stored in Spring H for a number of spring extensions. Error bars are included to provide an indication of the measurement error for both the independent and dependent variable. A simple linear regression was used to model this relationship (see Fig. 4.9(a)). Based on the ran-

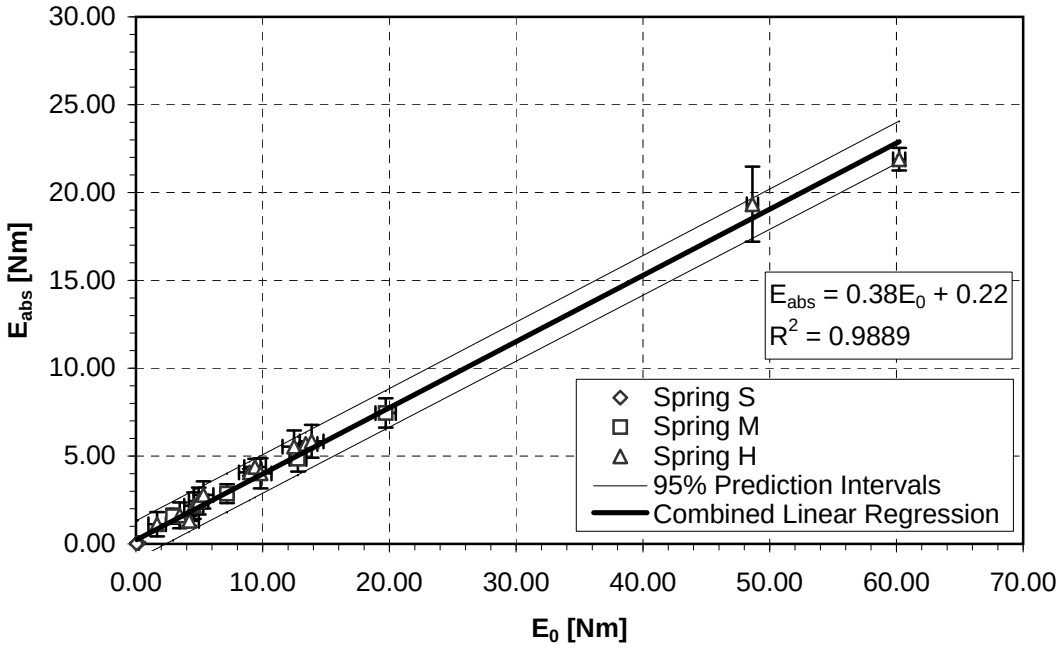

(a) Simple Linear Regressions of Combined Data Set from Springs S, M, and H

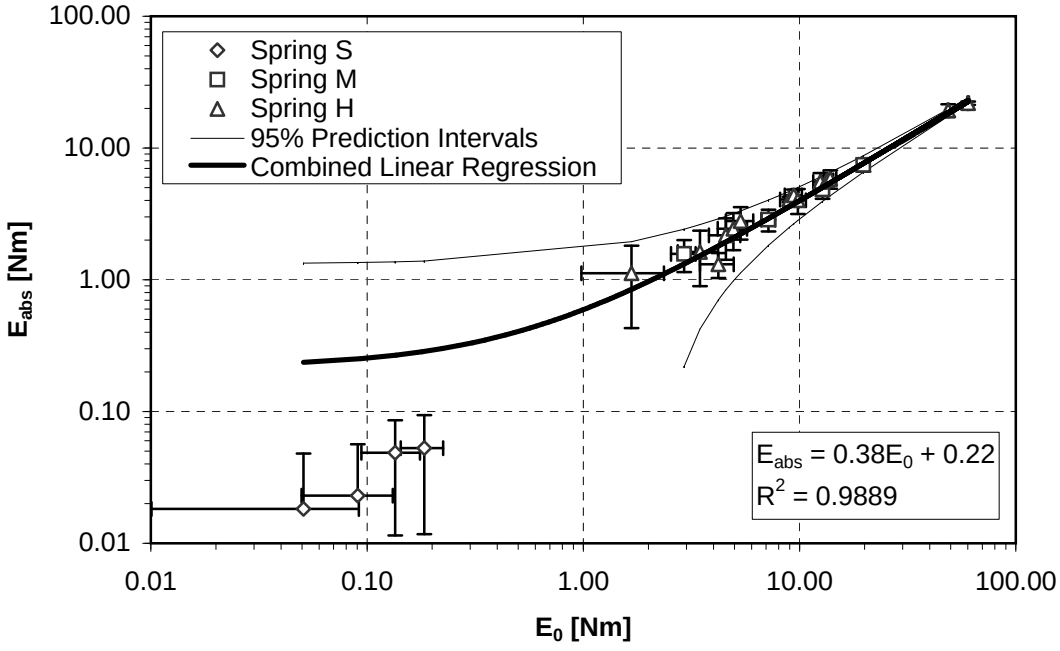

(b) Simple Linear Regression of Combined Data Set from Springs S, M, and H plotted on Log-Log Axes

Figure 4.8: Energy Absorbed by Spring Coil Impact vs. Initial Potential Energy, Combined Free Flight Experiments

domly distributed residuals given in Fig. 4.9(b), the linear model is a good approximation of the data. The model shows us that as initial potential energy increases, the amount of kinetic energy remaining after contraction also increases, even at small initial energies.

The data and model given in Fig. 4.10 relates the percentage of energy absorbed by Spring H during contraction to the initial potential energy stored in Spring H for a number of spring extensions. Error bars are included to provide an indication of the measurement error for both the independent and dependent variable. A simple linear regression was used to model this relationship (see Fig. 4.10(a)). The residuals given in Fig. 4.10(b) appear to be randomly distributed. Based on this, the model seems like a good approximation of the data. The model shows us that as initial potential energy increases, the percent of energy absorbed during contraction decreases.

If we plot the energy absorbed by contraction versus the initial potential energy of Spring H, we obtain a model in units that can be easily compared to Springs S and M. This relationship can be seen in Fig. 4.11. Error bars are included to provide an indication of the measurement error for both the independent and dependent variable. A simple linear regression was used to model this relationship (see Fig. 4.11(a)). The residuals given in Fig. 4.11(b) appear to be normally distributed. Therefore, the use of a simple linear regression yields adequate approximation of the data.

When energy absorbed vs. initial potential energy is again compared for all three springs, similarities in energy absorption can be observed (see Fig. 4.12). Each of the three springs absorbs energy in a similar manner with models that have similar slopes. A linear regression of the combined data sets for the Accelerometer Experiments was not performed because of the low energies used in the experiments.

Two observations can be made about the data from the accelerometer experiments. First, the slopes of each linear model decrease as the spring constant of each spring increases, which is different than in the free flight experiments. The difference may be due to the added mass of the accelerometers attached to the springs. Alternatively, the difference might be attributed to testing the springs using small extensions. Some helical extension springs exhibit a nonlinear region at small extensions, as can be seen in Fig. 2.5 for Spring H. Second, the slope of each linear model is less than one; therefore, the majority of energy stored in the helical extension springs tested was not absorbed when the spring was released.

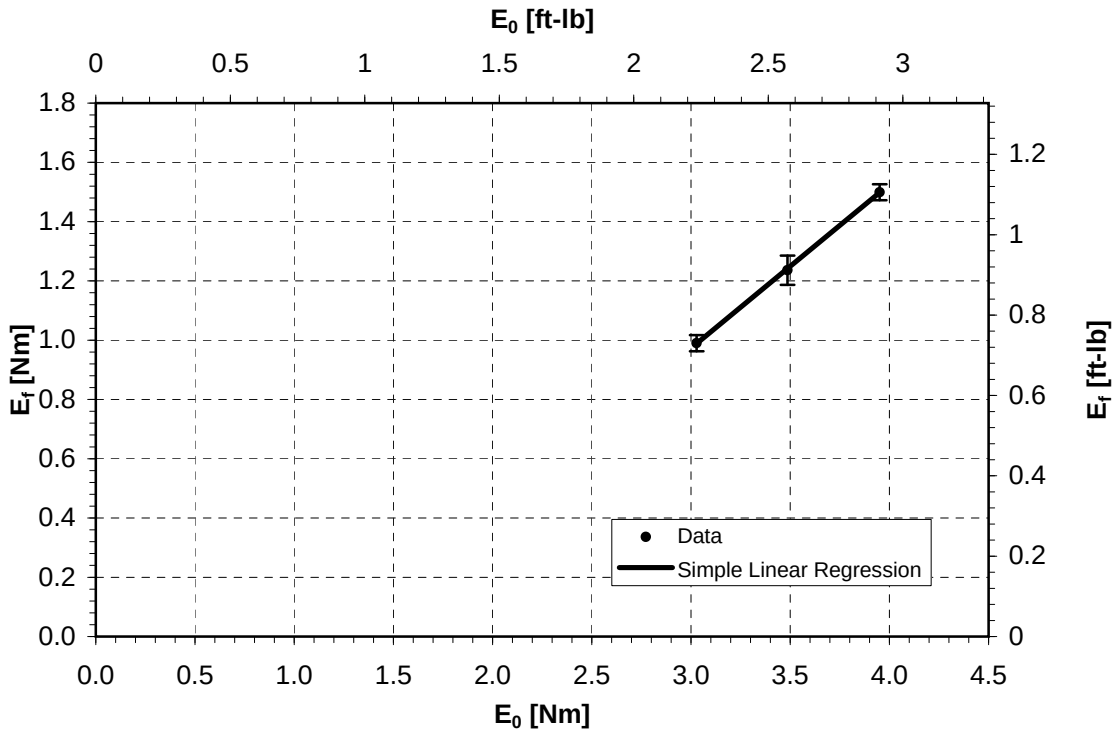

(a) Simple Linear Regression with Error Bars

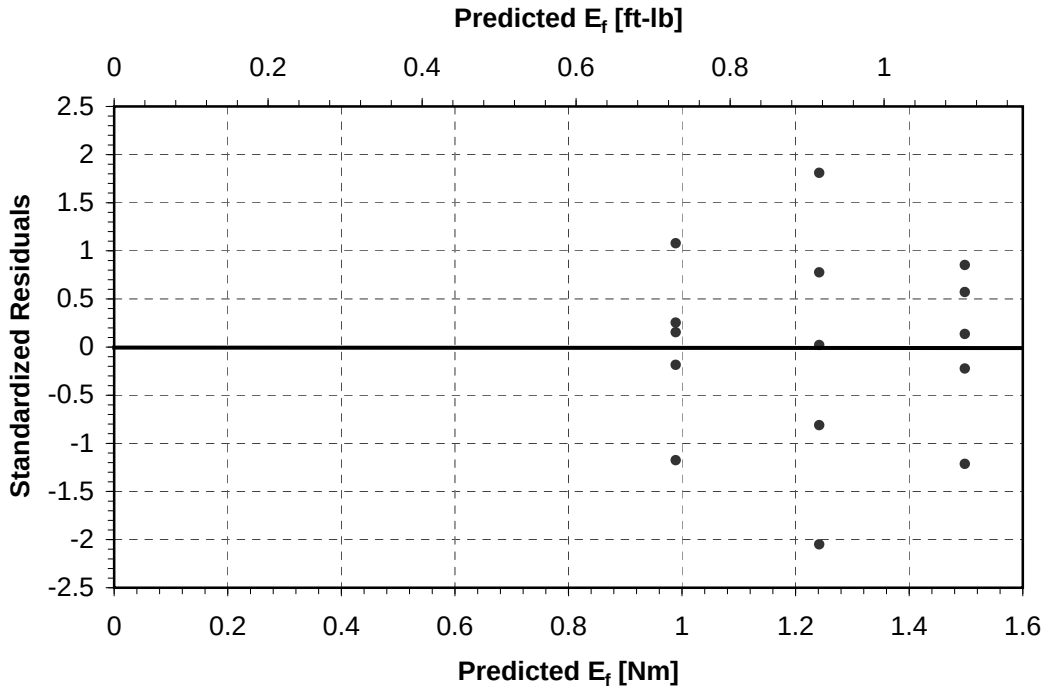

(b) Standardized Residuals from Regression Analysis

Figure 4.9: Final Kinetic Energy vs Initial Potential Energy, Spring H, Accelerometer Experiments

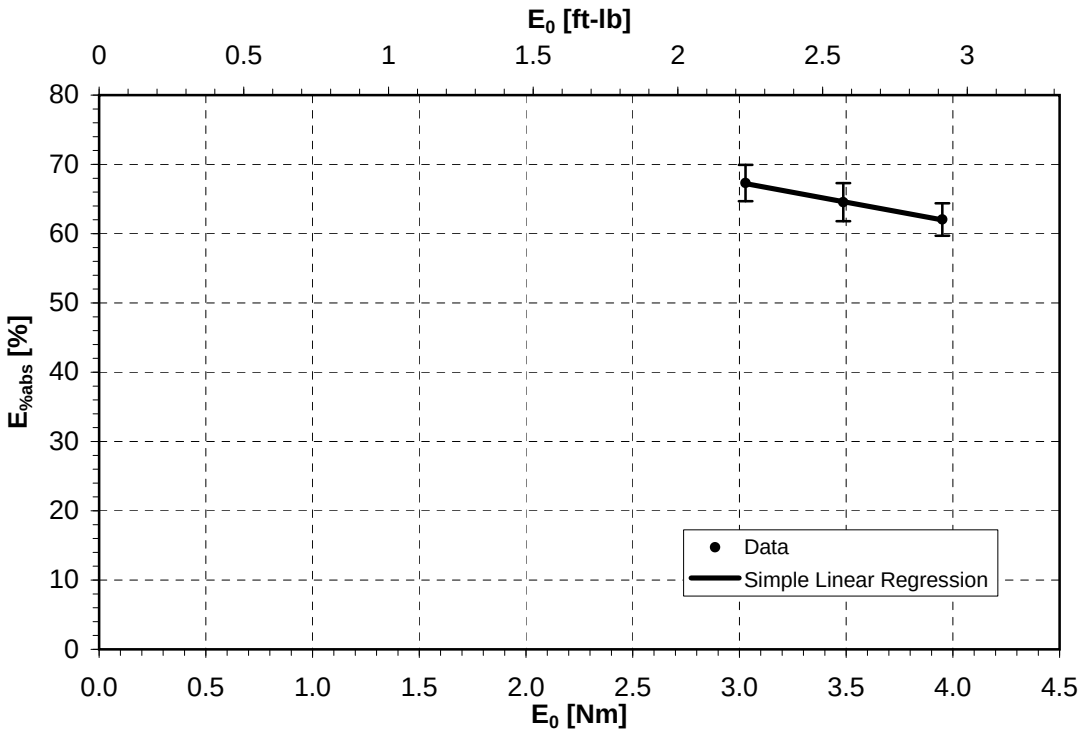

(a) Simple Linear Regression with Error Bars

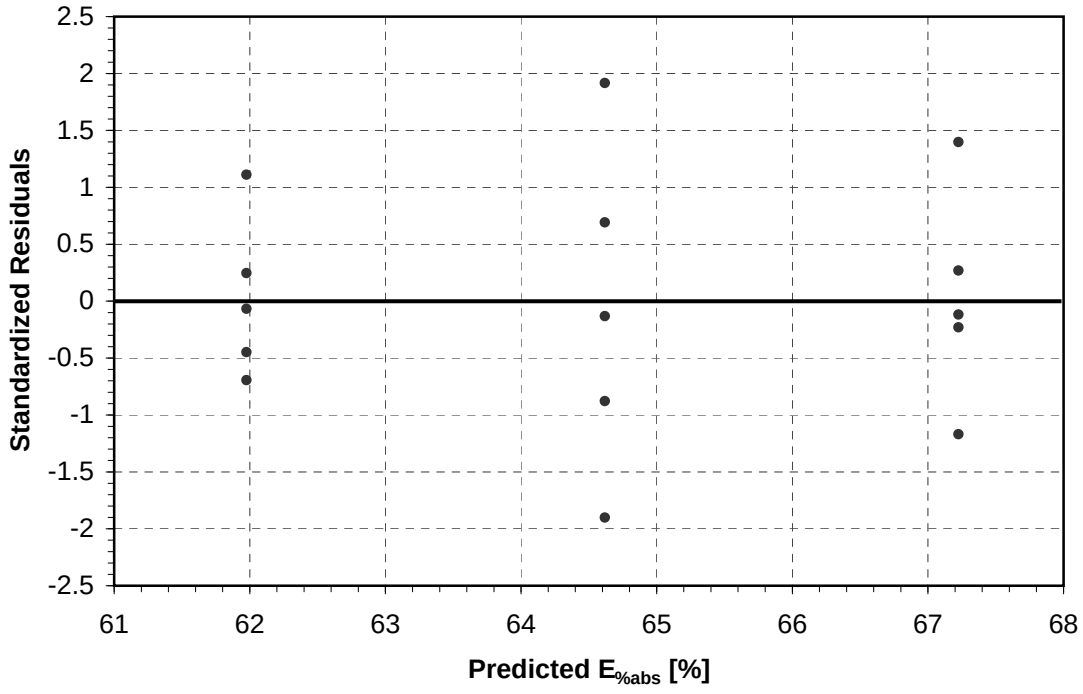

(b) Standardized Residuals from Regression Analysis

Figure 4.10: Percent Energy Absorbed vs Initial Potential Energy, Spring H, Accelerometer Experiments

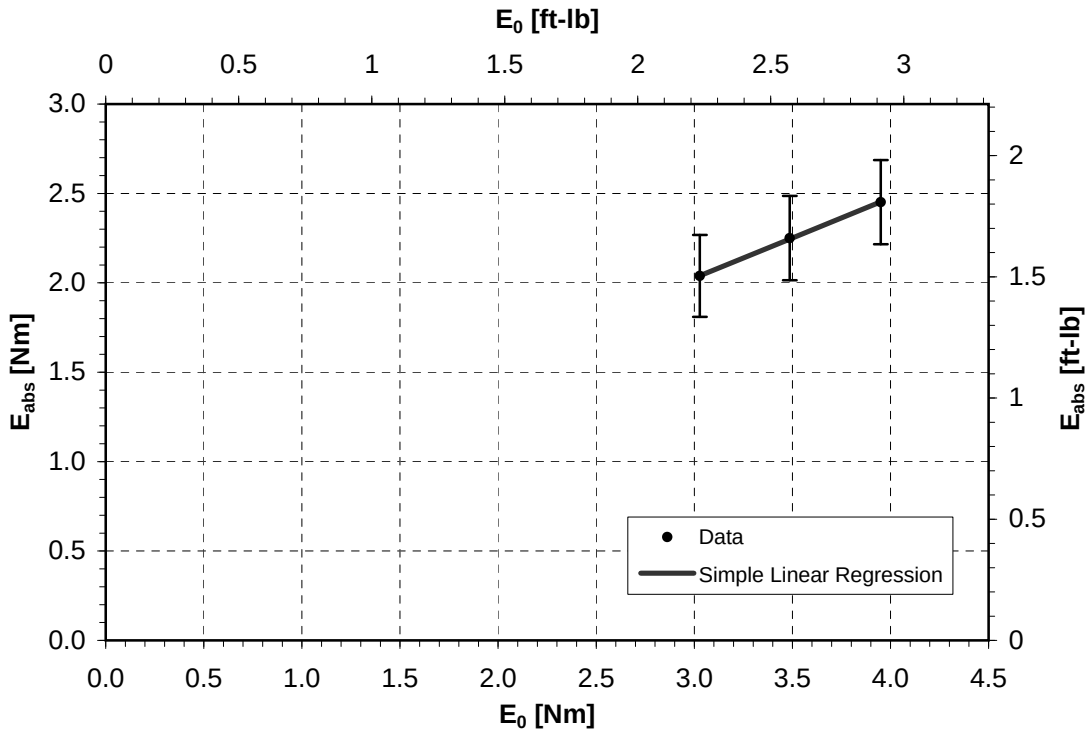

(a) Simple Linear Regression with Error Bars

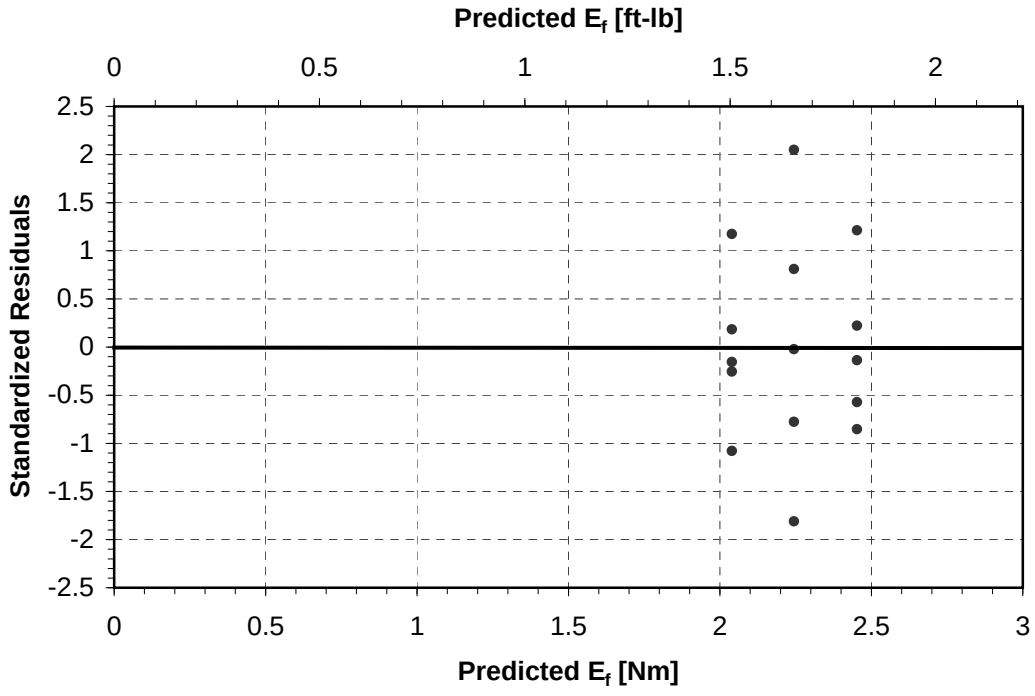

(b) Standardized Residuals from Regression Analysis

Figure 4.11: Energy Absorbed vs Initial Potential Energy, Spring H, Accelerometer Experiments

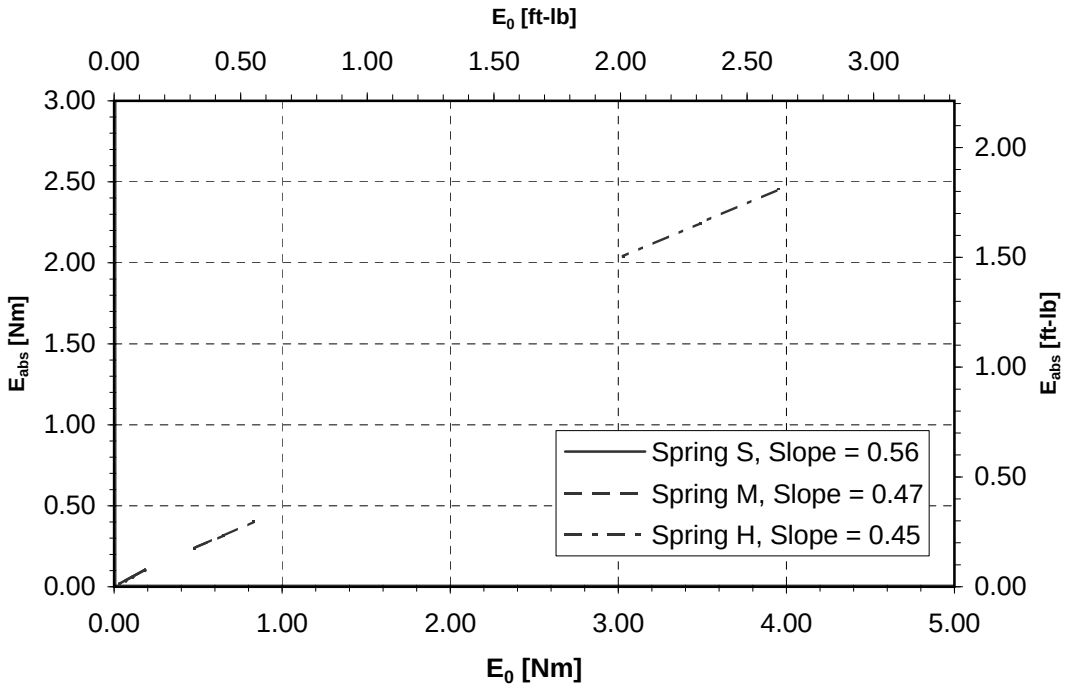

Figure 4.12: Linear Regressions of the Energy Absorbed by Spring Coil Impact vs. the Energy Stored in Spring S, M and H from Accelerometer Experiments

It is important to note that the three springs did behave similarly with respect to each other in both the free flight experiments and the accelerometer experiments. Each spring absorbs energy at a relatively similar rate given an increase in initial potential energy. This occurred consistently when testing springs with a wide range of spring constants.

4.1.5 Component Model and System Test Integration

We have created models for each component that was deemed to absorb a significant amount of energy in the system tests. These models can now be used inversely to determine the amount of energy each component absorbed in the system tests. This can be accomplished by measuring the amount of continuous or non-continuous damage sustained by each component in a particular system test. Inputing the damage values into the component models after undergoing inverse prediction will tell us how much of the energy input into a particular system test was distributed to each of the system's components.

Inverse prediction, also know as calibration [12], is accomplished by creating a regression of the data in question. A linear regression was made for each of the continuous component models discussed in the previous sections, similar to Eq. 4.2. These linear regressions were then inverted as detailed in Graybill [13]. The resulting equation gives the independent variable in terms of the dependent, see Eq. 4.7.

$$x = \frac{y - \beta_1}{\beta_0} \tag{4.7}$$

This new inverse equation is used in the system models, as seen in the following section.

4.2 System Model

System models were created for each of the four assemblies tested, AAB1, AAB2, AAB3 and AAB4. The models were created by analyzing the data obtained from the system tests. System wide comparison plots of the energy absorption of each component are obtained. Models relating the amount of energy absorbed by the system to the amount of energy stored in the helical extension spring are obtained.

The models discussed here are the simplified representations of the complex behavior of the system undergoing an impact event. They allow a better understanding of

the energies involved and potentially absorbed after an impact event occurs in the system.

4.2.1 Component Contributions to Energy Absorption of Subsystems

This section describes the role each system component plays in the overall energy absorption of the system. Using the data and analyses conducted in previous sections, we now gain an understanding of how much of the initial energy stored in the helical extension spring was absorbed by each of the components in the system. This system component data is plotted cumulatively along with the initial input energy.

Using the component damage data obtained from the system tests, Sec. 3.1, and combining it with the inverse component model equations, Sec. 4.1.5, we can now compute a theoretical energy absorption breakdown for each component in the system. Figures 4.13, 4.14, 4.15, and 4.16 show this breakdown for each of the assemblies tested.

In assembly AAB1, Fig. 4.13, components 1, 6, and 11 are the major energy absorbers. The theoretical energy absorbed levels are for the most part higher than the energy input levels. Since it is not possible to absorb more energy than that which is input, this means that we are predicting too great an energy absorption in one or all of the components. Based on the output of the inverse component models, it would appear that the inverse component models for component 11 and component 1 may be over estimating the amount of energy absorbed. This is most likely the case because a large amount of forward extrapolation occurred when the inverse models are used with the system test data. During the system tests component 11 experienced deformation ranging from .3 mm to 10.2 mm (.12 in to .40 in) while the component tests for component 11 were conducted with energy levels resulting in deformation between 3.8 mm to 5.8 mm (.15 in and .23 in). During the system tests component 1 experienced deformation ranging from .8 mm to 6.4 mm (.03 in to .25 in) while the component tests for component 1 were conducted with energy levels resulting in deformation between 1.3 mm to 4.8 mm (.05 in and .19 in).

In assembly AAB2, Fig. 4.14, components 1, 6, and 11 are again the major energy absorbers. Unlike Fig. 4.13, it appears from the system data that only a small amount of forward extrapolation occurred with the inverse models of components 11 and 1. The theoretical energy absorbed by the system now appears to be at or near the levels which were input. A small degree of over estimation still occurs in some tests,

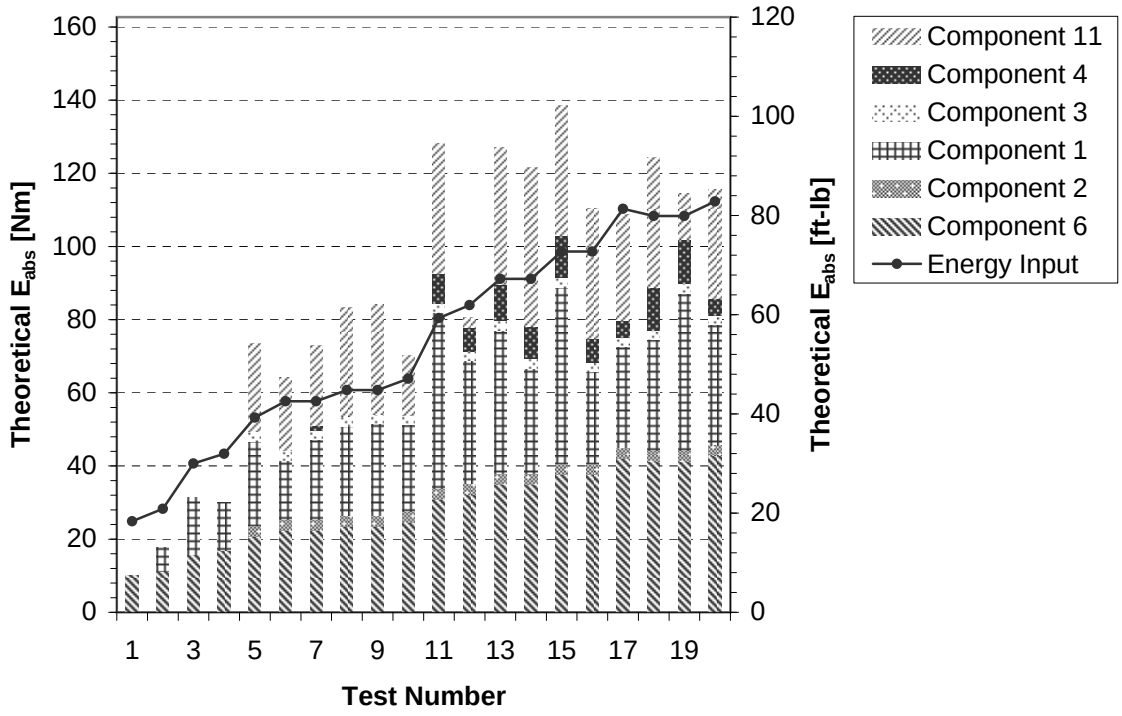

Figure 4.13: Energy Absorption in System Tests, Assembly AAB1

but the total absorption for each test seems to follow the general trend of the energy input.

Assembly AAB3, Fig. 4.14, utilizes component 5 where the earlier assemblies did not. The major energy absorbers are components 5 and 6. Less forward extrapolation of the inverse component models occurs for this assembly. This may account for the theoretical energy absorption levels having a lower level than the energy input levels. This leads us to believe that additional energy absorbers may exist in the system that have not been modeled.

Assembly AAB4, Fig. 4.16, behaves in a similar manner to assembly AAB3. The theoretical energy absorption levels are somewhat lower relative to the energy input levels as compared to assembly AAB3.

Assumptions were made that the method of energy absorption estimation used in the system model given above would not be able to account for all energy absorbed by the system. Nevertheless, these models seem to do an adequate job of predicting the amount and source of energy absorption in the system.

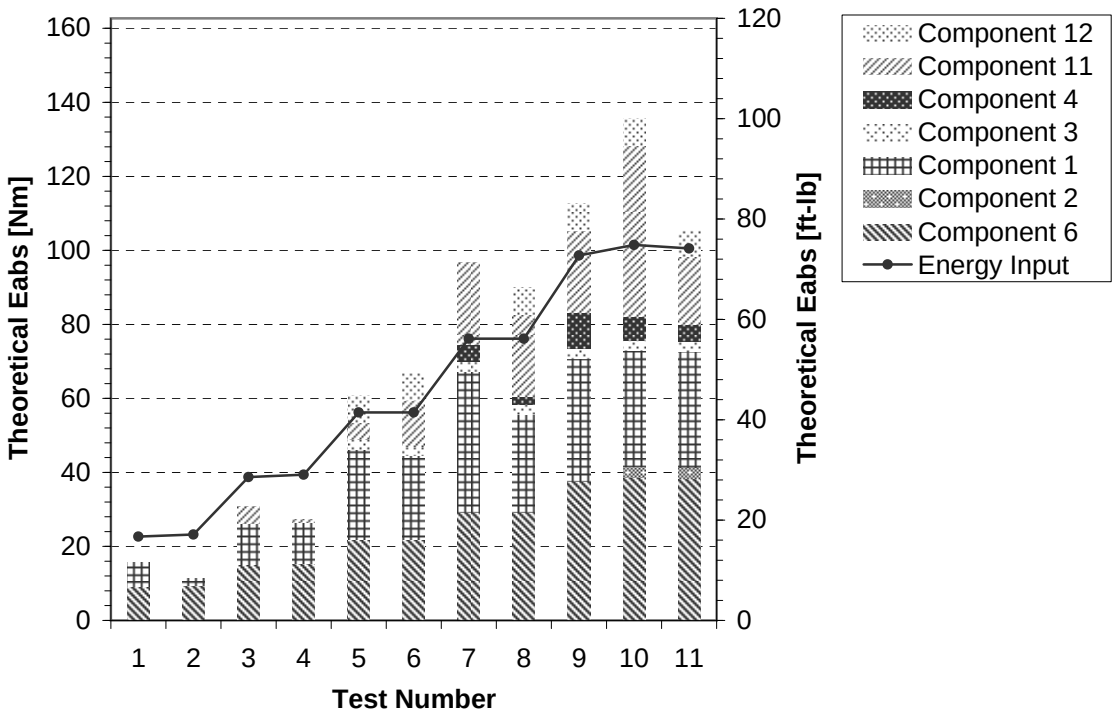

Figure 4.14: Energy Absorption in System Tests, Assembly AAB2

4.2.2 System Model for Energy Absorption

The results of the system tests and modeling are displayed and discussed in this section. The results have been summarized graphically, relating theoretical energy absorbed by the system to initial potential energy stored in component 6, the helical extension spring. For each assembly tested, AAB1, AAB2, AAB3 and AAB4, a model and the lower bound of a prediction interval is created.

The model created is a simple linear regression of the data. The independent variable is the initial potential energy stored in the helical extension spring before it is suddenly released. The dependent variable is the sum of all the computed component energies for each initial potential energy. A prediction interval is similar to a confidence interval, discussed in section 4.1.2. Where confidence intervals are used to describe intervals for the expected response at different values of the dependent variable, a prediction interval specifies a region for the future response value of the dependent variable at a given confidence level [9]. A lower bound is used to specify that energies at or below this level should be used for predicting future energy absorption levels. It should also be stated that these models constitute very rough estimates of actual

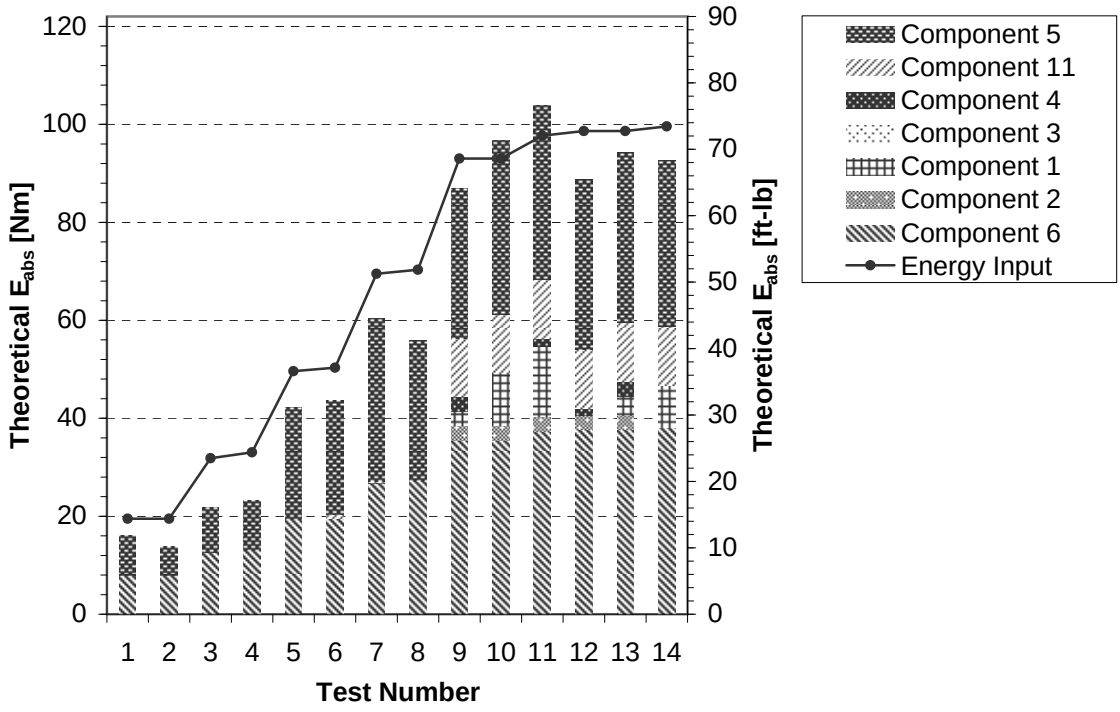

Figure 4.15: Energy Absorption in System Tests, Assembly AAB3

future energy absorption levels. They should be used as references only and any absorption levels should be tested.

The model for assembly AAB1, Fig. 4.17, displays the same behavior seen in Fig. 4.13. The lower bound prediction interval tempers some of the over estimation in this model. The over estimation can be seen in that the slope of the model is greater than one.

Assembly AAB2, Fig. 4.18, also shows some over estimation. Again, this is tempered by the prediction interval.

The linear regression of Assembly AAB3, Fig. 4.19, is almost one to one. This means that the system is predicted to absorb almost all of the energy input. The prediction interval is closer to the predicted mean than the previous two models.

The linear regression of Assembly AAB4, Fig. 4.20, is less than one to one. This means that the energy input into the system will not be completely absorbed.

We have now gained an understanding of the energy absorbing properties of the components in the given system. Conclusions about the methods used to determine the amount of energy absorbed by a multi-body system under impact can now be

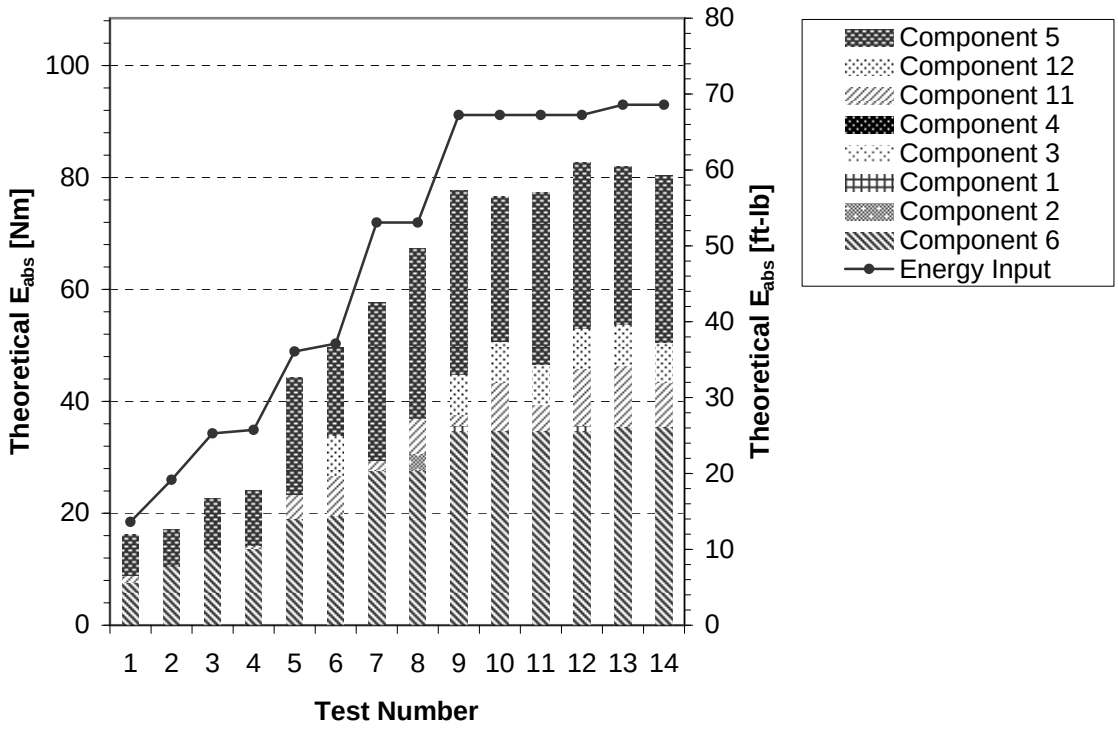

Figure 4.16: Energy Absorption in System Tests, Assembly AAB4

made.

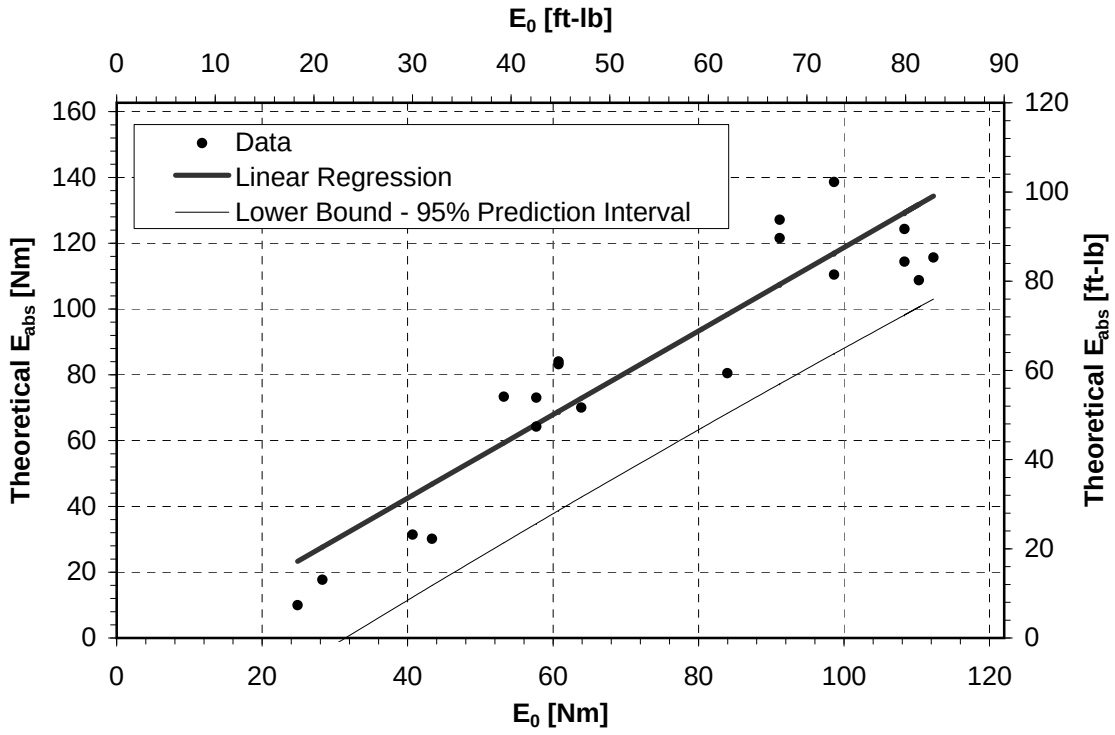

Figure 4.17: Theoretical Energy Absorption vs. Stored Energy of Assembly AAB1

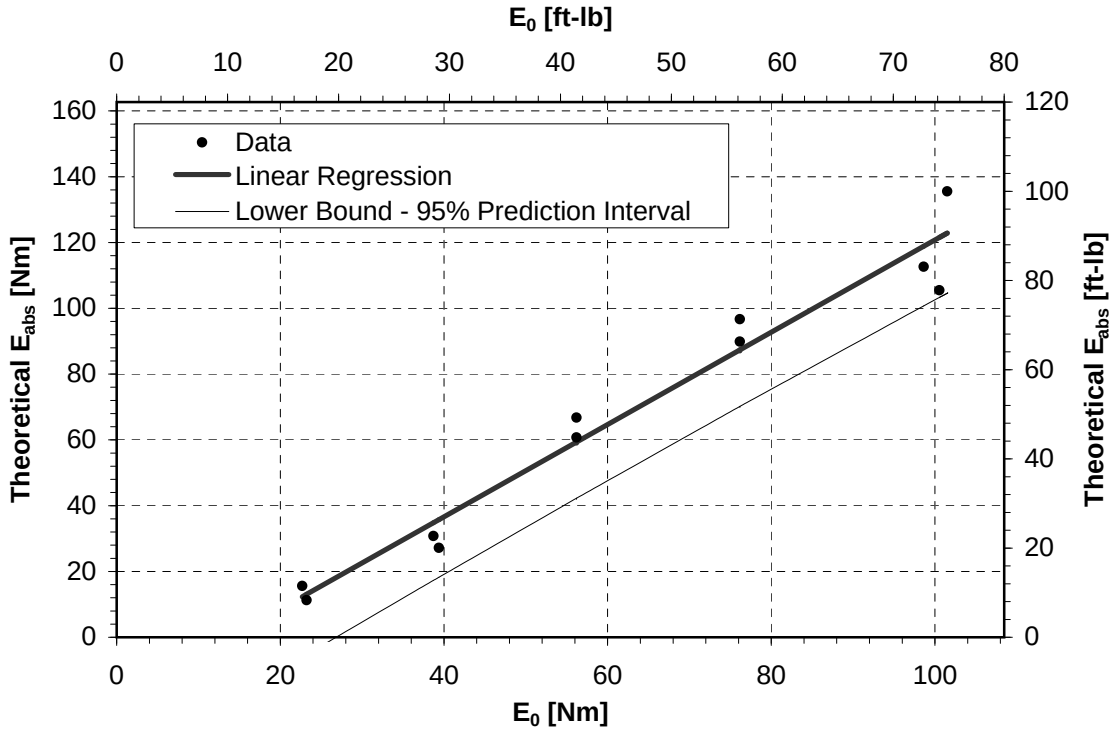

Figure 4.18: Theoretical Energy Absorption vs. Stored Energy of Assembly AAB2

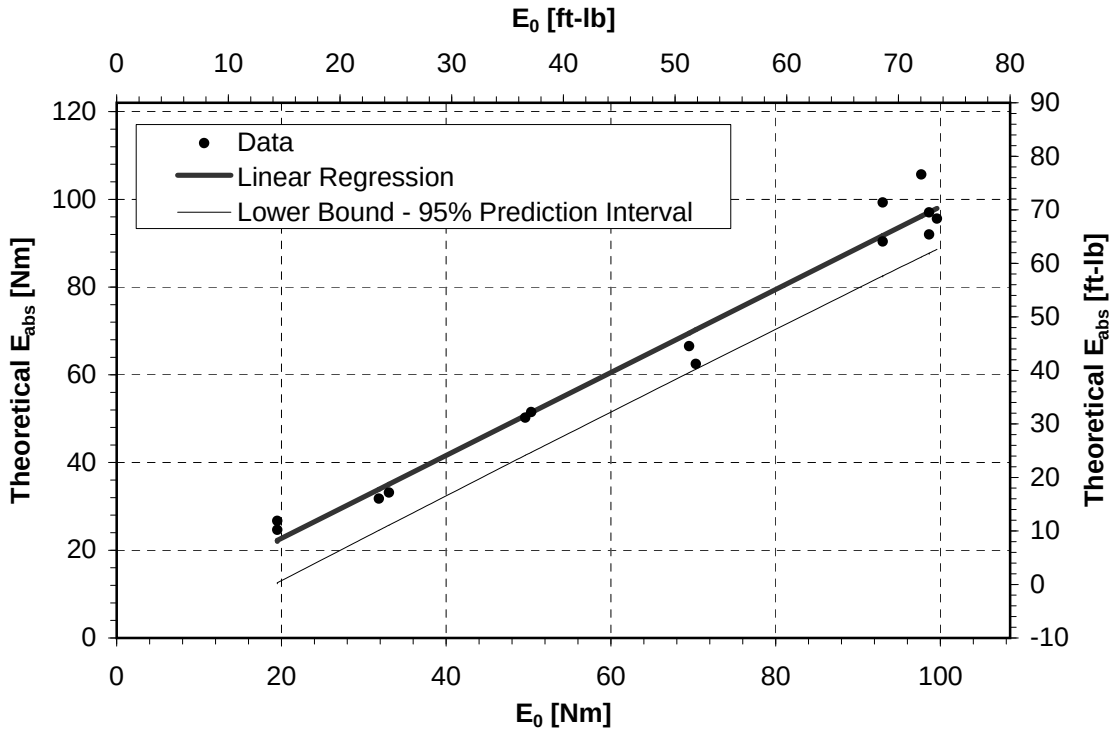

Figure 4.19: Theoretical Energy Absorption vs. Stored Energy of Assembly AAB3

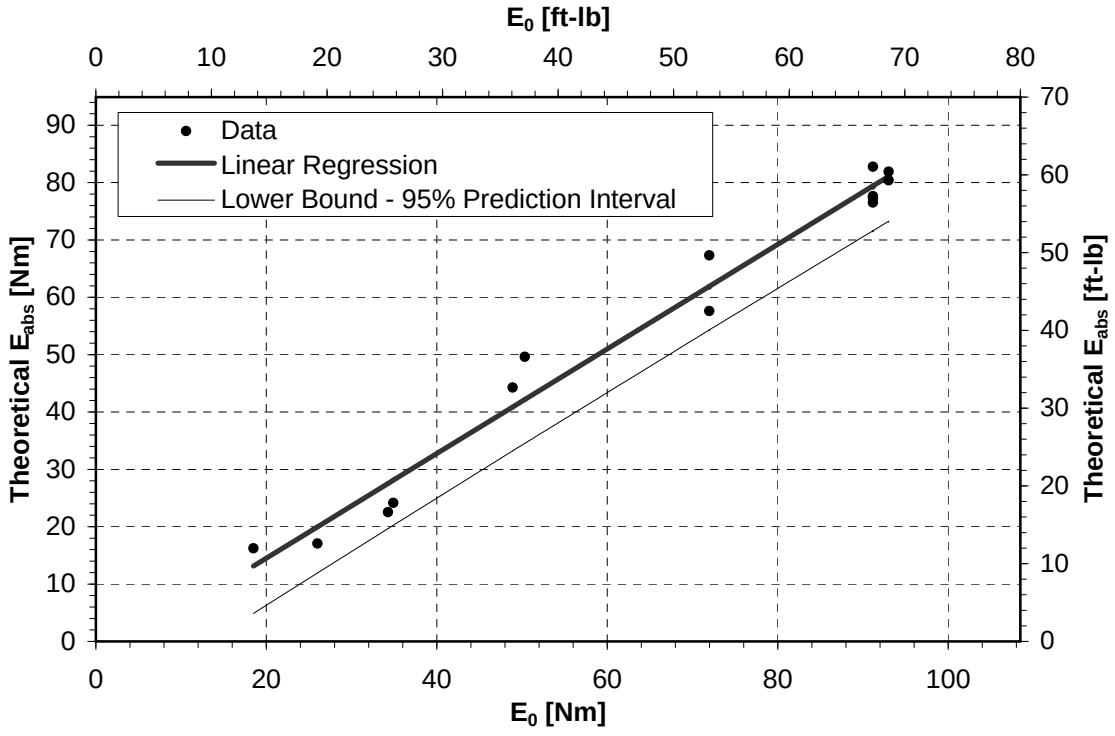

Figure 4.20: Theoretical Energy Absorption vs. Stored Energy of Assembly AAB4

Chapter 5

Conclusions

Chapter 5 concludes this thesis in three sections. The first reviews the previous chapters, the second states conclusions made concerning the research conducted and the last poses recommendations for future work.

5.1 Review

This section reviews the previous chapters. Chapter 1 discussed the background for this research. It reviewed literature related to the finite element analysis of impact scenarios, empirical methods used in impact analysis, and the types of impact regimes related to impact velocity.

Chapter 2 described the multi-body system under investigation in which an impact event occurred. It detailed the subsystems and components that make up the system while making special note of the helical extension spring.

Chapter 3 discussed the system and component tests that were conducted to better understand the behavior of the system after an impact event. Test setup, procedure and results were discussed for both the system and component tests.

Chapter 4 discussed the models created to approximate the component and system behavior. Models were created from the component test data to understand the relationship between the amount of damage sustained to the amount of energy absorbed. These models were then used to create models of the system as a whole, relating the amount of energy input into the system and the total amount of theoretical energy absorbed by all of the components in a system test.

5.2 Conclusions

This section summarizes conclusions detailed in this thesis. The process used to investigate energy absorption in a multi-body system under impact has resulted in models of the system that appear to approximate the impact energy. Much of the energy input into the system was accounted for by observing the damage to components and creating models relating damage to energy absorption. During the course of investigation the energy absorption properties of contracting helical extension springs was also studied, yielding interesting insight into the amount of energy absorbed by spring coil impact.

The process used to create the models outlined in this thesis is given in Fig. 5.1. Using only linear approximations for data obtained in both the component tests and the system tests, models were created that theoretically accounted for 88% to 120% of the energy input. A large variance in the energy absorption predictions exists but overall the methods produced useful data when attempting to gain a general understanding of the energy being absorbed in the system due to an impact event.

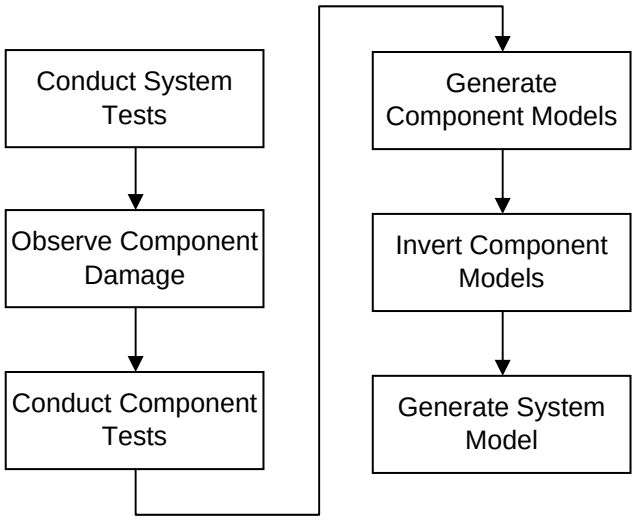

Figure 5.1: Experimental Energy Absorption Process Flowchart

The helical extension spring used in this research exhibited energy absorption properties. When a pretensioned helical extension spring is extended and then suddenly released, the coils of the spring contract until the solid height of the spring is reached. Between 37 and 68 percent of the initial potential energy was absorbed during this

process. The larger the initial potential energy, the lower the percentage of energy absorbed by the spring.

Further analysis of the data obtained in Meyer [11] was conducted to better understand the energy absorption properties of pretensioned helical extension springs. The three pretensioned helical extension springs studied in Meyer, which included the spring used in this research, were tested to determine their energy absorption properties. A summary of these properties for the free flight experiments is given in Fig. 5.2.

As seen in Fig. 5.2(a), spring M and H behave in similar manners. Looking at the confidence intervals, the behaviors of springs M and H are not statistically different because the confidence intervals overlap. As seen in Fig. 5.2(b), the behavior of spring S is similar to Spring H and M. Because the input energy values of spring S and springs M and H do not overlap, it can not be said that they are statistically similar.

Using free flight experiment data for springs H, M and S we have created a model, Fig.4.8(a), of the energy absorption of pretensioned helical extension springs during solid height contraction based on the initial potential energy stored in the spring. The model's mean is given by Eq. 4.6.

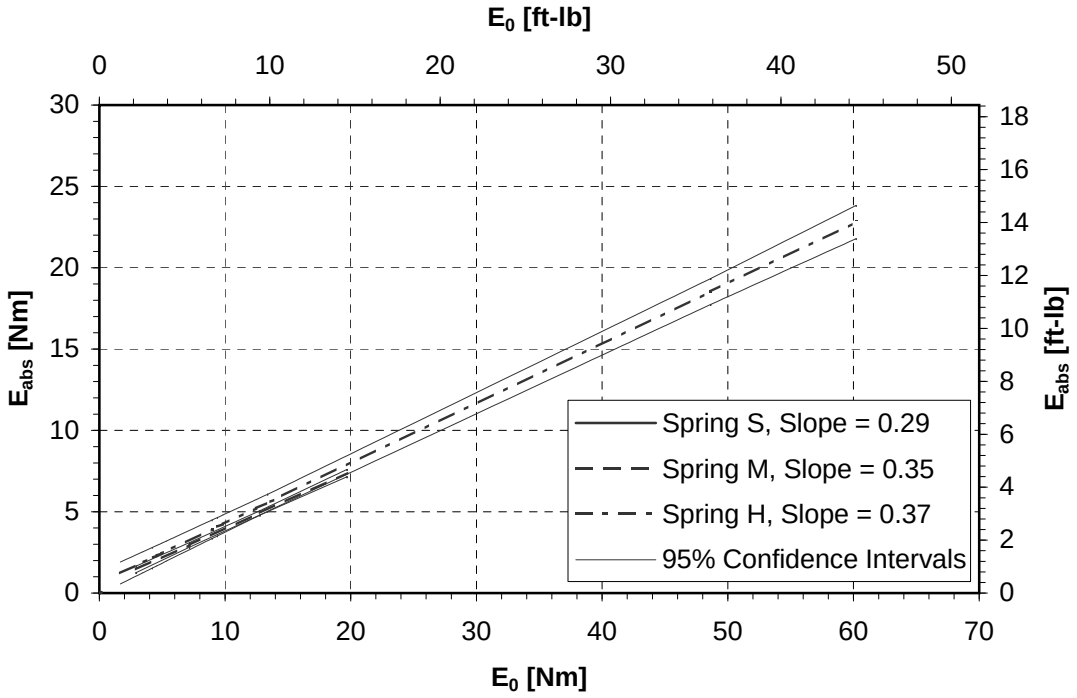

(a) Simple Linear Regressions of Spring S, M, and H with Confidence Intervals

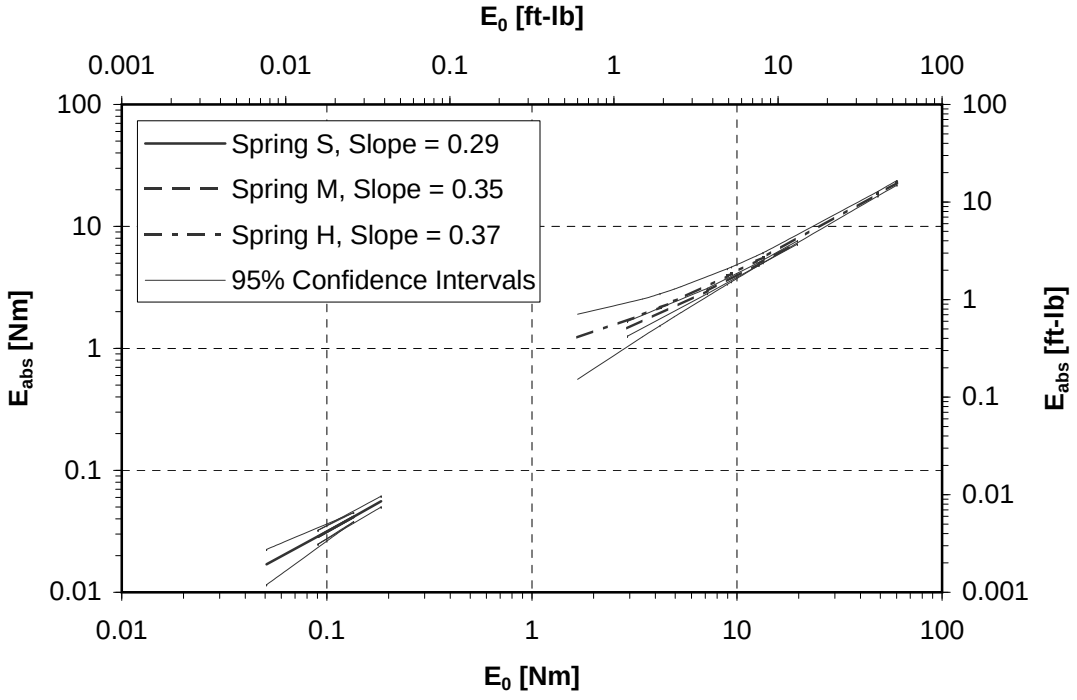

(b) Simple Linear Regressions of Spring S, M, and H with Confidence Intervals Plotted on Log-Log Axes

Figure 5.2: Energy Absorbed by Spring Coil Impact vs. Initial Potential Energy, Free Flight Experiments

5.3 Recommendations for Future Work

This section describes areas for future work. Eight different components were used in the component tests. These components were chosen based on the amount of permanent damage that they sustained in the system tests. These components absorbed the majority, but not all, of the energy that was input into the system. Further investigation of other possible energy absorbing components would allow for a more detailed understanding of the overall energy absorbing properties of the system. Of particular interest are the components that absorbed energy elastically, leaving no permanent signs of the energy they absorbed.

The component models, used inversely to determine the energy absorbed by components from the system tests, were extrapolated frequently when used to create the system models. Additional component tests with a wider range of input energies would allow for greater confidence in the system models.

Measurement error or error variance was obtained for all of the continuous component models. This data is useful in understanding how well the model represents the true relationship between the energy input into the component and the resulting energy absorbed by the component. The error in the component models was not propagated into the system models when the inverse component models were used with the system data. Finding the error variance of an inverse prediction is particularly difficult [13] and was not attempted in this work. Propagation of this error from component models into the system models would increase the predictability of the system model.

It is difficult to predict the energy absorption in a multi-body system under medium velocity impact where high levels of permanent deformation occur. The empirical methods used to create the models in this thesis gave a reasonable representation of the distribution of energy absorption throughout the system using simple linear models.

References

[1] Goldsmith, W., 1960. *Impact, The theory and physical behaviour of colliding solids*. Edward Arnolds Publishers LTD.

[2] Gilardi, G., 2002. "Literature survey of contact dynamics modelling". *Mechanism and Machine Theory,* **37**(10), pp. 1213–1239.

[3] Stronge, W. J., 2000. *Impact Mechanics*. The Press Syndicate of the University of Cambridge.

[4] Gobbi, M., 2008. "Numerical-experimental analysis of metal bars undergoing intermediate strain rate impacts". *Computational Mechanics,* **43**(2), pp. 191–205.

[5] Frendo, F., 2005. "Simulation of motor-scooter drop testing by a multi-body finite element integrated approach". *Proceedings of the Institution of Mechanical Engineers - Part K - Journal of Multi-body Dynamics,* **219**(4), pp. 383–391.

[6] Chou, C. C., 2007. "A review of side impact component test methodologies". *International Journal of Vechicle Safety,* **2**(1-2), pp. 141–184.

[7] Pearson, D., 1988. "Dynamic behavior of helical springs". *The Shock and Vibration Digest,* **20**(7), pp. 3–9.

[8] Macaulay, M., 1987. *Introduction to Impact Engineering*. Chapman and Hall.

[9] Hayter, A. J., 1996. *Probability and Statistics for Engineers and Scientists*. PWS Publishing Company.

[10] Montgomery, D. C., 1999. *Applied Statistics and Probability for Engineers*, second ed. John Wiley and Sons, Inc.

[11] Meyer, M., 2006. "Energy absorption in contracting pretensioned helical extension springs". Master's thesis, The University of Minnesota, May.

[12] *NIST/SEMATECH e-Handbook of Statistical Methods*. http://www.itl.nist.gov/div898/handbook/, October 1, 2007.

[13] Graybill, F. A., 1976. *Theory and Application of the Linear Model*. Wadsworth Publishing Company, Inc.

Appendix A

Component Tests

A.1 Raw Component Test Data

Test Number	Spring Extension	Length of Manufactured Rivet Head Hole
	[in +/- 1/16]	[in +/- 0.001]
1	3	0.310
2	3	0.305
3	1	0.240
4	2	0.270
5	4	0.330
6	4	0.345
7	4	0.299
8	5	0.373
9	6	0.326
10	6	0.340
11	2	0.264
12	2	0.221
13	1	0.223
14	1	0.211
15	3	0.244
16	4	0.299
17	4	0.295
18	4	0.255
19	4	0.286
20	4	0.238

Table A.1: Component 1 Test Data

Test Number	Spring Extension	Failure State
	[in]	[Fail / No Fail]
1	3.00	Fail
2	1.50	Fail
3	0.75	No Fail
4	1.13	Fail
5	1.00	No Fail
6	1.00	Fail
7	1.25	Fail
8	1.13	Fail
9	1.00	Fail
10	1.00	Fail

Table A.2: Component 2 Test Data

Test Number	Spring Extension	Failure State	Comments
	[in]	[Fail / No Fail]	
1	1.00	Fail	
2	0.50	No Fail	
3	0.80	No Fail	
4	0.90	Fail	
5	-	-	Invalid
6	-	-	Invalid
7	0.92	Fail	
8	0.81	No Fail	

Table A.3: Component 3 Test Data

Test Number	Spring Extension	Screw Deformation	Comments
	[in +/- 1/16]	[form straight +/- 0.5]	
1	1.0	10	
2	2.0	21	
3	3.0	30	
4	2.5	33	
5	-	-	Invalid
6	0.5	2	
7	0.5	3	
8	0.5	4	
9	1.0	8	
10	1.0	9	
11	1.5	18	
12	1.5	17	
13	1.5	15	
14	2.0	26	
15	2.0	25	
16	2.0	26	
17	2.5	30	
18	2.5	30	
19	3.0	35	
20	3.0	37	

Table A.4: Component 4 Test Data

Test Number	Spring Extension	Change in Length	Comments
	[in +/- 1/16]	[in]	
1	1	0.032	
2	2	0.088	
3	3	0.188	
4	4	0.189	
5	5	0.377	
6	6	0.430	
7	2	0.057	
8	2	0.072	
9	2	0.057	
10	3	0.132	
11	3	0.127	
12	3	0.093	
13	4	0.135	
14	4	0.160	
15	4	0.028	
16	-	-	Invalid
17	5	0.295	
18	5	0.309	
19	5	0.269	

Table A.5: Component 5 Test Data

Test Number	Spring Extension	Max. Height
	[in]	[in]
1	1.25	4.25
2	2.06	7.06
3	3.13	12.69
4	4.25	19.81
5	1.38	4.75
6	1.25	3.69
7	1.38	4.56
8	1.38	4.13
9	2.44	8.88
10	2.44	9.13
11	2.38	8.75
12	2.25	6.69
13	3.06	12.50
14	2.94	11.81
15	3.00	12.25
16	3.38	14.88
17	4.13	18.75
18	4.38	20.50
19	4.06	18.56
20	4.19	19.00
21	5.25	26.38
22	5.19	25.88
23	5.13	25.81
24	5.06	24.81
25	5.19	24.25
26	1.56	64.97
27	1.56	74.22
28	1.63	80.72
29	1.50	69.84
33	0.87	34.72
34	0.94	35.25
35	0.81	33.12

Table A.6: Component 6 Test Data

36	0.75	43.05
37	0.75	37.47
38	1.50	66.00
39	2.19	111.47
40	2.13	106.22
41	2.13	108.34
44	2.13	106.28
45	2.00	96.22
46	0.31	7.56
47	0.63	25.47
48	5.91	364.00
49	5.91	427.99
50	5.91	425.98
51	5.91	414.01
52	6.89	542.99
53	6.89	525.00
54	6.89	534.01

Table A.6: Component 6 Test Data

Test Number	Spring Extension	Elongated Hole Length	Comment
	[in +/- 1/16]	[in +/- 0.005]	
1	0.50	0.162	
2	1.00	0.164	
3	1.50	0.165	
4	-	-	Invalid
5	1.25	0.191	
6	1.75	0.198	
7	1.75	0.168	
8	0.50	0.171	
9	1.00	0.161	
10	1.25	0.184	
11	1.50	0.153	
12	2.00	0.210	
13	0.50	0.167	
14	1.00	0.170	
15	1.25	0.183	
16	1.50	0.203	
17	1.75	0.169	
18	2.00	0.215	

Table A.7: Component 11 Test Data

Test Number	Spring Extension	Failure	Comments
	[in]	[Fail / No Fail]	
1	0.50	No Fail	
2	1.00	No Fail	
3	1.50	No Fail	
4	2.00	No Fail	
5	3.00	No Fail	
6	6.00	No Fail	
7	-	-	Invalid
8	-	-	Invalid
9	-	-	Invalid
10	-	-	Invalid
11	-	-	Invalid
12	-	-	Invalid
13	-	-	Invalid
14	-	-	Invalid
15	-	-	Invalid
16	2.00	Fail	
17	2.00	Fail	
18	2.00	Fail	
19	1.50	No Fail	
20	1.50	No Fail	
21	1.75	No Fail	
22	1.75	No Fail	
23	2.00	No Fail	

Table A.8: Component 12 Test Data

A.2 Continuous Models

The residuals shown Fig. A.1(b) corresponding to Fig. A.1(a) indicate that a higher order regression may be appropriate. However, when a second order regression is performed and the coefficients of determination, R^2, are compared, they are found to be similar. The two regressions both approximate the data sufficiently, the linear regression was used for practical purposes.

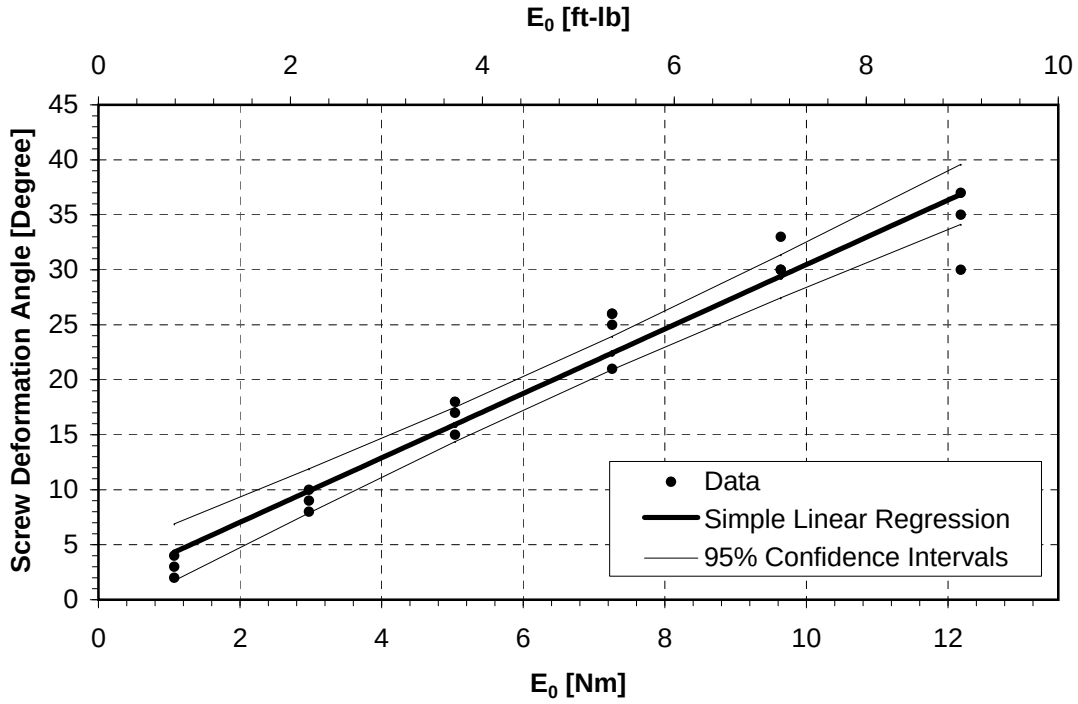

(a) Simple Linear Regression with Confidence Intervals

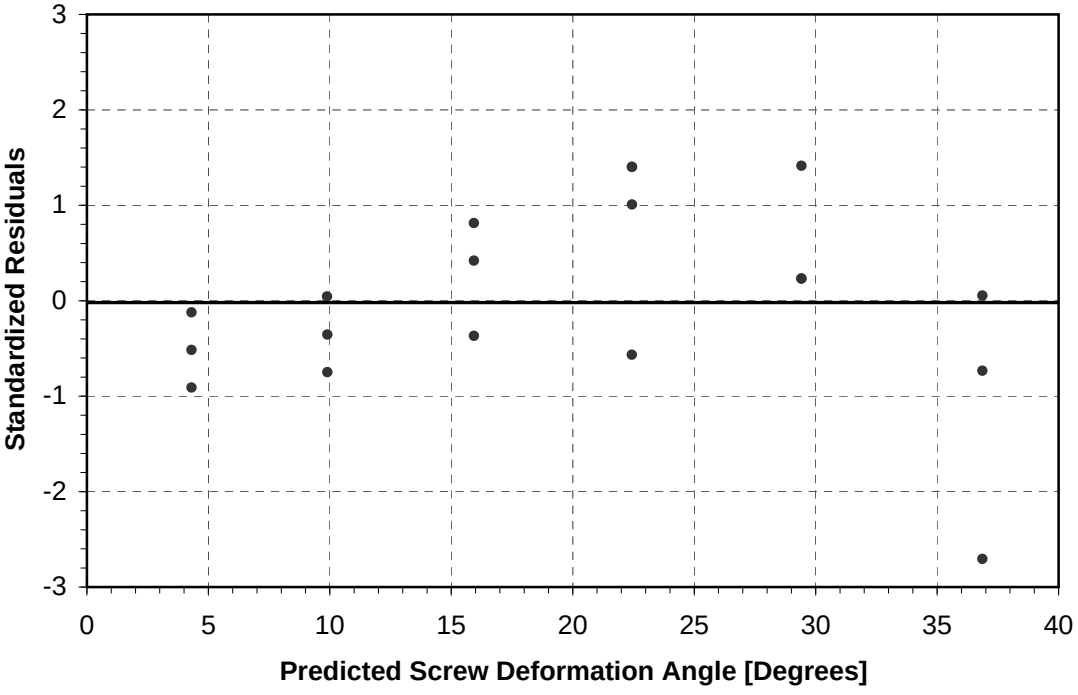

(b) Standardized Residuals from Regression Analysis

Figure A.1: Deformation Angle vs. Energy Absorbed, Component 4

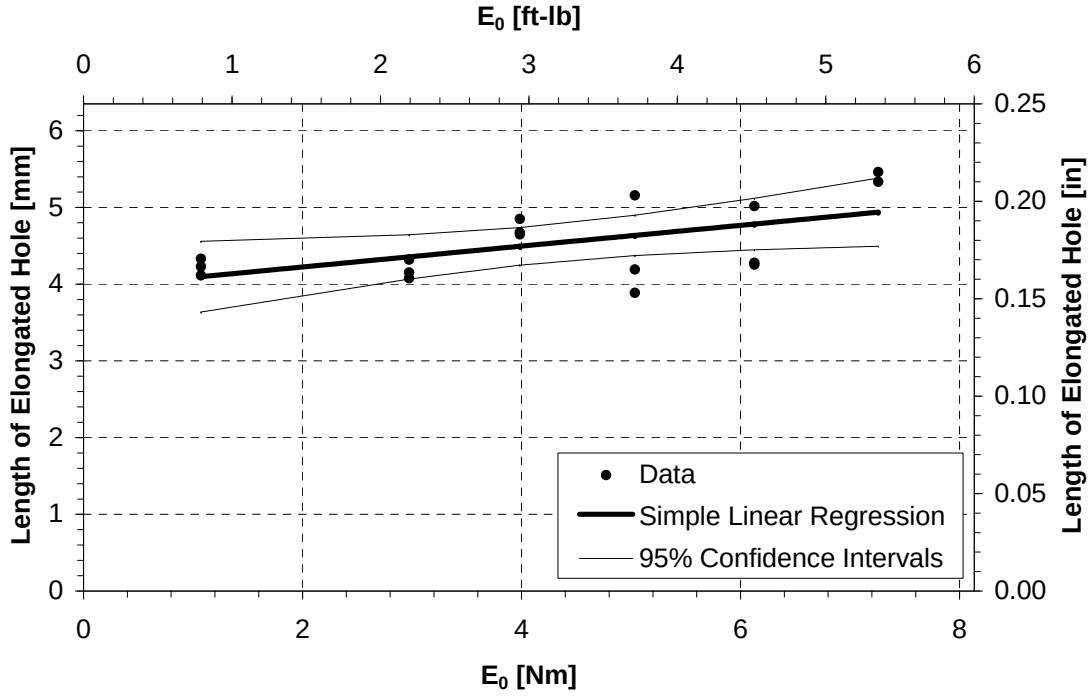

(a) Simple Linear Regression with Confidence Intervals

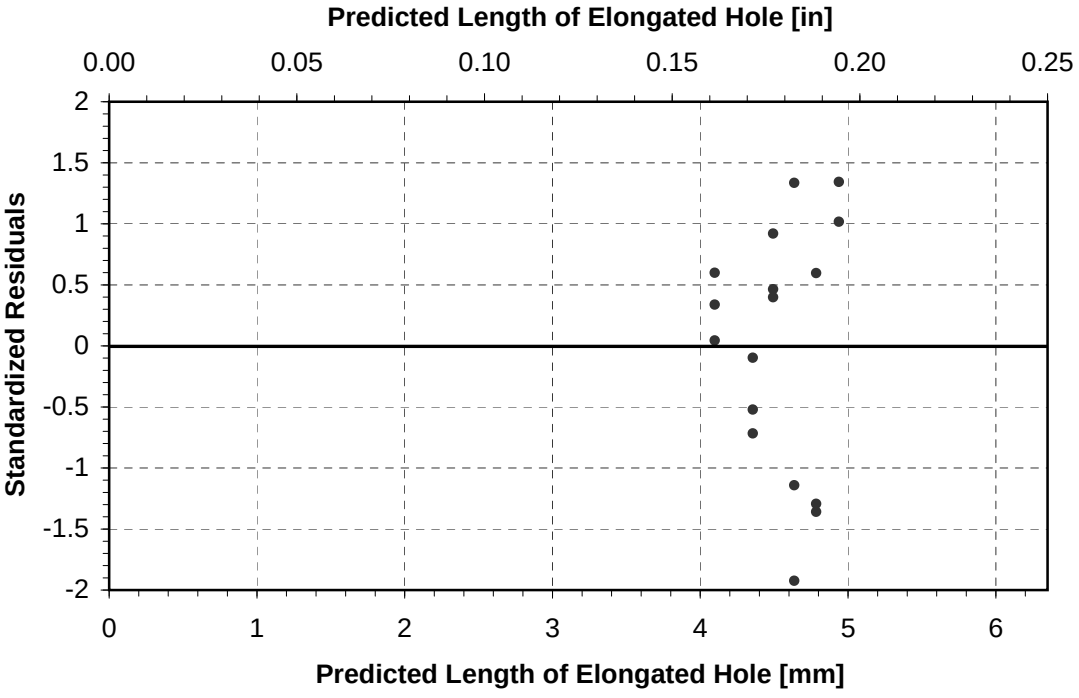

(b) Standardized Residuals from Regression Analysis

Figure A.2: Length of Elongated Hole vs. Energy Absorbed, Component 5

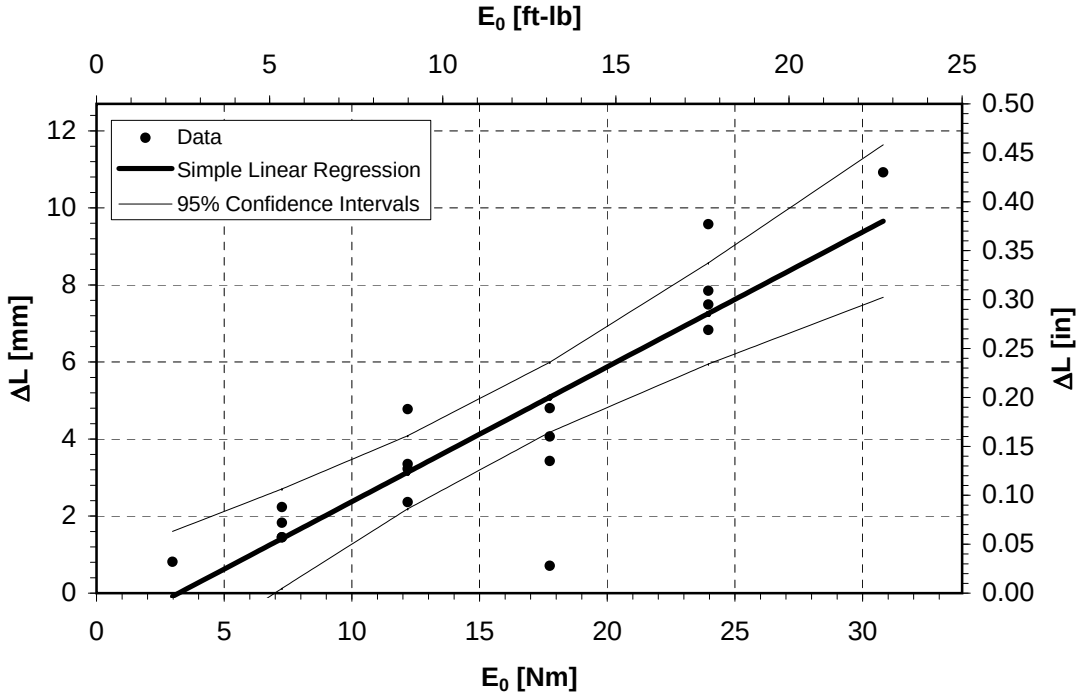

(a) Simple Linear Regression with Confidence Intervals

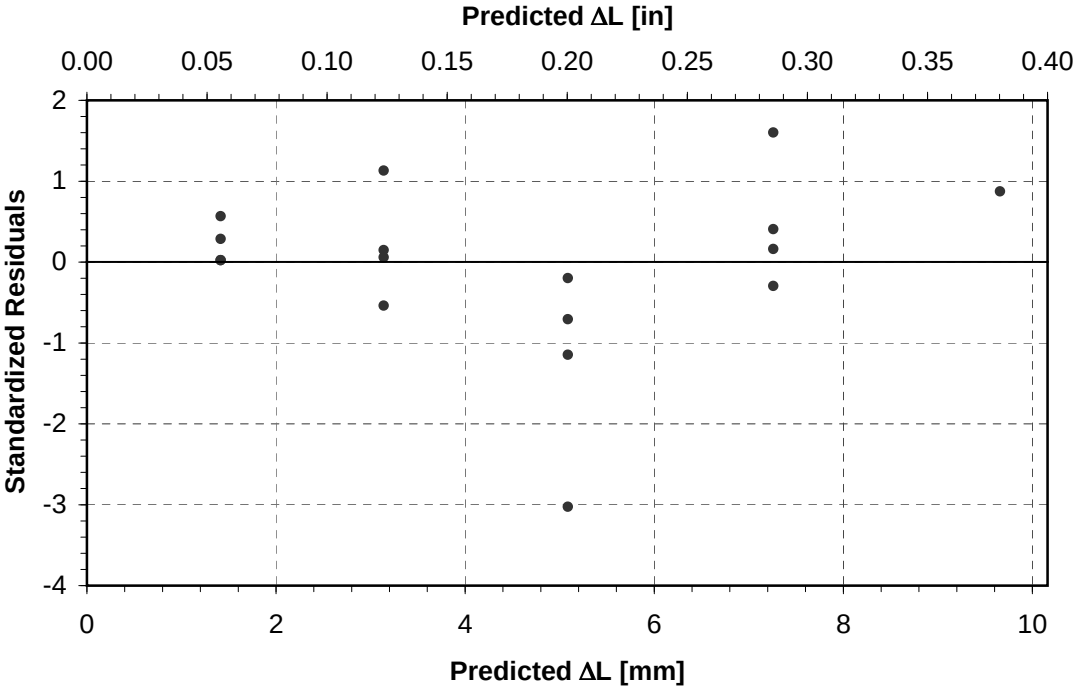

(b) Standardized Residuals from Regression Analysis

Figure A.3: Change in Length vs. Energy Absorbed, Component 7

A.3 Non-Continuous Models

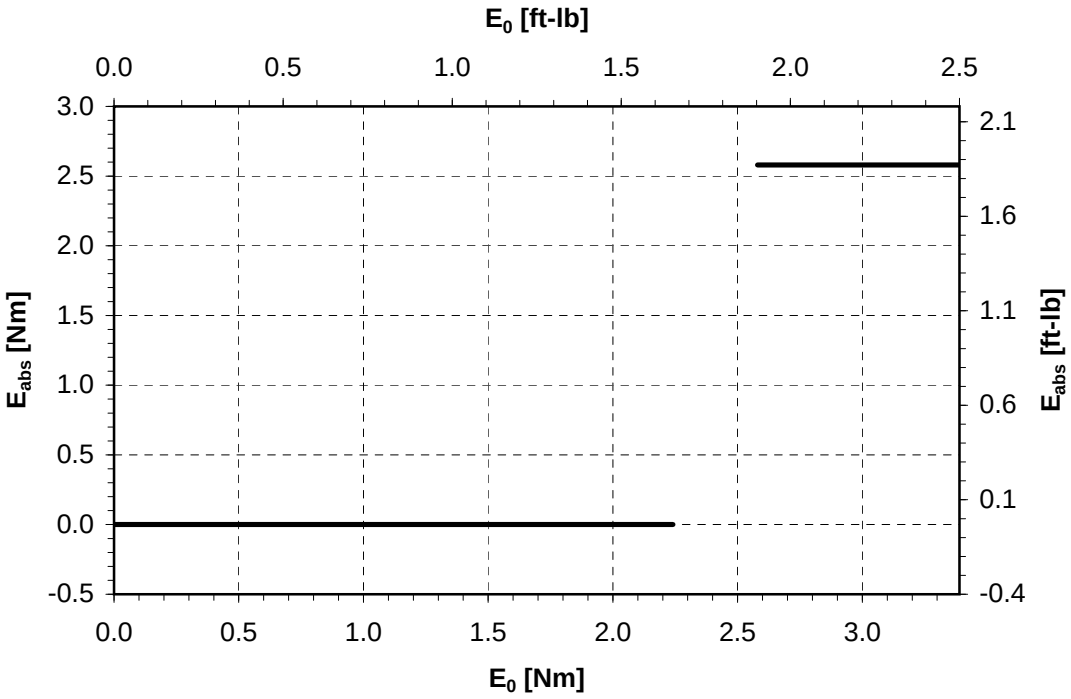

Figure A.4: Failure vs. Energy Absorbed, Component 3

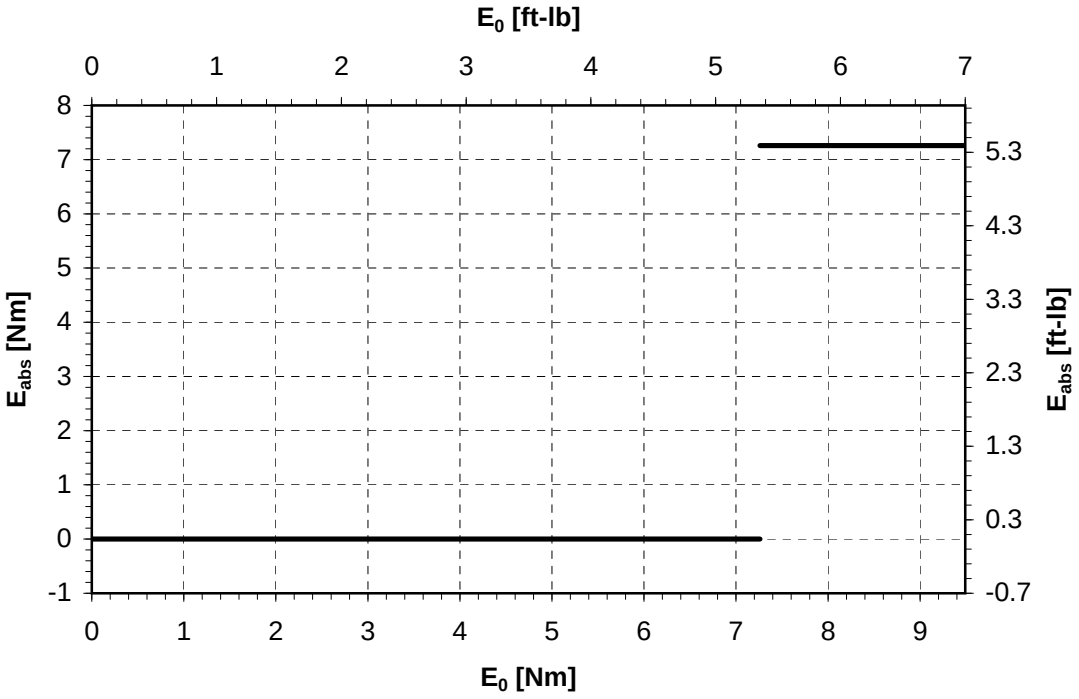

Figure A.5: Failure vs. Energy Absorbed, Component 6

A.4 Energy Absorption in Helical Extension Springs

A.4.1 Free Flight Experiments

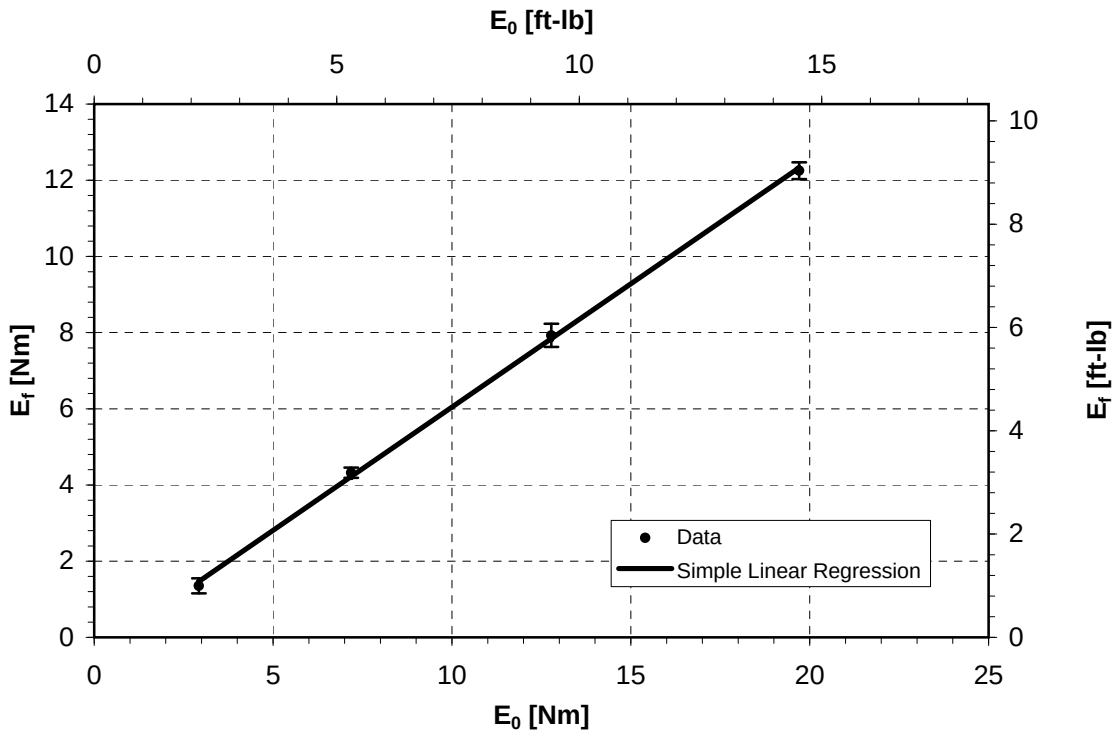

(a) Simple Linear Regression with Error Bars

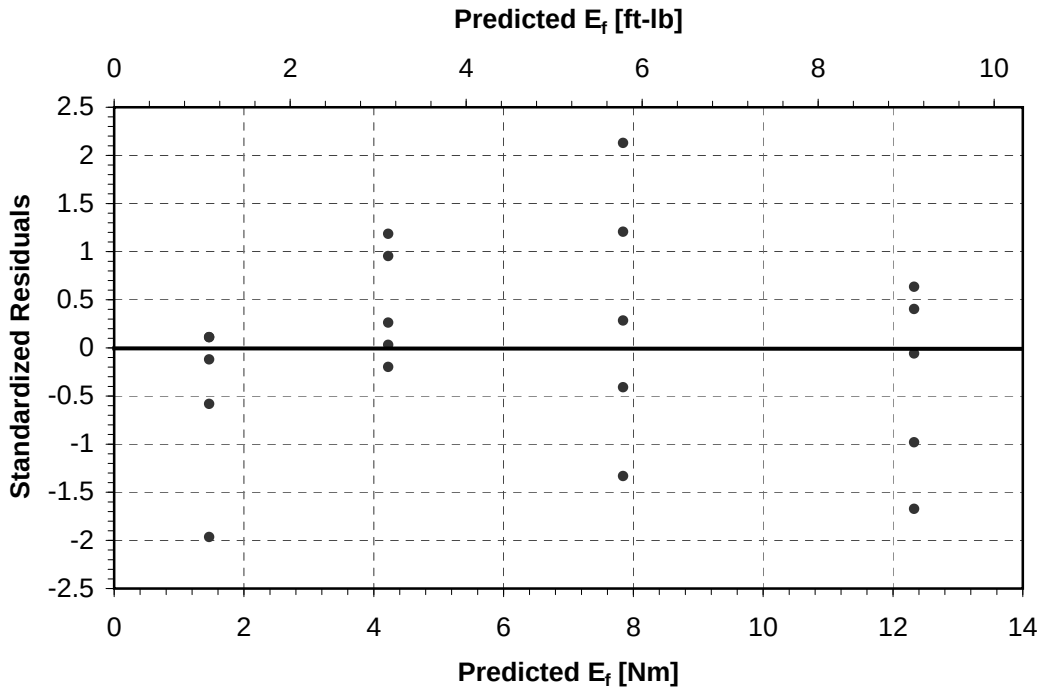

(b) Standardized Residuals from Regression Analysis

Figure A.6: Energy Final vs. Energy Initial, Spring M, Free Flight Experiments

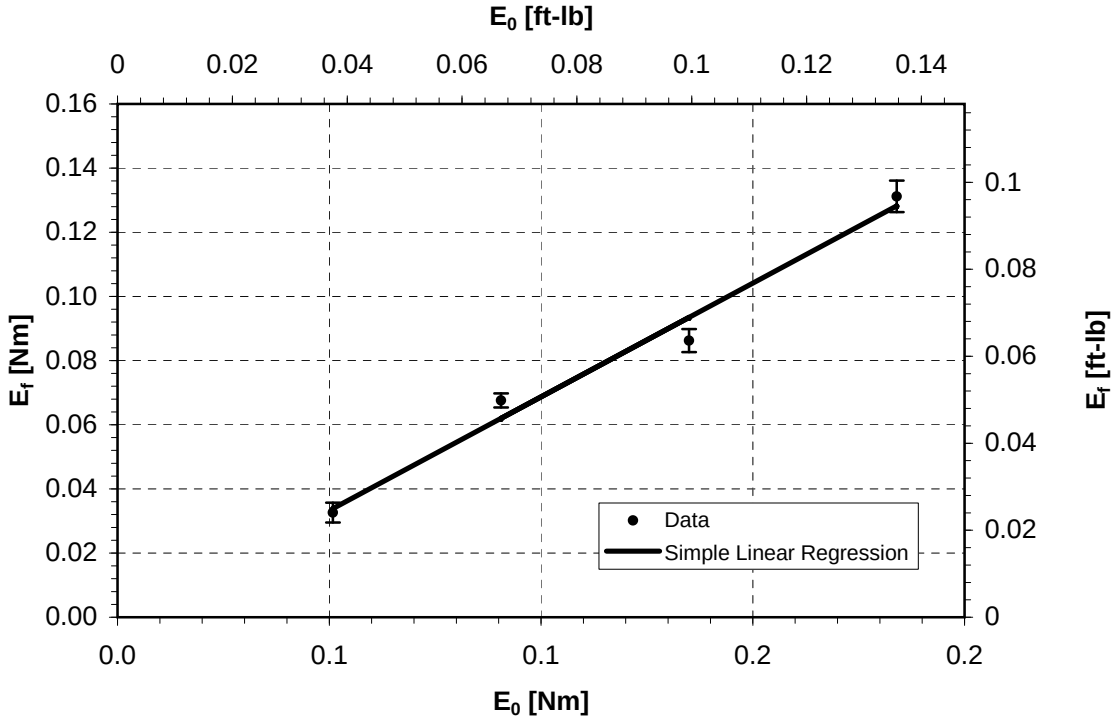

(a) Simple Linear Regression with Error Bars

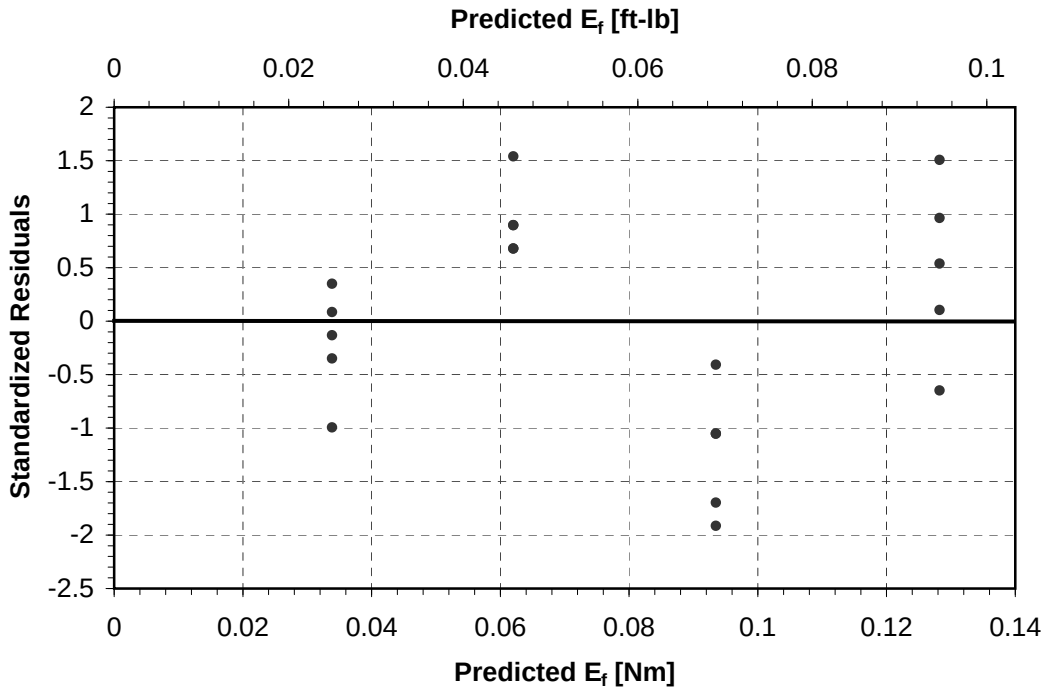

(b) Standardized Residuals from Regression Analysis

Figure A.7: Energy Final vs. Energy Initial, Spring S, Free Flight Experiments

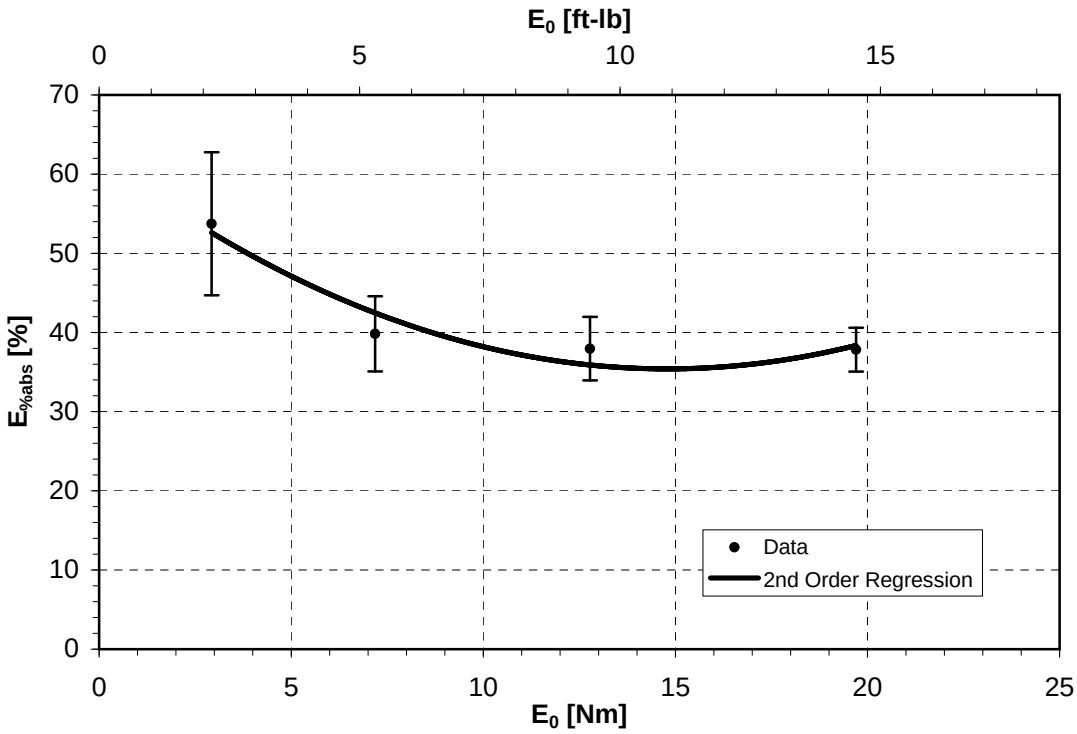

(a) Simple Linear Regression with Error Bars

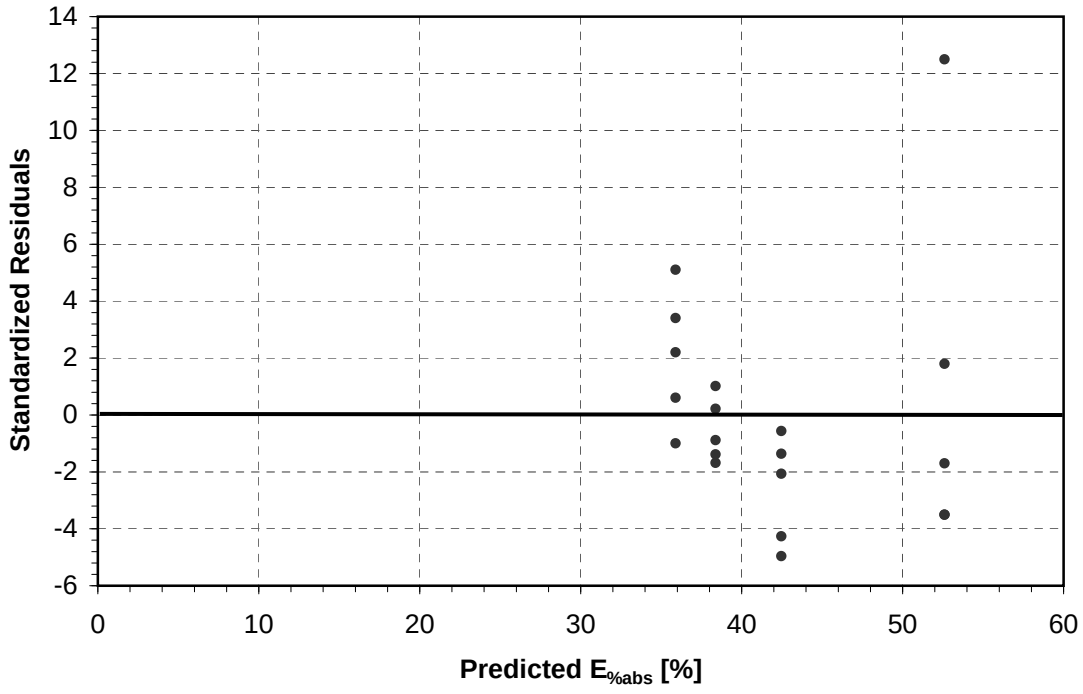

(b) Standardized Residuals from Regression Analysis

Figure A.8: Percent Energy Absorbed vs. Energy Initial, Spring M, Free Flight Experiments

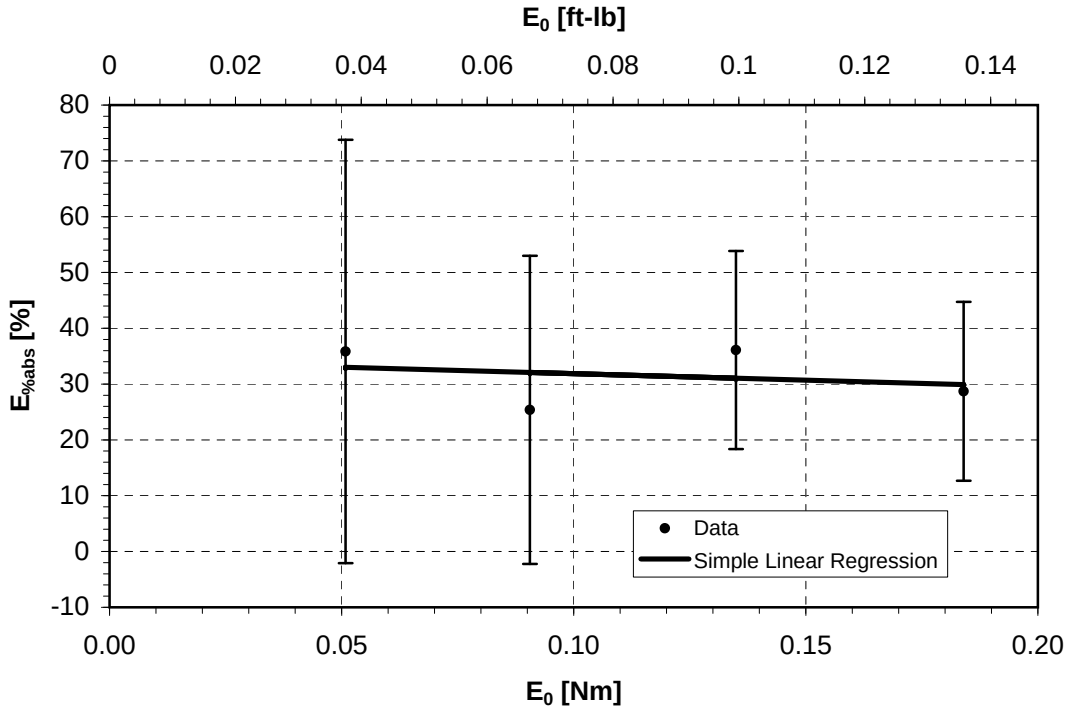

(a) Simple Linear Regression with Error Bars

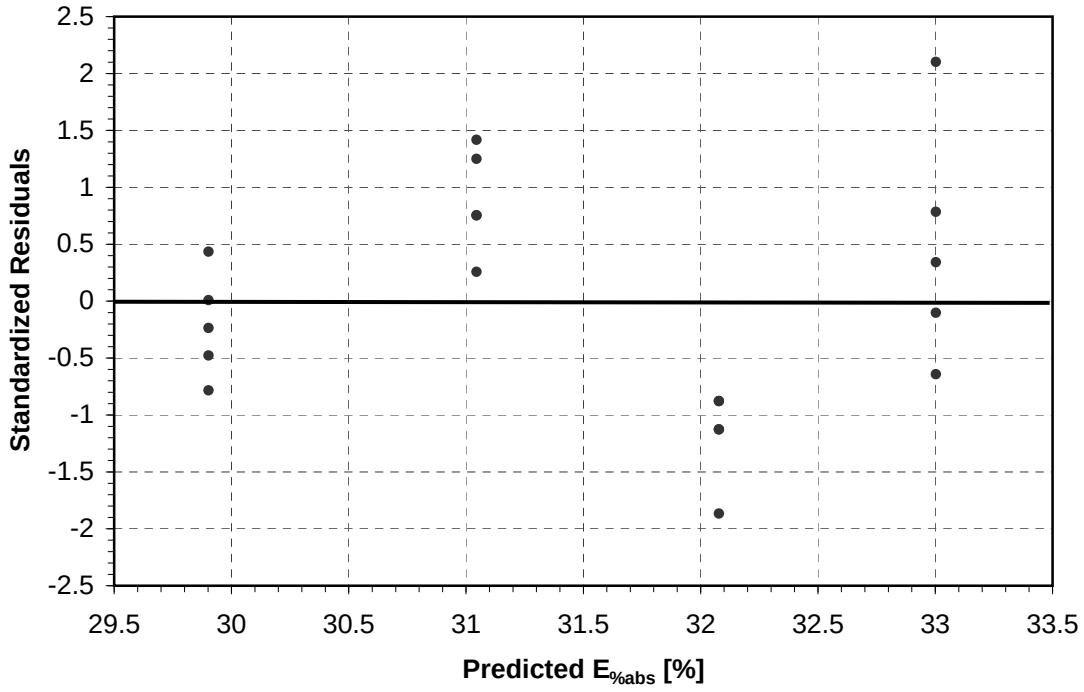

(b) Standardized Residuals from Regression Analysis

Figure A.9: Percent Energy Absorbed vs. Energy Initial, Spring S, Free Flight Experiments

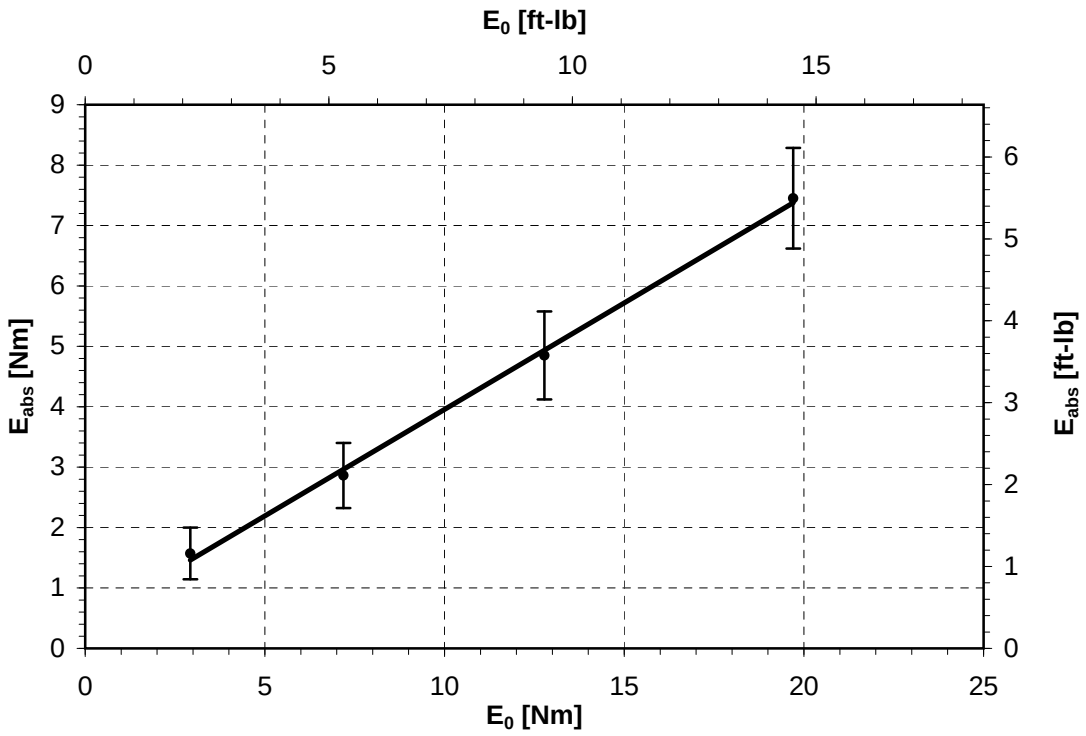

(a) Simple Linear Regression with Error Bars

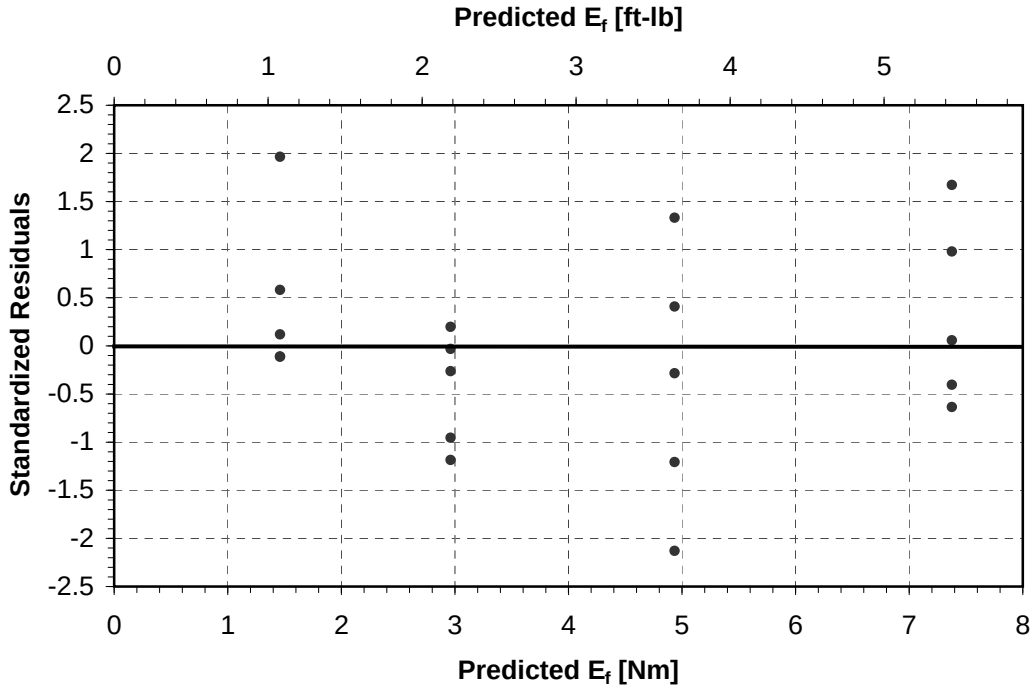

(b) Standardized Residuals from Regression Analysis

Figure A.10: Energy Absorbed vs. Energy Initial, Spring M, Free Flight Experiments

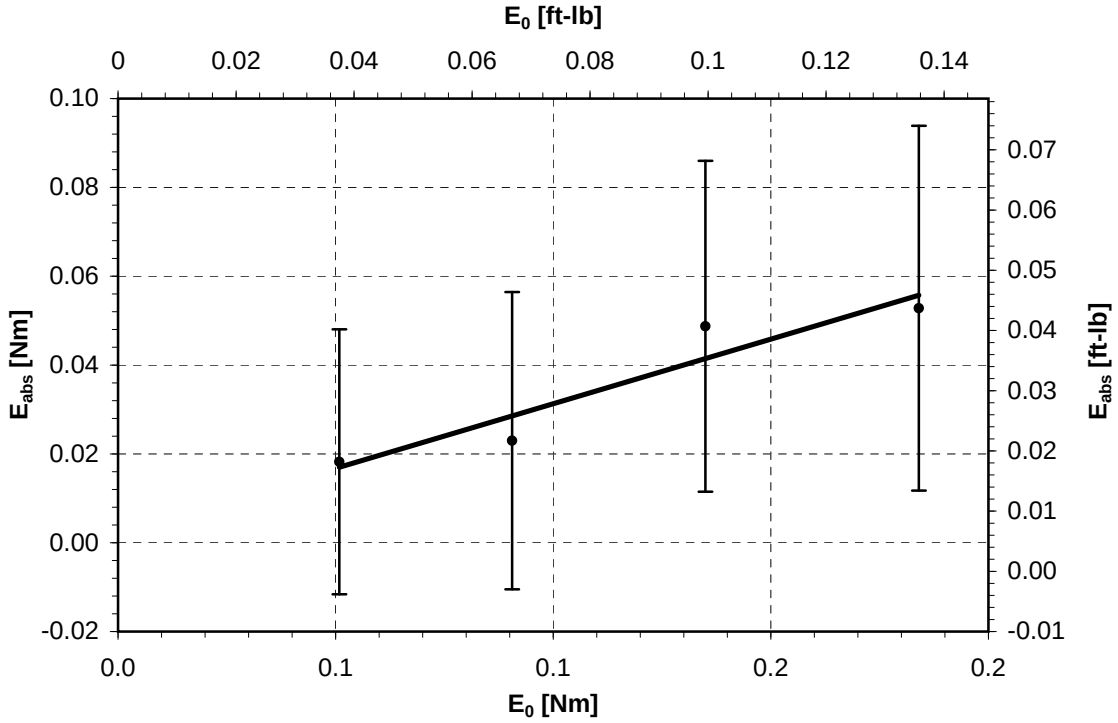

(a) Simple Linear Regression with Error Bars

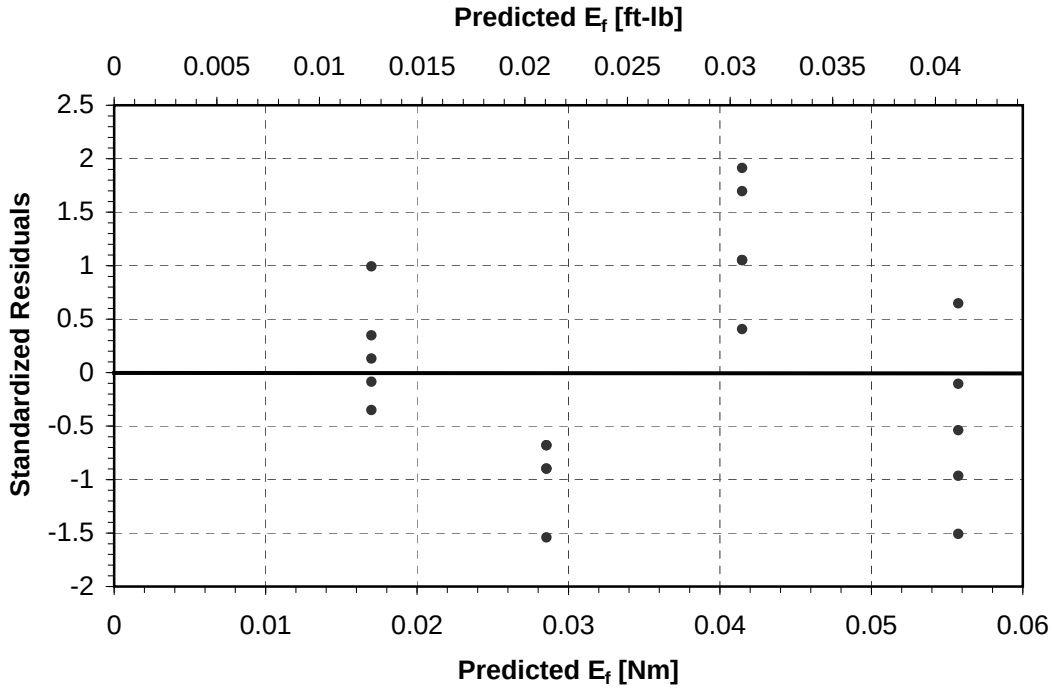

(b) Standardized Residuals from Regression Analysis

Figure A.11: Energy Absorbed vs. Energy Initial, Spring S, Free Flight Experiments

A.4.2 Accelerometer Experiments

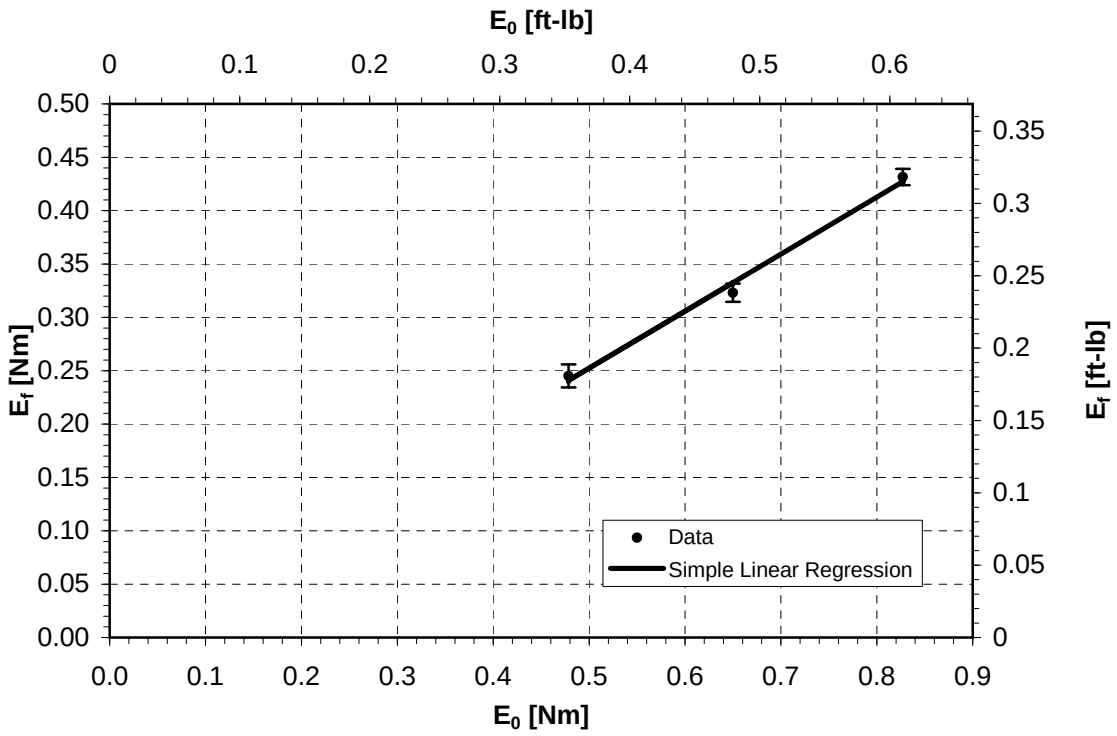

(a) Simple Linear Regression with Error Bars

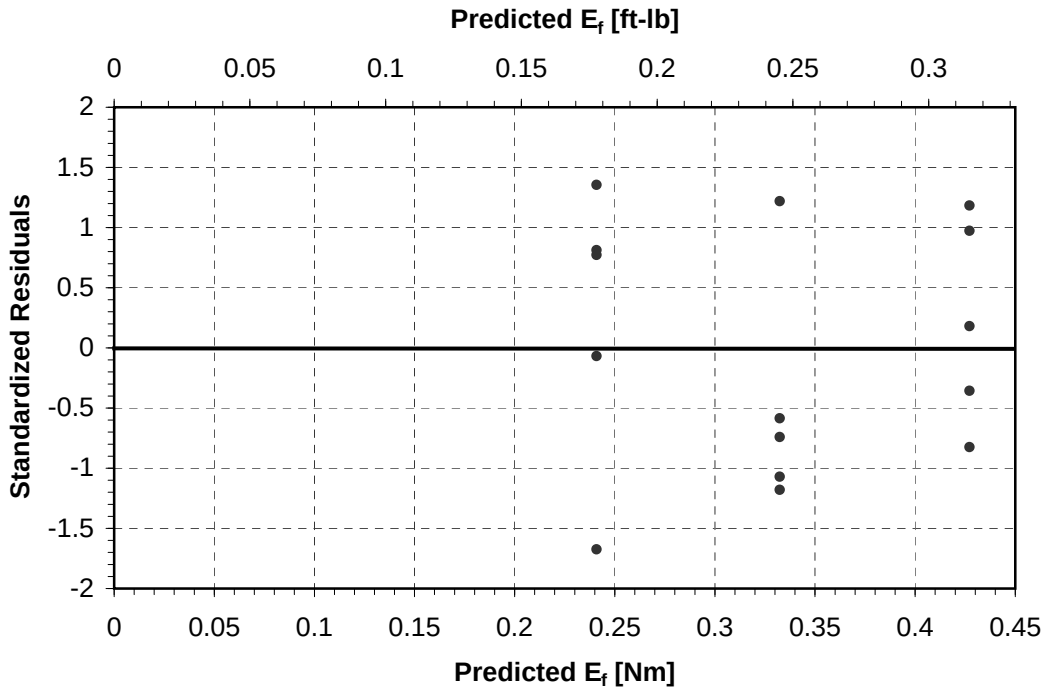

(b) Standardized Residuals from Regression Analysis

Figure A.12: Energy Final vs. Energy Initial, Spring M, Accelerometer Experiments

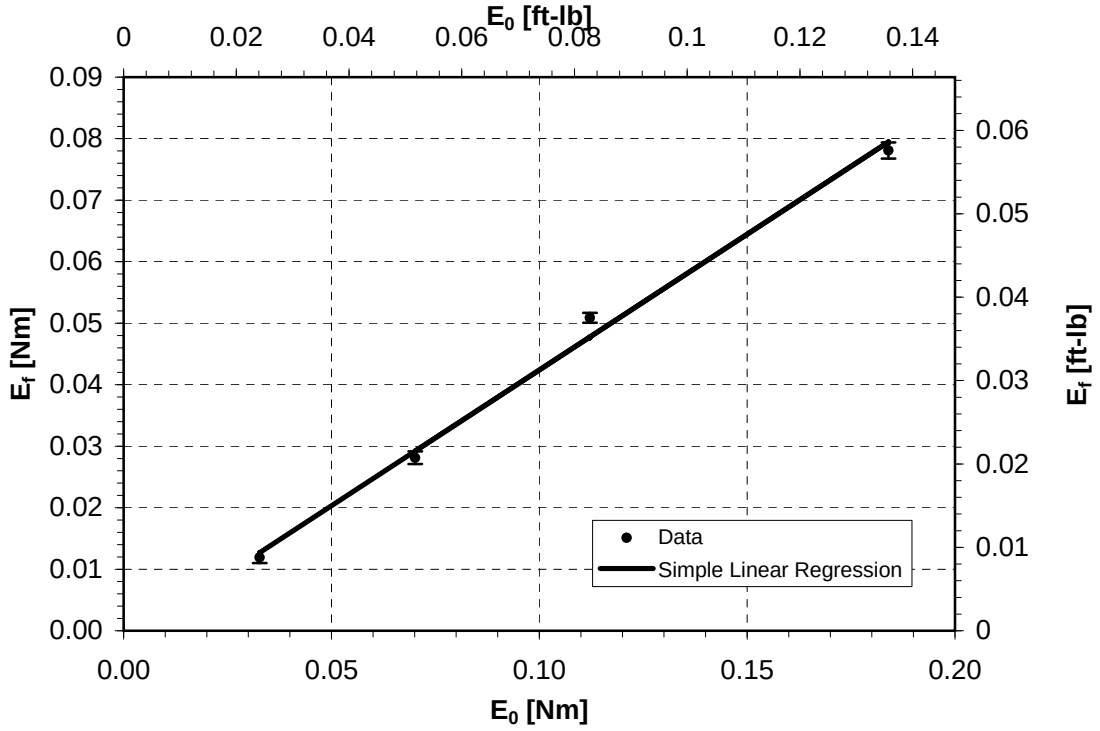

(a) Simple Linear Regression with Error Bars

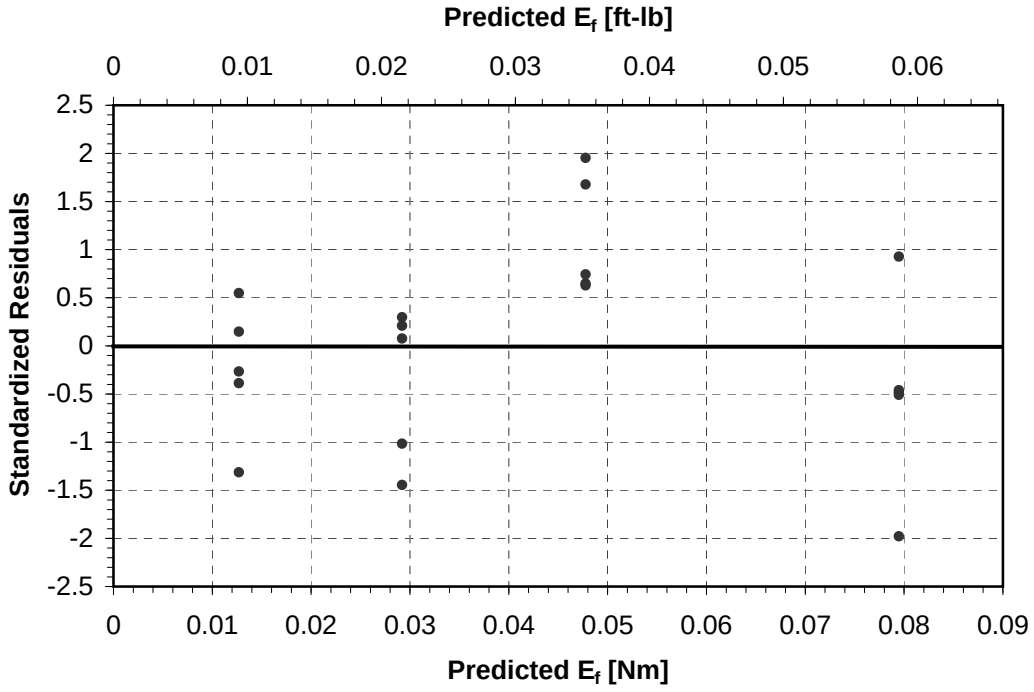

(b) Standardized Residuals from Regression Analysis

Figure A.13: Energy Final vs. Energy Initial, Spring S, Accelerometer Experiments

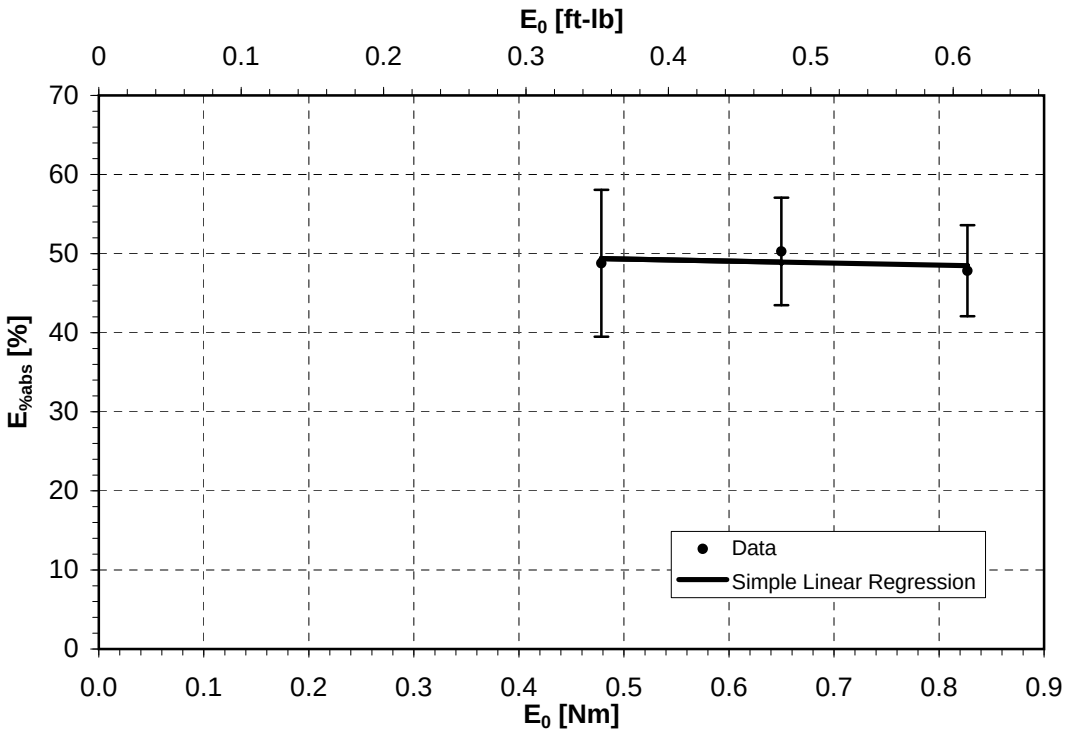

(a) Simple Linear Regression with Error Bars

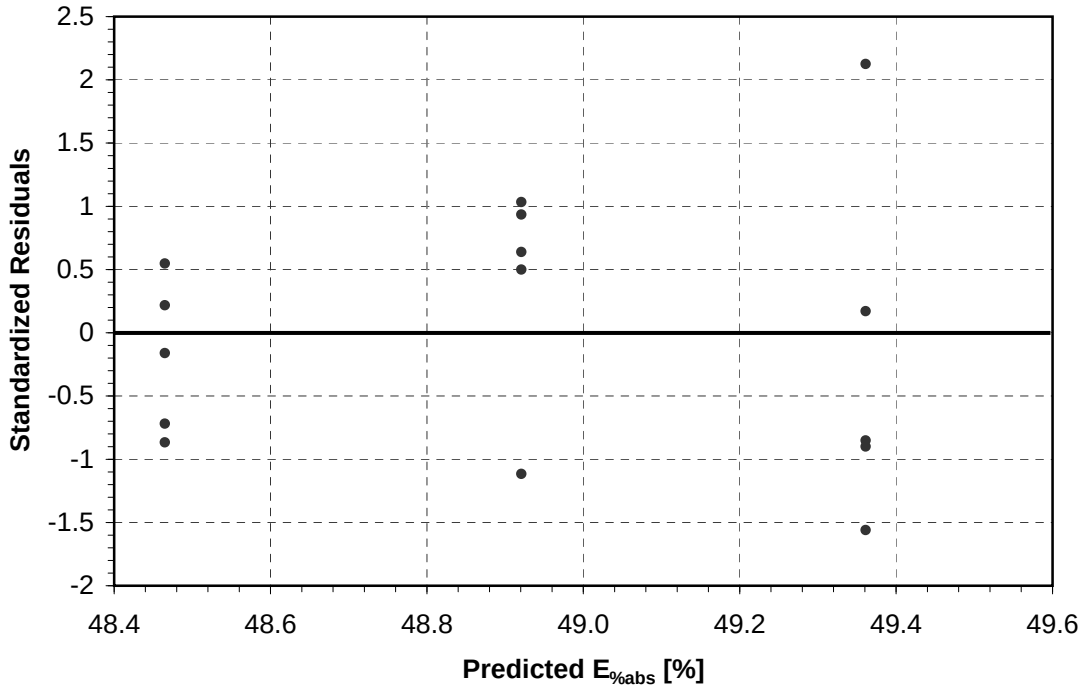

(b) Standardized Residuals from Regression Analysis

Figure A.14: Percent Energy Absorbed vs. Energy Initial, Spring M, Accelerometer Experiments

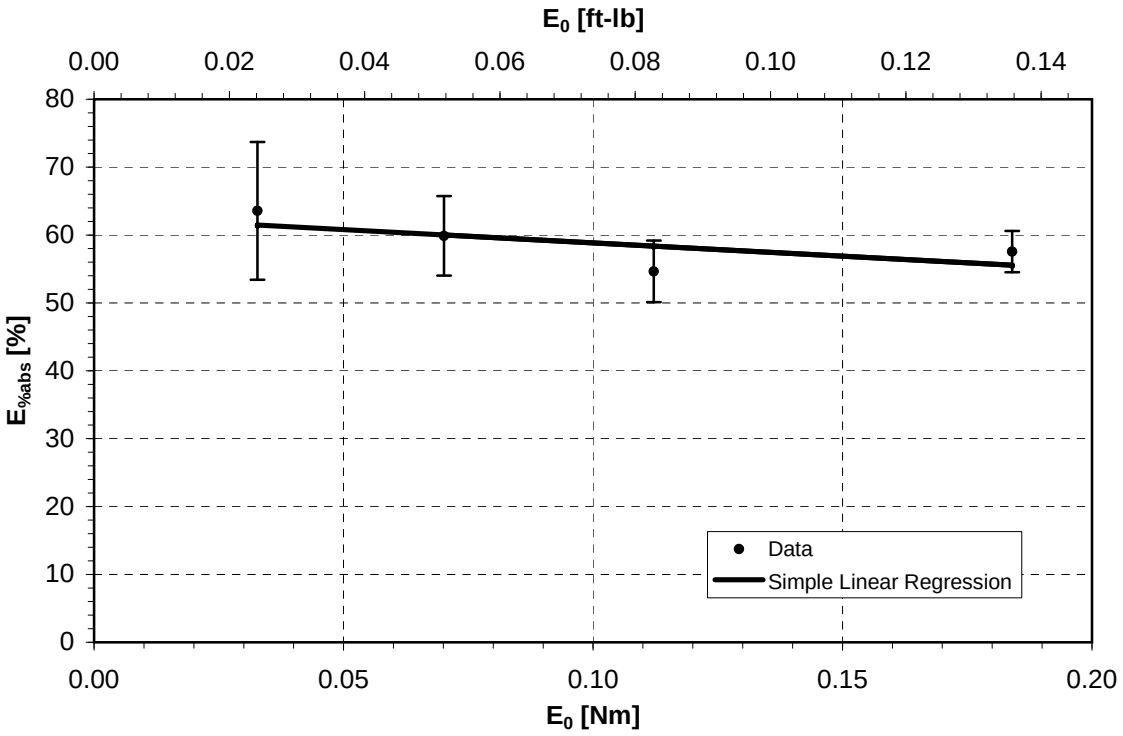

(a) Simple Linear Regression with Error Bars

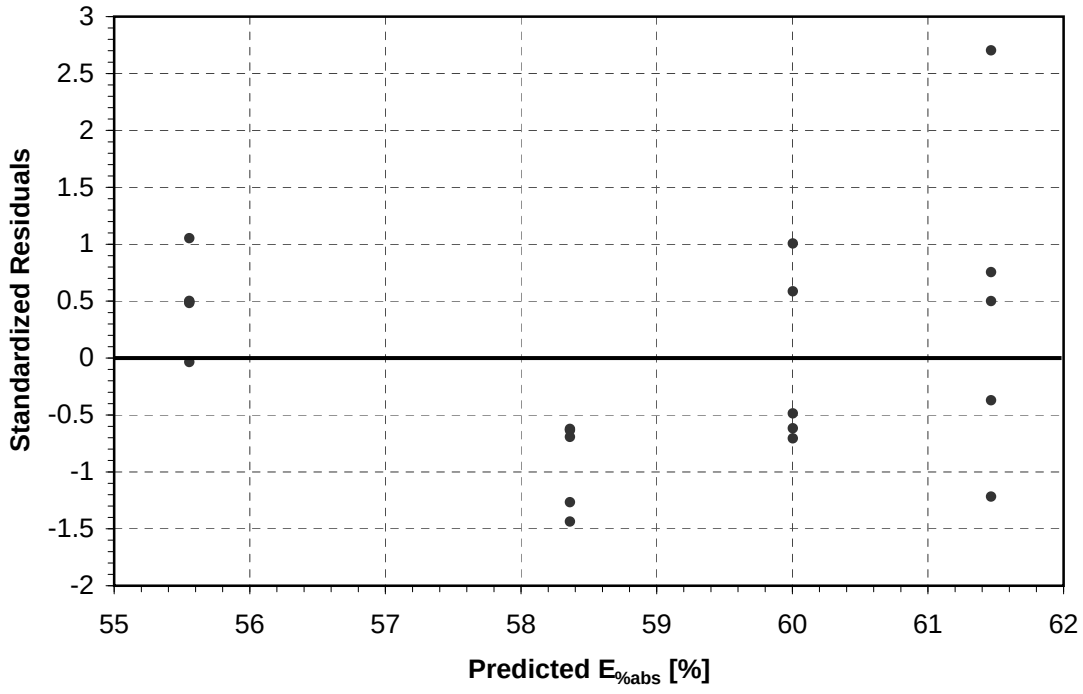

(b) Standardized Residuals from Regression Analysis

Figure A.15: Percent Energy Absorbed vs. Energy Initial, Spring S, Accelerometer Experiments

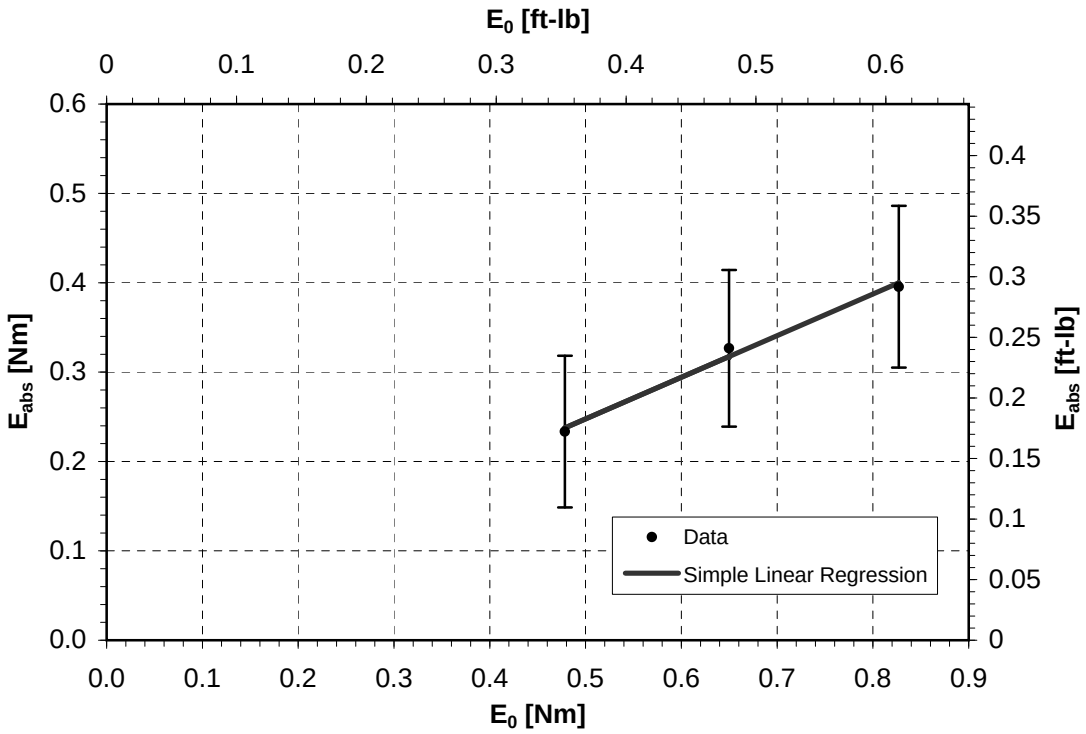

(a) Simple Linear Regression with Error Bars

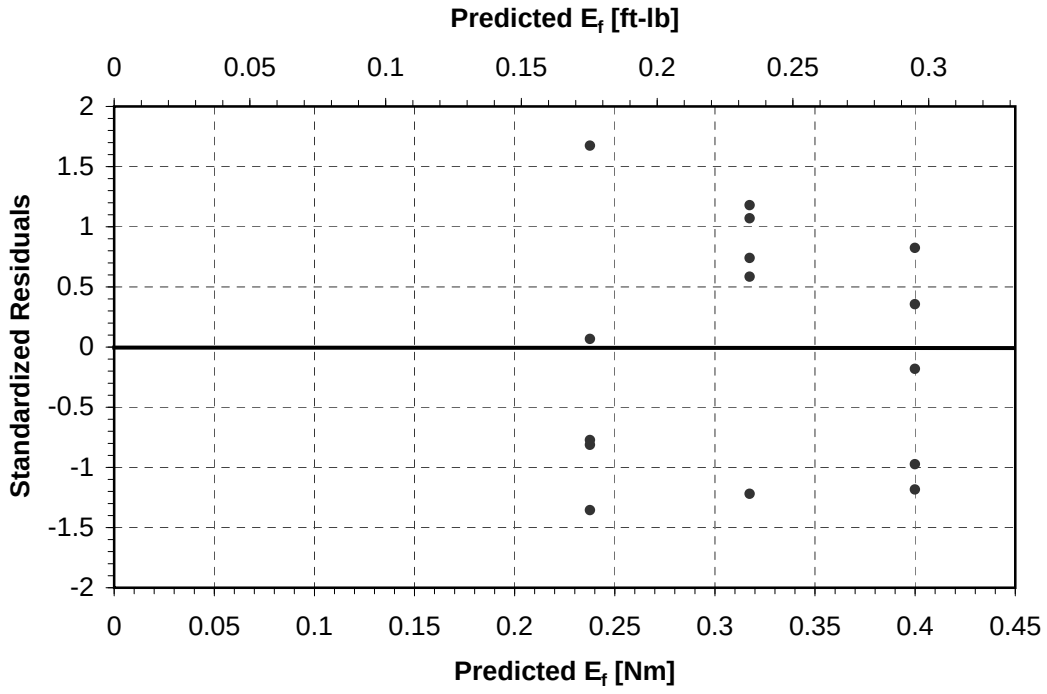

(b) Standardized Residuals from Regression Analysis

Figure A.16: Energy Absorbed vs. Energy Initial, Spring M, Accelerometer Experiments

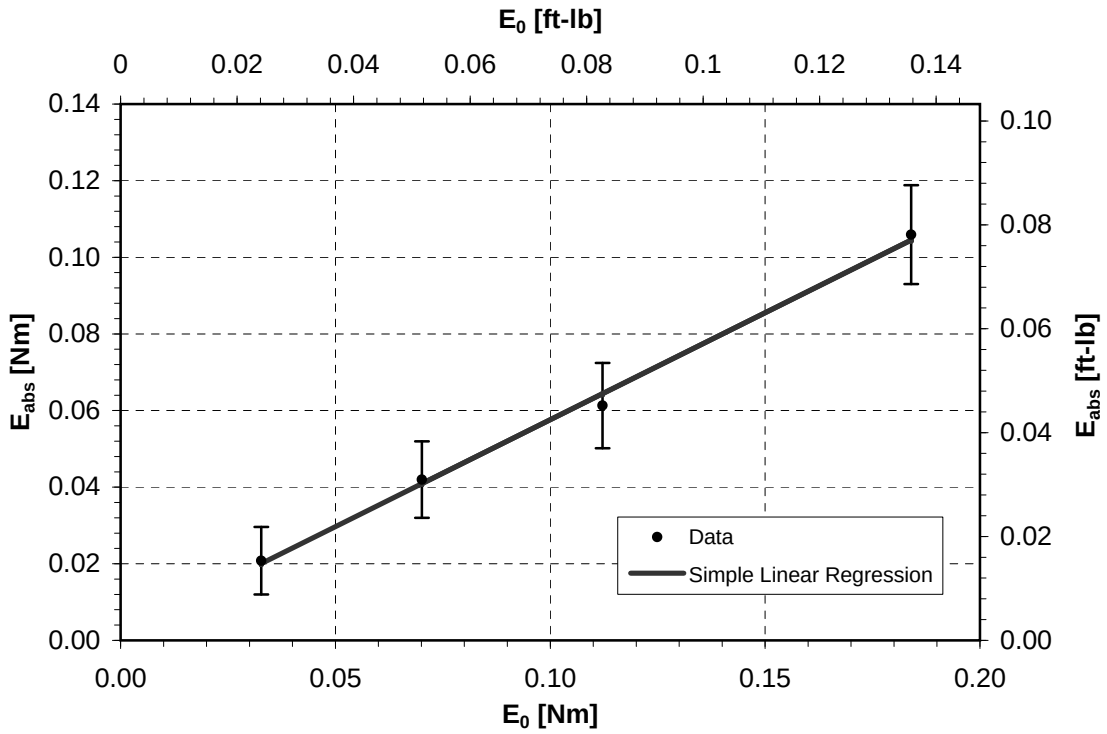

(a) Simple Linear Regression with Error Bars

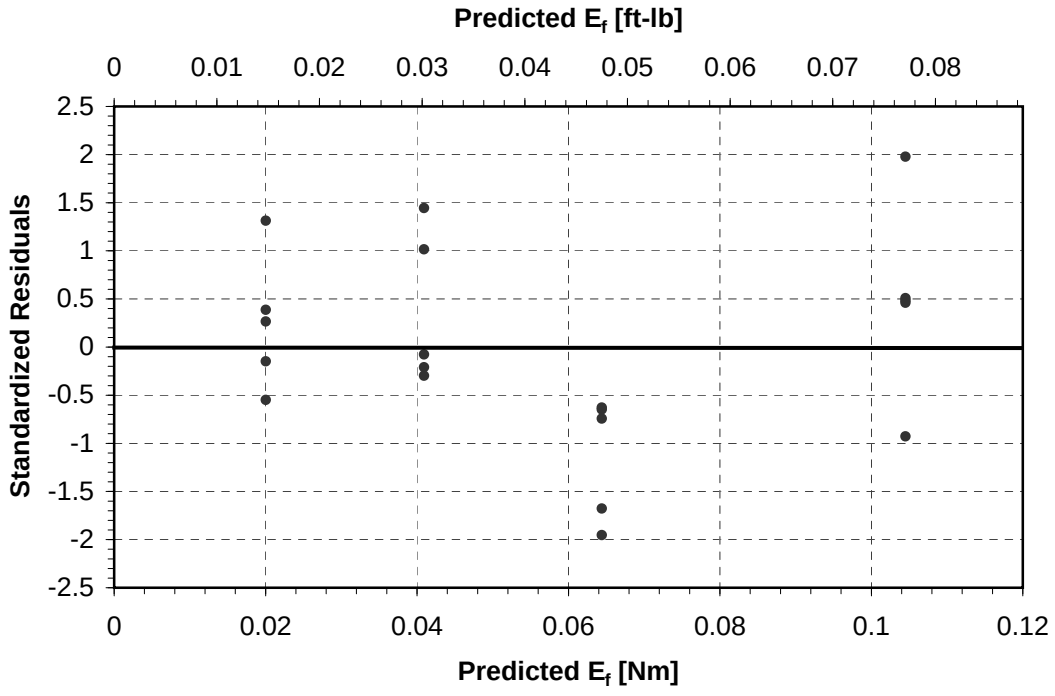

(b) Standardized Residuals from Regression Analysis

Figure A.17: Energy Absorbed vs. Energy Initial, Spring S, Accelerometer Experiments

Appendix B

Raw System Test Data

	Comp. 6	Comp. 1	Comp. 4	Comp. 11	Comp. 2	Comp. 3
Test Number	Spring Extension	Hole Elongation	Bending Deformation Angle	Length of Elongated Hole	Failure	Failure
	[in]	[in]	[deg]	[in]	[Fail / No Fail]	[Fail / No Fail]
5	9.13	0.208	30	0.350	Fail	Fail
6	9.13	0.162	27	0.380	Fail	Fail
7	6.88	0.142	0	0.310	Fail	Fail
8	6.88	0.146	0	0.310	Fail	Fail
9	6.63	0.106	0	0.260	Fail	Fail
10	6.63	0.131	5	0.270	Fail	Fail
11	7.13	0.139	0	0.240	Fail	Fail
12	6.25	0.137	0	0.280	Fail	Fail
13	10.38	0.156	15	0.305	Fail	Fail
14	10.25	0.168	35	0.340	Fail	Fail
15	9.63	0.248	35	0.340	Fail	Fail
16	9.63	0.146	20	0.340	Fail	Fail
17	10.25	0.224	37	0.220	Fail	Fail
26	10.50	0.179	15	0.310	Fail	Fail
30	3.88	0.063	0	0.124	No Fail	No Fail
31	3.50	0.033	0	0.124	No Fail	No Fail
32	5.13	0.103	0	0.124	No Fail	No Fail
33	5.38	0.093	0	0.124	No Fail	No Fail
34	8.38	0.247	25	0.340	Fail	Fail
35	8.63	0.183	20	0.170	Fail	Fail

Table B.1: System Test Data of Assembly AAB-1

	Comp. 6	Comp. 1	Comp. 4	Comp. 11	Comp. 2	Comp. 3	Comp. 12
Test Number	Spring Extension	Hole Elongation	Bending Deformation Angle	Length of Elongated Hole	Failure	Shearing	Failure
	[in]	[in]	[deg]	[in]	[Fail / No Fail]	[Fail / No Fail]	[Fail / No Fail]
18	8.06	0.203	15	0.270	No Fail	Fail	No Fail
19	8.06	0.151	8	0.270	No Fail	Fail	Fail
20	9.81	0.173	20	0.395	Fail	Fail	Fail
21	9.63	0.181	30	0.270	No Fail	Fail	Fail
22	6.50	0.143	0	0.180	No Fail	Fail	Fail
23	6.50	0.135	0	0.220	No Fail	Fail	Fail
24	4.94	0.083	0	0.180	No Fail	No Fail	No Fail
25	5.00	0.083	0	0.160	No Fail	No Fail	No Fail
27	9.75	0.173	15	0.250	Fail	Fail	Fail
28	3.31	0.043	0	0.124	No Fail	No Fail	No Fail
29	3.25	0.063	0	0.124	No Fail	No Fail	No Fail

Table B.2: System Test Data of Assembly AAB-2

	Comp. 6	Comp. 1	Comp. 4	Comp. 11	Comp. 5	Comp. 2	Comp. 3
Test Number	Spring Extension	Hole Elongation	Bending Deformation Angle	Length of Elongated Hole	Change in Length	Failure	Failure
	[in]	[in]	[deg]	[in]	[in]	[Fail/No Fail]	[Fail/No Fail]
1	9.25	0.081	0	0.22	0.455	Fail	No Fail
2	9.25	0.047	10	-	0.384	Fail	No Fail
3	7.56	0.035	0	0.16	0.422	No Fail	No Fail
4	7.63	0.024	0	0.13	0.360	No Fail	No Fail
5	5.94	0.013	0	0.14	0.278	No Fail	No Fail
6	6.00	0.017	0	0.16	0.282	No Fail	No Fail
7	4.38	0.028	0	0.16	0.099	No Fail	No Fail
8	4.25	0.000	0	0.15	0.084	No Fail	No Fail
9	2.88	0.000	0	0.13	0.038	No Fail	No Fail
10	2.88	0.000	0	0.15	0.070	No Fail	No Fail
21	9.63	0.032	5	-	0.443	Fail	No Fail
22	9.56	0.098	6	-	0.455	Fail	No Fail
23	9.69	0.073	0	-	0.432	No Fail	No Fail
24	9.63	0.051	10	-	0.443	Fail	No Fail

Table B.3: System Test Data of Assembly AAB-3

	Comp. 6	Comp. 1	Comp. 4	Comp. 11	Comp. 5	Comp. 2	Comp. 3	Comp. 12
Test Number	Spring Extension	Hole Elongation	Bending Deformation Angle	Length of Elongated Hole	Change in Length	Failure	Failure	Failure
	[in]	[in]	[deg]	[in]	[in]	[Fail/No Fail]	[Fail/No Fail]	[Fail/No Fail]
11	9.13	0.038	0	0.17	0.416	No Fail	No Fail	Fail
12	9.13	0.038	0	0.21	0.372	No Fail	No Fail	Fail
13	7.75	0.015	0	0.17	0.352	No Fail	No Fail	No Fail
14	7.75	0.021	0	0.19	0.382	Fail	No Fail	No Fail
15	5.88	0.014	0	0.18	0.249	No Fail	No Fail	No Fail
16	6.00	0.018	0	0.19	0.176	No Fail	No Fail	Fail
17	4.56	0.018	0	0.16	0.095	No Fail	No Fail	No Fail
18	4.50	0.000	0	0.16	0.083	No Fail	No Fail	No Fail
19	2.75	0.000	0	0.16	0.058	No Fail	No Fail	No Fail
20	3.63	0.000	0	0.16	0.049	No Fail	No Fail	No Fail
25	9.25	0.000	0	0.21	0.351	No Fail	No Fail	Fail
26	9.25	0.014	0	0.20	0.375	No Fail	No Fail	Fail
27	9.13	0.000	0	0.20	0.319	No Fail	No Fail	Fail
28	9.13	0.025	0	0.18	0.386	No Fail	No Fail	Fail

Table B.4: System Test Data of Assembly AAB-4